FINAL REPORT

for

RADIO ASTRONOMY EXPLORER-B

IN-FLIGHT MISSION CONTROL SYSTEM

DEVELOPMENT EFFORT

Contract Number NAS 5-11900

Report Number 73-8

March 1973

Prepared by:

Analytical Mechanics Associates, Inc.
11691 National Boulevard
Los Angeles, California 90064

for

Goddard Space Flight Center
Greenbelt, Maryland

FINAL REPORT

Contract Number NAS 5-11900

Report Number 73-8

March 1973

Goddard Space Flight Center

Contracting Officer

Mr. Robert J. Flick

Technical Officer

Mr. Charles R. Newman

Prepared by:

D. A. Lutzky
W. S. Bjorkman
C. Uphoff

ANALYTICAL MECHANICS ASSOCIATES, INC.
50 JERICHO TURNPIKE
JERICHO, N. Y. 11753

TABLE OF CONTENTS

List of Tables

List of Figures

List of Figures

(continued)

SECTION 1

INTRODUCTION and SUMMARY

This report is a description of the development effort for the MAESTRO program to be used for the in-flight decision-making process during the translunar and lunar orbit adjust phases of the flight of the Radio Astronomy Explorer - B (RAE-B). MAESTRO is an acronym for Mission Analysis Evaluation and Space Trajectory Operations. The program serves two functions, performance and evaluation of preflight mission analysis and in-flight support for the midcourse and lunar orbit insertion command decisions that must be made by the flight director.

The all-FORTRAN program was designed to be a flexible mission analysis tool that can be readily modified to analyze and support different types of spaceflight missions. One of the principal guidelines in the MAESTRO development effort has been to reach an equitable balance between efficiency and flexibility. The advantage of this type of development was demonstrated in the summer of 1972 when, within a few months, the program was modified to support the IMP-H mission analysis and in-flight operations.

This document supplements a previous report on the mission control system design study (Final Report for NAS5-11796). The skeleton system developed in the earlier contract is described there at length along with the analyses that helped set the criteria for development of the actual working program.

The development of the system has been divided into three basic tasks as follows:

I System Integration

II On-line Control and Displays

III Operational Logistics and Testing.

The report is arranged according to these tasks except that the extensive midcourse guidance analysis has been included as a separate section.

Section 2 contains a basic description of the program capabilities along with discussions of the analyses that accompanied the development of those capabilities. The program options are divided into operational modes that are invoked by the setting of a single control flag. Each of the options uses the basic trajectory propagation software that forms the heart of the program. This trajectory propagation software itself contains several options for selection of the trajectory propagation method, numerical integration technique or analytic propagation technique. The program options include straightforward trajectory propagation or ephemeris generation, orbit insertion retro- or kick-motor firing analysis, midcourse guidance analysis with any of a number of guidance laws and targeting constraints and a fully integrated midcourse verification mode. The program contains orbit prediction capability in two forms of different speed and accuracy, a post injection trim analysis with several levels of sophistication, along with shadowing, occultation and tracking visibility calculations as options. These capabilities are not mutually exclusive and the options can be run in tandem to form the Monte Carlo mode that provides statistical information on expected fuel requirements, orbit trim requirements, spin-axis-sun angles at maneuvers, distributions of execution errors and a great deal of more detailed information related to the specific goals of the RAE-B mission.

The Monte Carlo capability can be run either as a production type, pre-launch mission analysis tool or on-line during the flight to help the flight director make decisions on the basis of maximizing the probability of mission success. These capabilities and the available optional features are described in detail in Section 2.

Section 3 contains an extensive discussion of the midcourse guidance capabilities of MAESTRO. Detailed descriptions, with explicit examples, are given for the various quidance laws. These laws, and the entire guidance philosophy, have evolved through a combination of theoretical and numerical experiments aimed at providing flexibility and speed of computation.

The midcourse quidance calculations are normally accomplished with the

Multiconic trajectory propagation technique because of its speed and flexibility. These calculations can, however, be performed with full numerical integration if desired. The guidance end-point constraint variations are evaluated by the secant method and the required midcourse velocity is obtained by the usual linear analysis in each iteration of a numerical search procedure.

The midcourse quidance analysis features an analytic pre-targeting procedure that is based upon a modified sphere of influence patched conic technique and internal gradient evaluation control logic that greatly reduces the required iterations in the midcourse analysis.

The results of the quidance calculations are further used in the evaluation of expected second midcourse fuel requirements, expected errors in the lunar approach trajectory, and the expected variations in the post-injection lunar orbit. These quantities are available, on option, to the flight director to aid in the selection of the best overall midcourse maneuver time and attitude. The guidance analysis mode provides for selection of minimum fuel, fixed time of arrival, fixed pre-retro selenocentric energy, fixed post-retro energy, variable target inclination procedures and a variety of overburn or underburn options for these guidance modes.

Section 4 is a description of the methods for on-line control and the printed displays of the MAESTRO program. The program includes an input editor that assigns preset values to the control variables according to the setting of the mode flag. These preset values can be changed with little effort but the objective of the automatic input scheme is to permit the program operation to be semi-automatic. The preset inputs have been arranged in a hierarchy so that certain analyses can be run by the setting of the single control variable. This scheme greatly reduces the chances of human error in operation, especially under conditions of stress during an actual flight.

Also in Section 4 are brief descriptions of the printed displays that are used to form a director's book for reference and presentation of results. These displays

are designed to be comprehensive but also readily understandable. Many of the displays are split apart with the bulk of the information printed separately from a concise summary sheet that presents a readily-grasped evaluation of the situation. Several examples of the displays are included in this report and the reader is referred to separate documents for additional examples and explanation.

Section 5 contains explanations of the methods of using the program for in-flight operations support. The first subsection includes a typical flight profile outline along with an approximate time-line for the in-flight control operations. The hypothetical flight pro file is only one of several similar possibilities but the outline contains all the operations that might be required in a "worst case" situation. The discussion emphasizes the importance of a close man-computer relationship during the in-flight operations and the need for a smooth flow of information between the separate parts of the overall control system is made obvious.

A second subsection contains discussions of possible failure modes with fairly detailed outlines of three of what appear to be the most likely contingincies. The areas of possible failure are catagorized in such a way that the reader can associate his own specialty with one of the modes. The presentation is intended to stimulate the reader's imagination so that possibilities that may not have been considered will be brought to light. Failures are classified broadly as 1) Hardware malfunctions, 2) Computer Software Errors, and 3) Human errors. In addition to this generalized classification of possible failures, the three specific areas of most import are suggested to be: 1) Midcourse and trim propulsion sytem failure, 2) Attitude control and determination system malfunction, and 3) Retro rocket failure. These three possibilities are discussed in some detail.

A third subsection contains descriptions of the system testing procedures, the simulations that have been held to date, and recommendations for the extensive testing that is to take place during the next few months. Several of our early mistakes are discussed and suggestions are made for minimizing the possibility

of such mistakes in the future. Emphasis is placed upon the need for complete and rapid communication between the components of the mission control system and upon the need for a close man-computer relationship during the in-flight operations. Also stressed is the need for a smooth flow of information between the three major components of the computer software system.

A closing section includes a brief summary of the important aspects of the MAESTRO system development and operation. A short list of recommendations is presented along with some suggestions for the future development, use, and upkeep of the MAESTRO program. The reader is reminded that this document is complemented by four other reports: the MAESTRO Programmer's Manual Reference (6), the design study final report Reference (1), the MAESTRO User's Manual Reference (2), and the Parameter Estimation Notebook Reference (7) which might be considered an appendix to this report. The non-technical reader who wishes to skip to the conclusions and recommendations should first examine the operations flow diagram of figure 4.1.

SECTION 2

SYSTEM DEVELOPMENT

The MAESTRO system is an outgrowth of the skeleton system described in Reference 1. The skeleton system demonstrated the feasibility of developing a mission control system that has the capability of propagating different kinds of trajectories as efficiently as possible. The trajectory propagator in the skeleton system was developed using the philosophy that no one trajectory propagation technique is most efficient for all trajectories. For example, it was found that Cowell was most efficient for a nearly rectilinear orbit and Encke's method is most efficient in other situations. Thus, the trajectory propagator in the skeleton system had various trajectory propagation techniques and numerical integration techniques. MAESTRO has the same trajectory propagation tool as the primary workhorse in the system. There are several mission analysis modes built around the trajectory propagator. These modes are:

1. trajectory propagator
2. retro motor firing analysis
3. midcourse analysis
4. Monte Carlo analysis
5. midcourse verificiation analysis
6. orbit evolution
7. post injection trim analysis

The following sections describe each of these modes.

It is important to note that MAESTRO was not designed to be restricted to a particular mission. Although many of the displays are concerned with the mission objectives of the RAE-B mission, the entire system can be easily adapted to interplanetary or Earth orbit missions. In the Summer of 1972, MAESTRO was quickly modified and implemented as the mission control program for the IMP-H mission.

2.1 TRAJECTORY PROPAGATION MODE

In this mode MAESTRO is used as a three-degree-of-freedom trajectory simulation program with the capability of propagating the trajectory with any of the following trajectory simulation schemes:

a. Cowell's method

b. Encke's method

c. numerical integration of the classical elements with true anomaly as the fast variable

d. numerical integration of the classical elements with mean anomaly as the fast variable

e. averaging of equations in "d"

f. multiconic

g. numerical integration modified elements

h. averaging of equations in "g"

The first four trajectory propagation schemes are commonly used techniques. A description of how they were incorporated into MAESTRO is described in Reference 1. The averaging used in schemes "e" and "h" are detailed in Section 2.6 of this report. Multiconic is an approximate method which gives very good results for Earth-Moon trajectories. Its chief advantage is that it is extremely fast. A description of this technique was also presented in Reference 1. Scheme "g" is similar to the integration of the classical elements except that the elements used do not have a discontinunity as the eccentricity approaches zero. The terms to be integrated are:

1. semilatus rectum, p
2. $\dot{e} \sin \omega$
3. $e \cos \omega$
4. $\omega + f$
5. inclination, i
6. longitude of the ascending node,

where e is the eccentricity

ω is the argument of perigee

f is the true anomaly

The derivatives of the above quantities are numerically integrated to obtain the instantaneous orbital elements. The equations which define these derivatives are presented in Appendix A.

The user also has the option of selecting any one of a variety of numerical integration schemes. The schemes available are

a. Ten-cycle seventh-order Runge-Kutta

b. Twelfth-order multistep

These schemes were described in Reference 1. Reference 1 also presented an analysis to determine the relative accuracy of these schemes. In that report it was stated that the seventh-order Runge-Kutta appeared "best." This integration scheme is still considered the best with most of the trajectory propagators; however, it was found that Cowell can achieve greater accuracy in the same computing time when used with the twelfth-order multistep. The twelfth multistep method possess the limitation that it cannot be easily used with a varying compute interval, and requires a cumbersome startup procedure.

The other capabilities of the trajectory propagator in MAESTRO are

1. Planetary Ephemerides
   a. DE69 tape read for all planets
   b. mean elements for Sun
   c. mean elements for Moon
   d. osculating elements for Moon
   e. DE69 disk read utilizing direct read feature on IBM computer
2. Lunar Gravity Models
   a. L1 field
   b. JPL - 15 by 8 field
      (a high-order geopotential can be included in the same logic for close-Earth orbit analysis)
   c. Post Mariner 9 Mars field
3. Input Coordinate Systems
   a. mean equator and equinox of 1950
   b. mean equator and equinox of date

c. mean equator and ecliptic of date

d. true equator and prime meridian

e. true equator and equinox of date

f. true equator and node

g. spherical Earth centered

4. Output Coordinate Systems

a. mean equinox and ecliptic of date

b. true equator and prime meridian

c. mean equator and equinox of 1950

d. true equator and equinox of date

5. Rocket motor firing with variable thrust/weight flow capability

6. Transfer orbit and in-orbit shadow calculations for both umbral and penumbral passages

7. Solar pressure

8. Run termination at

a. input final time

b. closest approach to a target planet

c. farthest distance from a target planet

9. Compute interval

a. preset table with up to ten values as a function of time

b. automatic

10. Variable printing logic

2.2 RETRO MOTOR FIRING ANALYSIS

The retro motor firing analysis or approach analysis is used to determine the attitude and time to fire a retro motor to achieve desired mission constraints. In this analysis it is assumed that all midcourse maneuvers have already been completed, thus the approach trajectory (trajectory before retro firing) is fixed. The analysis can be performed in either of two levels of accuracy. In the most accurate level, all segments of the approach trajectory are numerically integrated and retro motor is also numerically integrated. In the lower accuracy level the orbital elements of the approach trajectory are determined. The state at each firing time is determined by stepping along this constant set of elements. The retro motor is not numerically integrated; instead the impulsive velocity of the motor is used. The orbital elements of the approach trajectory are determined by numerically integrating the approach trajectory to the desired stop time (or closest approach if the appropriate inputs are set). The orbital elements at this time are used as the constant elements of the approach trajectory.

No matter which level of accuracy is used, the analysis is performed in the same manner. Firings of the retro motor are simulated along the approach trajectory at a series of attitudes. The mission constraints are determined for each firing at each attitude and displays are presented so that the user can rapidly determine the firing time and attitude which best satisfy the mission constraints. The range of firing times and attitudes are determined in the following manner:

1. Firings are made between input range of true anomaly about the stop time of the approach trajectory. The attitude range is an input cone angle about the velocity vector at the stop time.
2. Firings are made from asymptote to asymptote on the approach hyperbola. The attitude range is input as initial right ascension and declination, increment in right ascension and declination, and the number of right ascensions and declinations to be tried. The approach trajectory must be hyperbolic.

3. Firings are made between input times. The attitude range is input as in 2.

Although the displays currently available are designed for the RAE-B mission, displays could easily be changed to accommodate other missions. In this mission the most important mission criteria is achieving the desired Lunar orbit with sufficient maneuver fuel. Thus, a display is presented to rapidly access the retro firing attitude which results in the minimum maneuver fuel. Other displays are presented which have more complete information about the firings made at each of the attitudes. Samples of these displays are presented in the user's guide, reference 2.

2.3 MIDCOURSE ANALYSIS

The midcourse analysis capability in MAESTRO is described in Section 3. This section contains the theory, run setup and practical results.

2.4 MONTE CARLO ANALYSIS

The purpose of the Monte Carlo analysis is to determine the probability of mission success. The probability of mission success is determined by "flying" the mission numerous times with errors applied to the initial state and to each of the maneuvers. Each of the samples are analyzed to determine whether they satisfy mission constraints. The probability of satisfying a particular constraint is determined from the sum of the number of samples which satisfy the constraint divided by the total number of samples tried. A typical mission flight plan could consist of the following:

1. Apply tracking errors to the initial state and fly to the first midcourse execution time.
2. Determine the first midcourse correction, apply errors to the correction and fly to the second midcourse execution time.
3. Determine the second midcourse correction, apply errors to the correction and fly to the Moon.
4. Determine the retro motors firing time and attitude. Apply errors to the retro and burn retro.
5. Determine if final Lunar orbit satisfies mission constraints.

The analysis currently has the capability of simulating a flight plan similar to the one outlined above or a plan with only one midcourse and retro or only a retro maneuver. The Monte Carlo analysis also has the capability to determine the first maneuver from the current state. This maneuver, with errors, is applied to all of the samples. This capability should be used when the errors in the estimation of the initial state approach a constant value. When this point is reached the state will not be known to a more accurate level in the future. Thus, the first maneuver must be determined using current state and not the current state with estimation errors.

The model used to simulate errors in the initial state is a covariance matrix. This matrix is calculated by the oribit determination program and passed to MAESTRO, or can be input.

Error Models

The tracking error covariance matrix, P, is a 6 x 6 positive definite matrix of anchor vector estimation errors.

$$P = E\ (x - \tilde{x})\ (x - \tilde{x})^t \qquad (\tilde{x} = \text{anchor vector},\ x = \text{true state})$$

There is a preferred coordinate system in which components of the error factor, y, are uncorrelated. The (similarity) transformation between y and $x - \tilde{x}$ is S, an orthogonal matrix which diagonalizes P.

$$x - \tilde{x} = S_y$$

The diagonal matrix, D, defined by

$$D = S^t PS,$$

has as its diagonal elements the variances of the uncorrelated components of y. Scaling a white noise (uncorrelated random numbers) sampled by the standard deviations of y, we obtain an error vector in uncorrelated coordinates with components, y_i.

$$y_i = d_i\ n\ (0,1)$$

(d_i is the i-th diagonal element of D, n (0,1) is a sample random number from a normal (Gaussian) distribution of mean 0 and variance 1.) A sampled errant trajectory state is then computed from

$$x = \tilde{x} + Sy.$$

Execution errors for the midcourse and retro maneuvers are computed from assigned standard deviations of pointing and velocity errors. The velocity error is treated as a proportional error normally distributed plus a resolution error uniformly distributed.

$$\epsilon_V = v\sigma_V n\ (0,1) + (.0001\ \text{km/sec})\ u$$

(v is the velocity impulse magnitude and u is a random number from a distribution uniform on the interval $\{-.5 \leq u \leq .5\}$). The retro velocity error is formulated without a resolution error. The pointing error is formulated as two independent errors normally distributed along mutually orthogonal axes which are both orthogonal to the maneuver impulse direction. Let the maneuver impulse be denoted by V and its direction by $\bar{V}$. If K is the unit polar axis of V's coordinate reference frame, we can construct unit vectors normal to $\bar{V}$.

$$\bar{E} = \frac{\bar{K} \times \bar{V}}{\bar{K} \times \bar{V}} = \frac{\begin{Bmatrix} -v_2 \\ v_1 \\ 0 \end{Bmatrix}}{v_1^2 + v_2^2} = \frac{\begin{Bmatrix} -v_2 \\ v_1 \\ 0 \end{Bmatrix}}{v \cos(\text{dec})}$$

$$\bar{N} = \bar{V} \times \bar{E} = \frac{\bar{K} - \bar{V}\ (\bar{K} \cdot \bar{V})}{\cos(\text{dec})}$$

The "eastward" and "northward" pointing errors, θ_e and θ_n, are computed by scaling random numbers with the input pointing errors, σ_a. They are then converted to velocity deviations using the small angle approximation.

$$\epsilon_e = v\sigma_a n_1\ (0,1)$$

$$\epsilon_n = v\sigma_a n_2\ (0,1)$$

The misdirected velocity vector has the direction

$$\bar{V}' = (v\bar{V} + \epsilon_e \bar{E} + \epsilon_n)\bar{N} / \sqrt{v^2 + \epsilon_e^2 + \epsilon_n^2}$$

And the magnitude $v = \epsilon_v$, so that it may be programmed as follows,

$$V' = \frac{v + \epsilon_v}{v\sqrt{1 + \sigma_a^2 (n_1^2 + n_2^2)}} \left\{ \left(1 - \frac{\sigma_a N_2 V_3}{v \cos(\text{dec})} \right) \begin{pmatrix} v_1 \\ v_2 \\ v_3 \end{pmatrix} + \frac{\sigma_a}{\cos(\text{dec})} \begin{pmatrix} -n_1 & v_2 \\ n_1 & v_1 \\ n_2 & v \end{pmatrix} \right\}$$

The Monte Carlo analysis demonstrated the necessity to develop some method to automatically determine the retro motor's firing time and attitude. In earlier analysis models, the retro was simulated at closest approach to the Moon opposite to the velocity vector. This firing strategy was sufficient when the spacecraft passed close to the aiming point at the Moon. However, small midcourse execution errors will cause relatively large errors at the Moon. Thus, some other retro firing strategy had to be determined. The approach finally selected used a steepest ascent optimization procedure to determine the attitude which minimizes a particular function. The function minimized is the minimum post injection trim velocity on a Lunar approach hyperbola. This velocity is determined by firing the retro at various points along the approach hyperbola and calculating the trim velocity to achieve the desired final Lunar orbit. The minimum of all of the calculated trim velocities is the value used in the function to be minimized.

The trim philosophy is to perform a two- impulse Hohmann transfer to achieve the desired circular orbit and to make a third plane-change maneuver at the largest node of the intermediate orbit. Whether or not this new policy is optimal is difficult to decide. It is certainly not "fuel optimal," as the literature shows, for large plane change situations. In the normal case of small plane change, the fuel optimal policy will probably yield fuel savings that are inconsequential in comparison with the complexity and risk of performing additional attitude reorientations and engine ignitions. In any case, the logic for determining the required trim fuel, given a specific post-retro orbit, is an isolated subroutine which can be easily modified as more sophisticated trim maneuver logic is incorporated. The point important to the above discussion is that a value can be determined that represents the minimum fuel required to change the orbit from its post-retro size and orientation to the desired lunar orbit suitable for long-term antenna stability.

A more detailed description of the steepest ascent optimization procedure is shown in Appendix B.

The Monte Carlo output presents the running means and standard deviations of the variables of interest. These variables include the fuel requirement and spinaxis - sun angle for each maneuver as well as the post-retro orbital elements. A statistical summary is printed at the end of the run. This summary contains the mean, standard deviation, maximum value encountered and minimum value encountered of the quantities mentioned above. The analysis also has the provision to output starting conditions for each sample so that any particular sample can be studied in detail.

2.5 MIDCOURSE VERIFICATION ANALYSIS

The midcourse verification analysis was included in MAESTRO in order to provide a check of other analysis and provide data useful for real time decision making. The mode can be used to verify any midcourse motor firing. This includes firing for midcourse corrections on the transfer trajectory or firings in orbit for post injection trim.

In this analysis, the percise numerical integration techniques are used to propagate the state from the initial time to motor ignition. Next, the motor is numerically simulated and the spacecraft propagated to closest approach to the target planet if desired. The final time can be set to the engine burn-out time so that the analysis ends there. This would probably be desired for post injection trim verification.

A doppler analysis of the motor burn is also presented. The output from this analysis provides histories of the nominal spacecraft thrust, weight and the velocity away from the visible tracking stations assuming nominal thrust characteristics. The velocity away from the tracking stations can be used to calculate the doppler shift expected during the motor firing. The expected doppler shift can be compared to the actual shift experienced in real-time and correction actions can be initiated if a non-nominal burn is indicated.

The midcourse verification analysis also presents a list of tracking station elevation and azimuth angles at motor ignition time. Thus, tracking station coverage is automatically available for any motor ignition time by the use of this mode.

The post maneuver orbit is presented at closest approach to the target planet (or final time). This orbit should be compared to the orbit predicted by the midcourse analysis or post injection trim analysis. The orbits should be the same if same techniques were simulated in both analyses. For example, if impulsive velocity was assumed in the midcourse analysis and not used

in the verification run, differences arrising from the impulsive velocity approximation will appear when comparing the two runs.

The displays obtained from this mode are shown in the user's guide.

2.6 LUNAR ORBIT PREDICTION - Numerical Averaging

One of the primary objectives of the RAE-B mission is to establish a lunar orbit whose eccentricity will remain near zero for at least a year. The complexity of the lunar gravity field makes it difficult to perform approximate predictions of the orbit evolution by the usual analytic techniques. Because of this difficulty and because of the need to predict the long-term motion of the orbit, a numerical averaging technique has been developed and implemented in the MAESTRO program. This technique was described briefly in Reference (1) and more thoroughly in Reference (5). The following subsections contain discussions of the averaging method, a newly implemented numerical startup procedure to obtain initial mean elements, and some examples of the method's efficiency in the RAE-B orbit prediction problem.

2.6.1 The Averaging Technique

The method as implemented in MAESTRO is described in detail in Reference (5). The essence of the technique is the averaging of the planetary equations (see Appendix A) by numerical quadrature over one revolution of the spacecraft in its orbit. It is shown in Reference (5) that the system of ordinary differential equations describing the osculating orbital elements can be transformed, by the averaging operation, into a system of ordinary differential equations describing the mean values of the orbital elements.

Let the system of planetary equations given in Appendix A be represented by

$$\dot{E}_i = F_i(E_j, t) \qquad i=1,6; \quad j=1,6.$$

The time average of this system is defined as

$$\bar{\dot{E}} = \frac{1}{\tau} \int_{t-\tau/2}^{t+\tau/2} F_i(E_j, t)\, dt \qquad i=1,6; \quad j=1,6,$$

where τ is the orbital period.

The integration variable is transformed to the Keplerian true anomaly, f, as

$$\overline{\dot{E}} = \frac{n p^2}{2\pi \mu p} \int_{f(t-\tau/2)}^{f(t+\tau/2)} \frac{F(E,f)\, df}{(1 + e \cos f)^2}$$

It should be noted that

$$\overline{\frac{dE}{dt}} = \frac{1}{\tau} \int_{t_o-\tau/2}^{t_o+\tau/2} \dot{E}(t)\, dt = \frac{E(t_o+\tau/2) - E(t_o-\tau/2)}{\tau}$$

and that in terms of similarly defined mean values of the elements,

$$\frac{d}{dt}(\bar{E}) = \frac{d}{dt}\left\{ \frac{1}{\tau} \int_{t-\tau/2}^{t+\tau/2} E(t)\, dt \right\} = \overline{\frac{dE}{dt}}$$

provided that we maintain the understanding that the orbital elements remain constant during the averaging integration. Thus, by these few assumptions we have traded the system (1) of ordinary differential equations in terms of the osculating elements for the system (4) of ordinary differential equations in terms of the mean orbital elements.

The exact form of the averaging as implemented in MAESTRO is described in the MAESTRO programmer's manual under subroutine AVEQNS and the averaged equations are given in Reference (5).

2.6.2 Numerical Startup

For some time there have been discussions of how to start the numerical averaging technique (Methods 5 and 8). Past studies have been conducted with the assumption that the averaging integrations were started with known values of the mean orbital elements. These initial mean elements were assumed to be available by virtue of some process whereby they can be related to osculating elements at some epoch. This assumption has not been unreasonable because of theoretical arguments that every almost-periodic function has a mean motion.

We can assume, then, that the time history of the mean orbital elements is approximately the same as the history of the running mean of the osculating elements. In practice, we can proceed as if for every set of osculating elements at some epoch, there is a corresponding set of mean elements representing the average values of the osculating elements over the almost-period of the osculating motion. The problem, in the real world, is to relate the osculating elements to the mean elements at some epoch.

In Reference 5, it is suggested that the relationship between mean and osculating elements can be obtained by performing a one-revolution integration of the osculating orbital elements and by simultaneously forming the integrals

$$\bar{E}_i = \frac{1}{t} \int_0^t E_i \, dt, \qquad i = 1, 6,$$

where E_i represents the osculating elements. Now when the Keplerian period given by the running mean semi-major axis is equal to the current time, t, we can obtain a mathematically and dynamically consistent one-to-one relationship between the mean elements at t/2 and the osculating elements at t = 0.

This suggestion has been incorporated into the MAESTRO program and the new option can be invoked by setting location 1098 to 1. The new option allows one to input osculating elements at some epoch and to obtain a numerically averaged solution for the subsequent motion that is dynamically consistent with the initial osculating elements.

Figure 2.1 shows the time history of the selenocentric argument of pericynthion and includes a comparison of the osculating and averaged values of that quantity. The motion of the mean elements through the center of the envelopes of the osculating elements is very encouraging. The figure is representative of all the orbital elements and success of the startup procedure implies a better representation of the long-term motion in the realistic case where we must use osculating elements to start the numerical averaging technique.

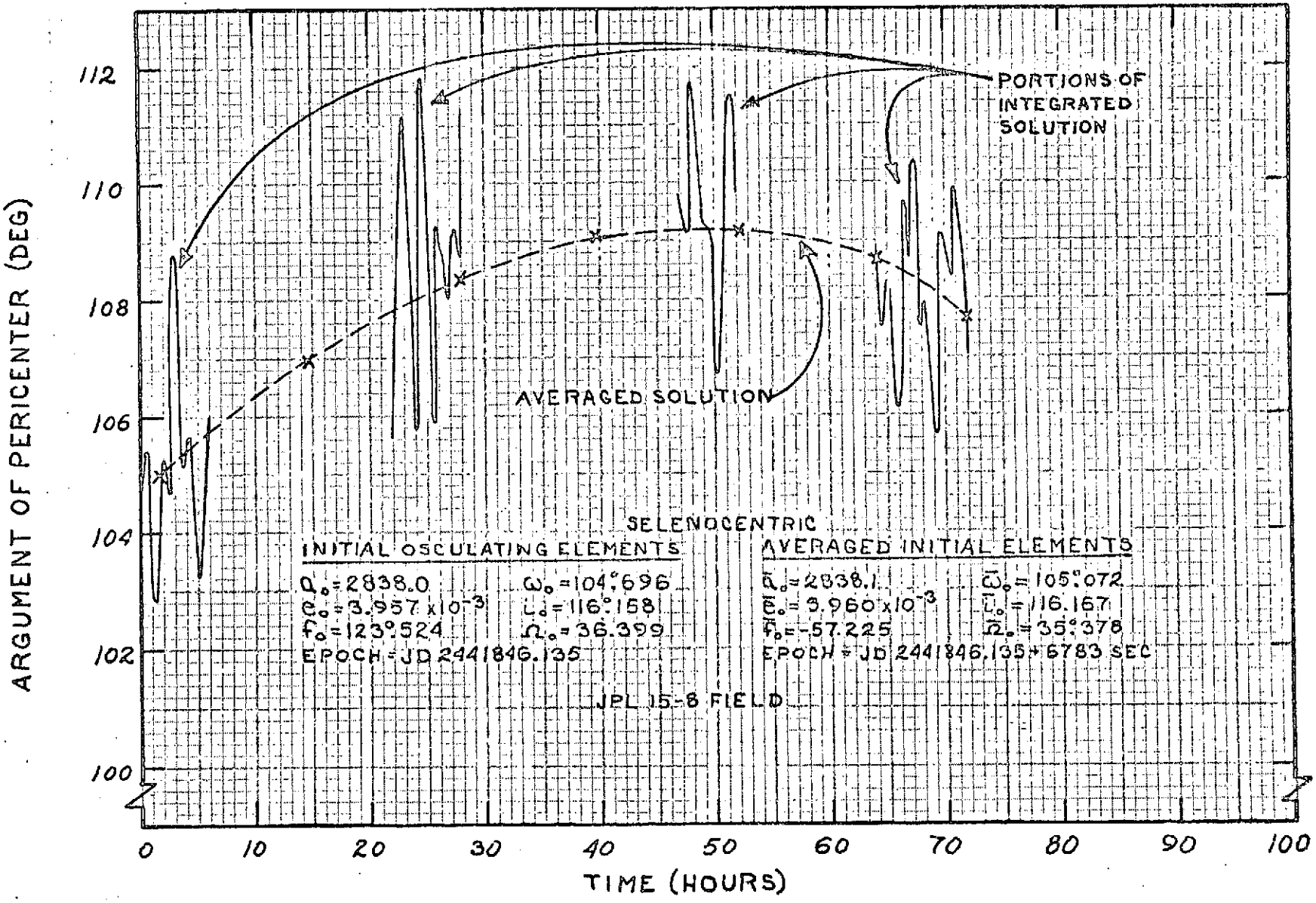

NUMERICAL AVERAGING WITH AUTOMATIC STARTUP

Figure 2.1

2.6.3 Comparison of Averaging with Actual Solutions

In Reference (5), several examples are given that indicate the speed, accuracy, and flexibility of the numerical averaging. It is carefully pointed out that the averaging is an intermediate technique that lies, in speed and accuracy, somewhere between full numerical integration and the usual analytic techniques. The principal advantage of the method is that all kinds of forces can be included in the dynamic model without the need for analytic approximation of the disturbing forces.

Throughout the MAESTRO development effort, experiments have been conducted to determine the "best" combination of intervals and ordinates to be used in the quadrature integration. For the RAE-B orbit, it has been found that excellent results are obtained if the averaging interval (the orbit period) is divided into three intervals each employing a 6 point Gaussian quadrature. Figure 2.2 shows the effect of changing the intervals and ordinates for a typical example of the tests conducted.

Finally, Figure 2.3 gives a 200 day time history of the eccentricity for a typical RAE-B orbit. This run was started with mean elements obtained by the numerical startup procedure and the agreement of the mean and osculating time histories represents an obvious improvement over the example shown in Reference (5) where the differences between initial osculating and mean elements were ignored. The accuracy and timing shown on the figure are typical of the performance of the averaging for RAE-B type orbits.

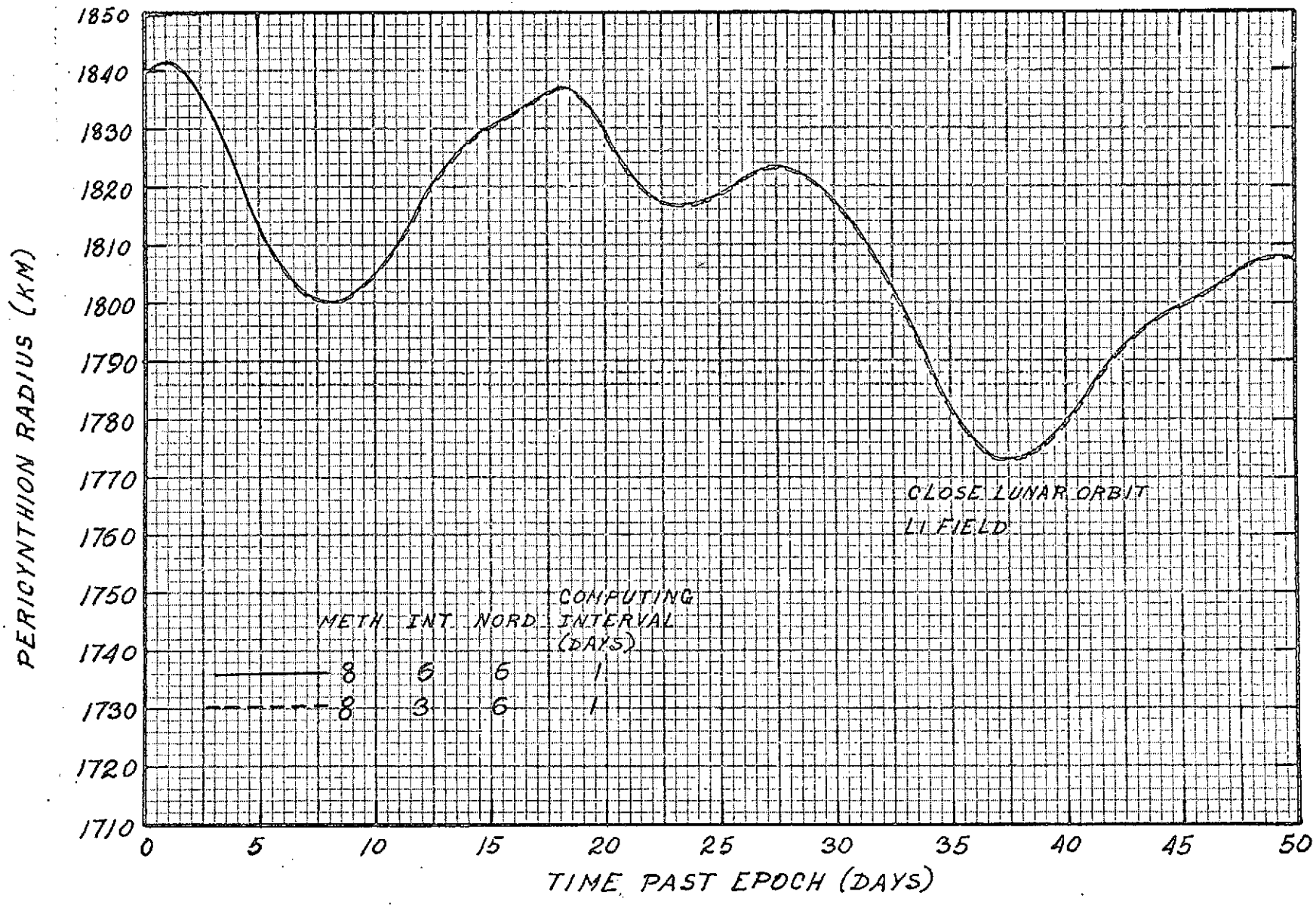

EFFECT OF NUMBER OF INTERVALS ON ACCURACY OF AVERAGING TECHNIQUE

Figure 2.2

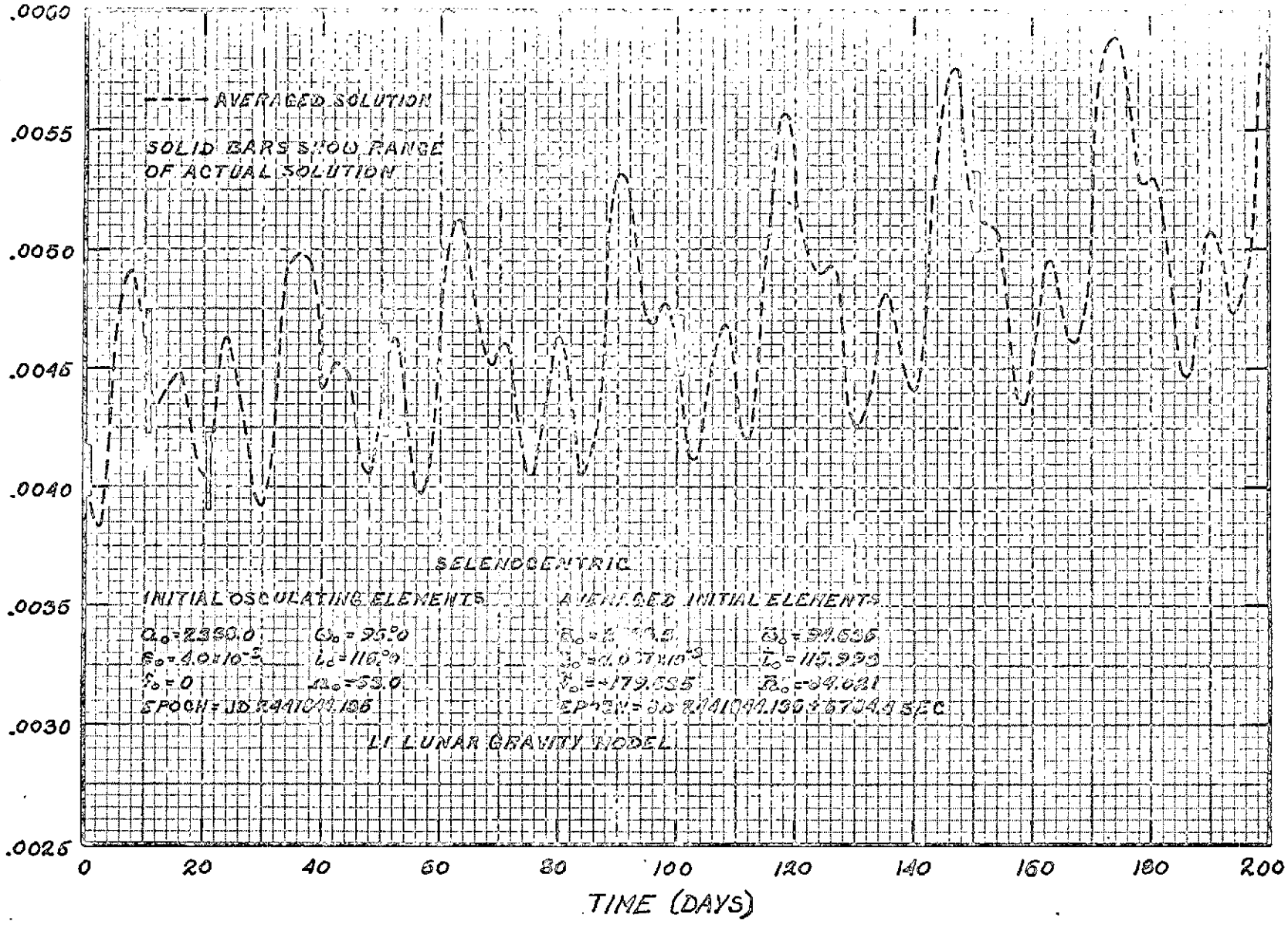

COMPARISON OF ACTUAL AND AVERAGED SOLUTION

Figure 2.3

2.7 POST INJECTION TRIM ANALYSIS

The post injection trim analysis is required to determine the maneuver(s) necessary to achieve a desired orbit. The orbit after retro will probably not be the desired orbit because the fixed retro velocity could not yield the desired orbit, or, if it could, the errors in the retro maneuver itself could yield substantial errors. The desired orbit is defined as a circular orbit with a specified radius and inclination. The position in the orbit or the argument of the ascending node is not important.

There has been many attempts to solve this complex problem analytically. Thus, a literature search was initiated to determine if any previous work could be adapted to our problem. The search was conducted by Dr. Mary Payne, reference 3. Her work indicated that there were a few techniques available that may solve our problem. Some of the techniques she suggested were techniques that utilize many impulses. It was decided not to use these techniques because the many motor firings and attitude changes would degrade the reliability without any large gain in system performance.

The work by T. Sun, reference 4, seemed the most promising. He developed the optimum solution to the two impulse 180° transfer between non-coplanon orbits. It is not necessarily true that the 180° transfer is optimum, however, it is optimum in certain planar cases (Hohmann transfer). Since the inclination changes in the orbit must be small because of system capabilities, it was concluded that the 180° transfer is near the optimum solution. Also, a two impulse maneuver is desirable from a reliability standpoint. The following paragraphs present a synopsis of Sun's method and describes how it was implemented.

Sun's method determines the optimal two impulse 180° transfer between non-coplanar orbits. Since a 180° transfer is specified, the first impulse must be applied at the intersection of the initial and final orbit planes. Thus, the angle between the initial and final orbit planes and the position on the initial orbit where the maneuver is made can be obtained from the spherical trigometric relationships, see figure below:

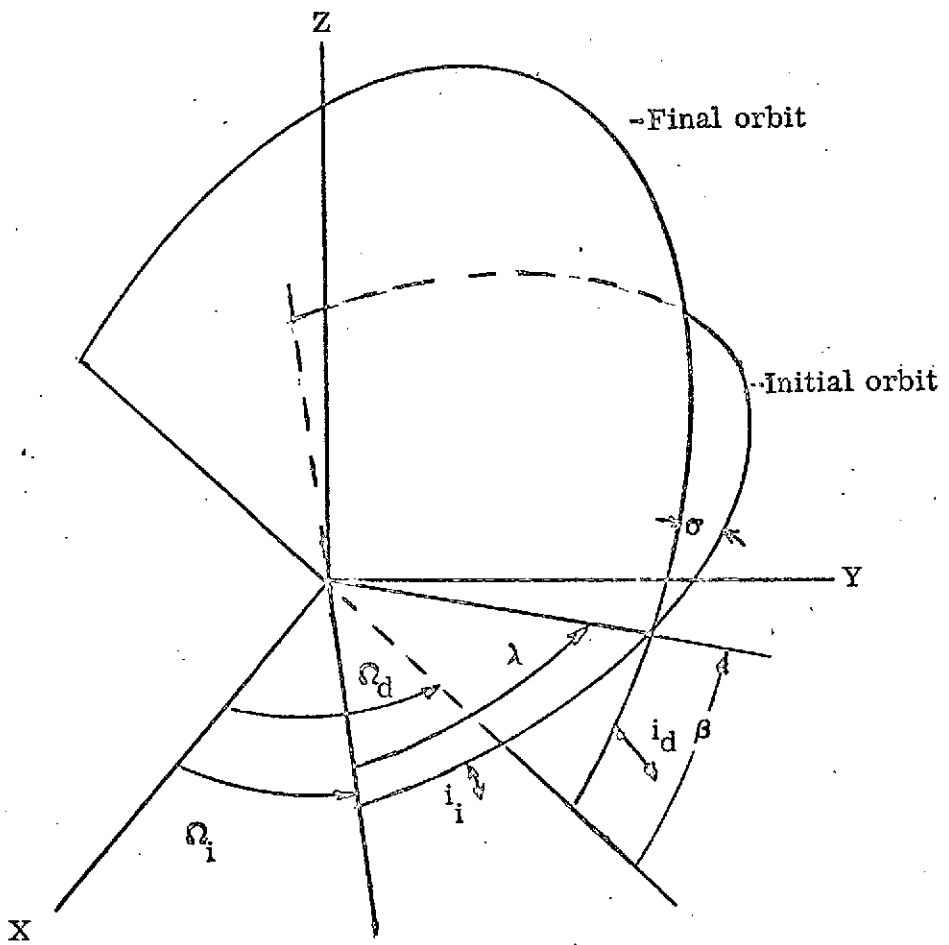

The angle from the reference plane to the common line of nodes in the initial orbit, λ, can be determined from the input initial true anamoly, f, and the argument of the ascending node of the initial orbit as,

$$\lambda = f + \omega \qquad (1)$$

Then, the angle between the two orbit planes, σ , can be determined from,

$$\sin \beta = \sin i_i \sin i_d / \sin \lambda \qquad (2)$$

$$\tan \frac{\sigma}{2} = \sin \left(\frac{\lambda - \beta}{2}\right) \overline{\sin \left(\frac{\lambda + \beta}{2}\right)} \tan \left(\frac{i_d - i_i}{2}\right)$$

where i is the inclination

β is the angle from the reference plane to the common line of nodes in the final orbit plane.

and the subscripts i and d refer to the initial and desired orbits, respectively.

The radius and velocity components can be determined from standard orbital relationships at the initial true anomaly, f.

The orientation of the transfer plane with respect to the initial and final orbit planes is described in the figure below:

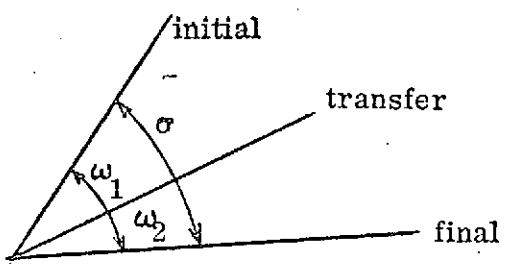

The angles ω_1 and ω_2 describe the orientation of the transfer plane with respect to the initial and final orbit planes, respectively.

If the inclination of the transfer plane with respect to the initial plane is specified, then the optimal velocity can now be determined using Sun's equation 10.

$$\Delta V = \sqrt{\frac{\mu}{r_1}} \left\{ V_{r1}^2 + \left[\left(V_{T1}^2 - 2 \sqrt{\frac{2n}{n+1}} V_{T1} \cos \omega_1 + \frac{2n}{n+1} \right)^{1/2} + \left(1 - 2 \sqrt{\frac{2}{n+1}} \cos \omega_2 + \frac{n}{n+1} \right)^{1/2} \right]^2 \right\}^{1/2} \qquad (3)$$

where μ is the gravitational constant

r_1 is the radius at $f = \lambda$

V_{r1}, V_{T1} are the radial and transversal velocity components on the initial orbit relative to local velocity ($V=\sqrt{\mu/r}$)

n is r_d / r_i

The equation above is somewhat simplified from Sun's equation since the final orbit is circular. Thus,

$$\begin{aligned} V_{r2} &= 0 \\ V_{T2} &= 1. \end{aligned} \tag{4}$$

If the velocity of each trim maneuver is desired, then

$$\frac{\Delta V_1}{\Delta V} = 1 + \frac{1}{\sqrt{n}} \left[\frac{1 - 2\sqrt{\frac{2}{n+1}} \cos \omega_2 + \frac{2}{n+1}}{V_{T_1}^2 - \sqrt{\frac{2n}{n+1}} V_{T1} \cos \omega_1 + \frac{2n}{n+1}} \right]$$

$$\frac{\Delta V_2}{\Delta V} = 1 + \sqrt{n} \left[\frac{V_{T1}^2 - 2\sqrt{\frac{2n}{n+1}} V_{T1} \cos \omega_1 + \frac{2n}{n+1}}{1 - 2\sqrt{\frac{2}{n+1}} \cos \omega_2 + \frac{2}{n+1}} \right] \tag{5}$$

where ΔV_1 and ΔV_2 denote the magnitudes of the first and second trim maneuvers.

The direction these impulses are applied can be determined by noting the following relationships.

$$\begin{aligned} \Delta V_{R1} &= V_{RT1} - V_{R1} \\ \Delta V_{N1} &= -V_{T1} \sin \omega_1 \\ \Delta V_{T1} &= V_{TT1} - V_{T1} \cos \omega_1 \end{aligned} \tag{6}$$

The second trim is determined in a similar manner as

$$\begin{aligned} \Delta V_{r2} &= V_{R2} - V_{RT2} \\ \Delta V_{N2} &= -V_{T2} \sin \omega_2 \\ \Delta V_{T2} &= V_{T2} \cos \omega_2 - V_{TT2} \end{aligned} \tag{7}$$

In the above equations the components of velocity are defined as follows,

$V_{R1,2}$	radial component of velocity of the initial or final orbit.
$V_{T1,2}$	Transversal component of velocity of the initial or final orbit, in the initial or final orbit plane.
$V_{TT1,2}$	Transversal component of velocity of the initial or final orbit written in the transfer plane.
$V_{RT1,2}$	Radial component of velocity of the transfer orbit at initial and final orbit crossings.

All components of velocity except the radial components of the transfer orbit in equations 6 and 7 are fixed by specifying the initial and final orbits. The radial component of velocity is determined from the condition that the total trim velocity is to be minimized. The total trim velocity is

$$\Delta V = \Delta V_1 + \Delta V_2 = \sqrt{\Delta V_{T1}^2 + \Delta V_N^2 + (V_{rT1} - V_{r1})^2} + \sqrt{\Delta V_{T2}^2 + \Delta V_{N2}^2 (V_{r2} - V_{rT2})^2} \quad (8)$$

Also,

$$V_{rT1} = -V_{rT2}$$

$$V_{r2} = 0 \quad (9)$$

since a 180^o transfer is specified and the final orbit is to be circular. Now, the partial derivative of the trim velocity with respect to V_{rT1} can be written as,

$$\frac{\partial \Delta V}{\partial V_{rT1}} = \frac{V_{rT1} - V_{r1}}{\Delta V_1} + \frac{V_{rT1}}{\Delta V_2} = 0$$

or

$$V_{rT1} = \frac{\Delta V_2 \, V_{r1}}{\Delta V_1} \quad (10)$$

The components of the trim velocity obtained from equations 6, 7 and 10 describe the trim velocity with respect to the transfer plane. The trim velocity vector in the same coordinate system of the initial orbit is obtained through a three Euler angle rotation pictured in the figure below.

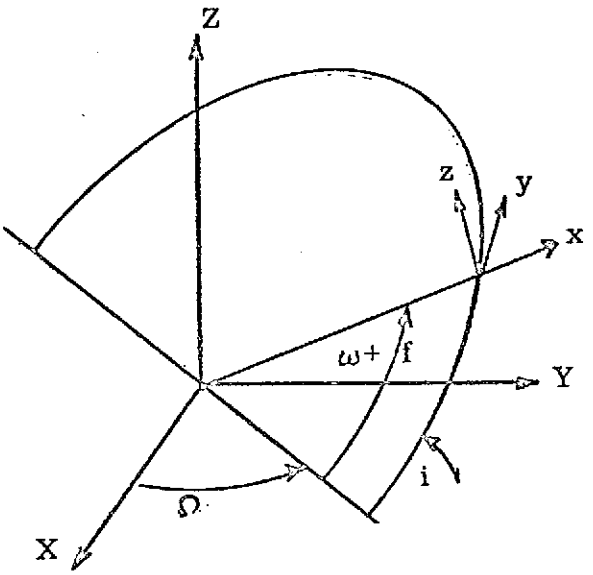

In the figure above, x corresponds to the radial direction, y to the transversal direction and z to the normal direction.

The angular elements of the reference orbit define the Euler angles. Thus the transformation from the x, y, z system to the X, Y, Z system is

$$\begin{Bmatrix} X \\ Y \\ Z \end{Bmatrix} = \begin{bmatrix} \cos\psi\cos\Omega & -\sin\psi\cos\Omega & \sin i\sin\Omega \\ -\cos i\sin\Omega\sin\psi & -\cos i\sin\Omega\cos\psi & \\ \cos\psi\sin\Omega & -\sin\psi\sin\Omega & -\sin i\cos\Omega \\ +\cos i\cos\Omega\sin\psi & +\cos i\cos\Omega\cos\psi & \\ \sin i\cos\psi & \sin i\sin\psi & \cos i \end{bmatrix} \begin{Bmatrix} x \\ y \\ z \end{Bmatrix}$$

where $\psi = f + \omega$

The above equation is used to transform the trim velocity components from an orbit plane coordinate system to the system of the reference orbit.

Optimum Inclination of the Transfer Plane

The condition for the optimal orientation of the transfer plane is expressed by

$$\frac{\sin\omega_2}{\sin\omega_1} = -n\left(\frac{1 - 2\rho_2\cos\omega_2 + \rho_2^2}{1 - 2\rho_1\cos\omega_1 + \rho_1^2}\right)^{1/2}$$

$$\text{where} \quad \rho_1 = \left(\frac{2\mu\, r_d/r_1}{r_d + r_1} \right)^{1/2} \frac{1}{V_{T1}}$$

$$\rho_2 = \left(\frac{2\mu\, r_1/r_d}{r_d + r_1} \right)^{1/2}$$

Equation 12 along with the condition

$$\omega_2 = \sigma + \omega_1$$

yields a set of equations which can be solved for ω_1 or ω_2 to yield the optimum orientation of the transfer plane. The solutions to equation 12 resulted in a sixth order polynomial in $\sin \omega$. The equation was solved numerically in order to avoid the cumbersome task of solving a sixth order equation. A Newton-Raphson procedure was employed to determine the solution to equation 13. Sun, in the reference, states that the solution is unique. Thus, the task of finding multiple solutions with the Newton-Raphson method is not required.

The optimum 180° transfer solution discussed above determines the maneuver to go from a fixed point on the initial orbit to the final orbit. We are not constrained to any specific point on the initial orbit, except for spin axis-sun angle considerations. Thus, it is necessary to determine the position on the initial orbit to make the first maneuver that results in the lowest trim requirement. The optimum position on the initial orbit is determined by a search of the entire orbit. A half-interval iteration is used to find the local minumum and the position used is the minimum of all the local minimums.

The post injection trim analysis also determines the Hohmann transfer maneuver to correct the eccentricity and raduis. This result is useful as a reference and shows how much fuel is expended to change the inclination of the initial orbit.

SECTION 3

MIDCOURSE GUIDANCE CAPABILITY

3.1 Theory

The constraint error vector, Ψ, is related to the control vector, U, by the non-linear functional expression

$$\Psi = \Psi(U).$$

The midcourse guidance problem can be stated in the form: "Find a particular control vector, U^*, which nulls the constraint error vector, Ψ." We shall now proceed to define Ψ and U specifically for the RAE-B mission and to describe the implemented solution to the midcourse guidance problem.

3.1.1 Controls

The control vector, U, for the RAE-B midcourse guidance capability is identified as the midcourse velocity correction impulse vector, ΔV_m. The program has capabilities for treating U:

1. strictly as a velocity impulse applied at midcourse ignition time and
2. as a set of numbers to be transformed to obtain burn duration and thrust direction which will render the post-burn state through integration of the powered equations of motion.

The transformation of U for finite burns is

$$\begin{aligned} \delta w &= w_o \left(1 - e^{-u/c}\right) \\ t_b &= f(\delta w) \\ \hat{T} &= \hat{U} \end{aligned}$$

The function, $f(\delta w)$, is the inverse of $\delta w(t_b)$. In the program at this writing, the weight flow rate is a piecewise-linear function of t_b, which permits a closed-form expression for $f(\delta w)$.

3. 1.2 Constraints

The arrival state, X_f, is an implicit function of U, obtained through trajectory propagation from midcourse to target closest approach, which occurs at time t_f. The constraint errors are defined explicitly as functions of desired (denoted by subscript d) and actual target (i. e. lunar) arrival conditions.

$\psi_1 = B\cdot T_d - B\cdot T(X_f)$ Equatorial miss-vector component

$\psi_2 = B\cdot R_d - B\cdot R(X_f)$ Perpendicular miss-vector component

$\psi_3 = t_{fd} - t_f$ Time of flight

$\psi_4 = v_{hed} - v_{he}(X_f)$ Hyperbolic excess speed

$\psi_5 = v_{prd} - v_{pr}(X_f, U)$ Post-retro speed, periapsis maneuver

$\psi_6 = f(U)$ Total correction fuel

$\psi_7 = r_{pd} - r_p(X_f)$ Radius of closest approach

$\psi_8 = i_d - i(X_f)$ Inclination to target's equatorial plane

Although MAESTRO allows targeting to input values of $B\cdot T_d$ and $B\cdot R_d$, it is more suitable (relative to orbiting mission objectives) to target to r_{pd} and i_d. Convergence is surer when targeting to $B\cdot T_d$ and $B\cdot R_d$, however, so these are defined in terms of r_{pd} and i_d. The specific definitions are found in appendices B, C and D. Nulling of ψ_1 and ψ_2 is a sufficient condition for nulling ψ_7 and ψ_8. The explicit definition of $B\cdot T$, $B\cdot R$, v_{he} and r_p as functions of X_f can be found in the description of subroutine BVE. We will now proceed to define $v_{pr}(X_f, U)$, $i(X_f)$ and $f(U)$.

The post-retro speed is defined by

$$v_{pr} = \sqrt{C_3 + 2\mu/r_{pd}} - \Delta V_r$$

which implies that the retro-velocity impulse, ΔV_r, is fired when the radius is r_{pd} and opposite to the velocity vector there. The retro-velocity impulse is a function of the midcourse velocity correction (i.e. of U) since the retro engine is a solid of fixed impulse and U determines how much fuel remains at retro time. When v_{prd} is $\sqrt{\mu/r_{pd}}$ and $\psi_5 = \psi_7 = 0$, the post-retro orbit will be circular.

Inclination is defined as that of the post-retro orbit relative to the target's equatorial plane, and therefore depends on the retro strategy adopted (see appendices D and E). If the angular momentum of the post-retro orbit is H, inclination is defined by

$$i = \cos^{-1}(h_3/h)$$

where h_3 is the polar component of H.

The total correction fuel, f(U), is the sum of the midcourse fuel and the trim fuel required to circularize the final orbit at the desired altitude. The midcourse fuel is computed from the rocket equation, assuming U to be the midcourse correction velocity impulse. The trim fuel is computed from the trim velocity, again using the rocket equation to provide the transformation from velocity to fuel weight. The trim velocity requirement is influenced by the retro strategy adopted and by the trim strategy. The normal strategy is to burn the retro at approach periapsis and to trim with two Hohmann impulses plus a plane-change, if necessary, at the larger-radius node on the target's equator.

3.1.3 Guidance Laws

Five guidance laws are considered. Each is designed to satisfy a different set of mission objectives, as seen from the following table.

Guidance Laws		
Law	Abbreviation	Constraint Errors Nulled
Minimum Midcourse Fuel	MFG	b_1, b_2, $\|U\|^*$
Fixed Time of Arrival	FTA	b_1, b_2, b_3
Fixed Target Energy	FTE	b_1, b_2, b_4
Variable Target Energy	VTE	b_1, b_2, b_5
Minimum Total Fuel	MTF	b_1, b_2, b_6^*

* Minimized, rather than nulled

The particular value of the MFG and MTF laws is that they achieve the final desired orbit with the least fuel. The FTA law is best from tracking visibility considerations, assuming that the arrival time was designed for good visibility. The FTE law is needed only if the arrival phase has been planned for a particular arrival energy and is inflexible to variations. The VTE law is useful in eliminating major trim maneuvers at the expense of midcourse and, usually, total correction fuel.

3.1.4 Pre-targeting

The pre-targeting method to be described is used as a device to provide "first-guess" midcourse corrections to initiate precise differential-correction targeting procedures. In this role, the method eliminates the need for non-linear targeting measures such as control limiting and gradient re-computation and greatly reduces the number of required trajectory computations. A gross description of the method would be "patched-conic targeting with constrained end conditions."

Transfer Phase

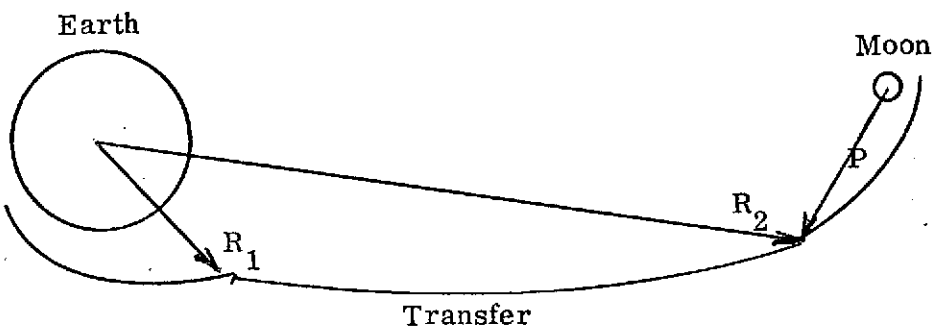

The transfer phase is treated as a single conic section relative to the central body (Earth). This phase begins at the midcourse correction position and time ends at the sphere of influence of the target body. The first terminal of this phase is the point of the midcourse correction on the uncorrected transfer trajectory -- at radius R_1, velocity V_1 and time t_1. The second terminal is on the sphere of influence of the target at a radius R_2 (referred to the central body) and time t_2. The second terminal's radius vector is computed from the target's state (relative to the central body) at t_2, R_t and V_t

$$R_2 = R_t + P$$

where P is a vector from the center of the target body to the point of entry of the target's sphere of influence. The time, t_2, of arrival at the sphere of influence

can be computed from

$$t_2 = t_f - \tau$$

where t_f is the time of arrival at closest approach (specified a priori) and where τ is the time required to travel on the approach hyperbola to the point of closest approach. The arrival phase parameters, P and τ, will be described later. An iterative solution of Lambert's problem (i.e. "Find the conic section passing from R_1 to R_2 in time $t_2 - t_1$") is employed. This solution provides V_1^*, the velocity on the transfer conic at the first terminal, and V_2^*, the transfer conic's velocity at the second terminal. The midcourse correction impulse, ΔV, is computed from

$$\Delta V = V_1^* - V_1$$

and the target-relative velocity, V, at t_2 is

$$V = V_2^* - V_t$$

where V_t is the target's velocity at t_2 relative to the central body.

The first transfer conic is computed with τ initially set to 66,000 seconds and P oriented in the Moon's orbital plane 10^o earthward from the Moon's velocity direction. The target-relative velocity derived from this first conic solution is used to initiate the arrival phase calculations. The arrival phase calculations predict a new value of P to which the transfer phase is targeted. An iteration initiated in this way can be made to converge to a steady-state value of ΔV.

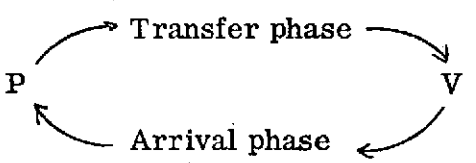

This answer is interpreted as the impulsive-correction, patched-conic, fixed-time-of-arrival midcourse maneuver.

Arrival Phase

The arrival phase computations use the target-relative approach velocity and the desired end conditions to develop the point of entry onto the sphere of influence and the time from "patch" to closest approach, assuming the approach trajectory to be a target-centered hyperbola. The desired arrival conditions are specified values of radius of closest approach and inclination. We develop characteristics which the approach hyperbola must possess in order to satisfy the desired arrival conditions. We assume that the target-relative approach velocity vector defines the direction of the arrival asymptote of the approach hyperbola. Furthermore, we assume that the point of entry into the sphere of influence can be changed without changing the direction of the arrival asymptote or the target-relative energy. It is this last assumption's inaccuracy that prompts the iteration.

The target-relative energy (Jacobian energy) is computed from the target-relative approach velocity, V. The energy of the approach orbit is corrected for perturbations which occur during the transfer phase but are not accounted for by the conic transfer trajectory.

$$C_3 = V \cdot V - 2\mu/a'$$

In the correction term, μ is the Moon's gravitational constant and a' is the semi-major axis of the Moon's orbit about the Earth. Note that the term $(2\mu/r_{soi})$ is absent from the calculation. When the fully-perturbed trajectory is flown to lunar closest approach, the energy computed there is always well-approximated by C_3 of the above equation. Together with desired values for closest approach distance, r_{pd}, and inclination, i_d, the energy and velocity direction, $\hat{V}$, can be used to compute the "desired" approach hyperbola and its corresponding point of entry into the sphere of influence, P.

The various parameters of the hyperbola are computed as follows.

v_{he}	$= \sqrt{C_3}$	hyperbolic excess speed
v_p	$= \sqrt{C_3 + 2\mu/r_{pd}}$	closest approach speed
α	$= \tan^{-1}(v_{he} v_p r_{pd}/\mu)$	half-angle between asymptotes
a	$= -\mu/C_3$	semi-major axis
b	$= (r_{pd} - a) \sin\alpha$	asymptotic miss distance
e	$= \sqrt{1 + (b/a)^2}$	eccentricity
p	$= -a\,(b/a)^2$	semi-latus rectum
n	$= \sqrt{\mu/\lvert a\rvert}/\lvert a\rvert$	mean motion
f	$= \cos^{-1}\{(p/66000-1)/e\}$	true anomaly at patch distance
M	$=$ TRMN(1, f, e)	mean anomaly at patch distance
τ	$=$ M/n	time from patch to closest approach

We next calculate the point of entry into the sphere of influence in such a way that the hyperbola has the desired inclination, i_d. We first define the arrival asymptote, S, as the direction of the target-relative velocity at patch, $\hat{V}$. Then, if K is a unit vector normal to the target's equatorial plane at time of closest approach, we can define vectors T and R normal to S as follows.

$$T = S \times K / |S \times K|$$

$$R = T \times S$$

The miss-vector, B, lies in the orbital plane and in the plane of T and R at an angle, θ, measured from T toward R.

$$B = T \cos\theta + R \sin\theta$$

The plane of the hyperbola is defined by a unit vector, H, in the direction of the angular momentum.

$$H = B \times S = R \cos\theta - T \sin\theta$$

The condition that the orbit's inclination is i_d is

$$H \cdot K = \cos i_d = R \cdot K \cos\theta ,$$

which can be solved for θ if $|R \cdot K| \leq |\cos i_d|$. If $|R \cdot K| > |\cos i_d|$, it means that i_d cannot be attained for the S under consideration. In that case, the best that can be done is

$$\cos\theta = 1 \cdot \text{sign}(\cos i_d / R \cdot K).$$

The sign on $\sin\theta$ $(= \pm\sqrt{1 - \cos^2\theta})$ can be chosen to make the miss-vector lie above or below the equatorial intersection in the miss-plane. Having now calculated B, we can form the vector, P, from the target's center toward the point of entry into the sphere of influence.

$$P = S \cos(f + \alpha) + B \sin(f + \alpha)$$

The computations above provide the point of entry of the sphere of influence and the time of passage to closest approach, which then can be used to establish a new aim point for the transfer trajectory.

Guidance Laws

The solution provided by the above process is the fixed time of arrival (FTA) guidance solution. The FTA guidance law constrains flight time, t_f, to closest approach to be a specific value while satisfying the desired end conditions of radius of closest approach and inclination. Other guidance laws of interest relative to the RAE-B mission are:

1. minimum fuel
2. fixed target energy
3. variable target energy

Each of the other guidance laws constrains radius of closest approach and inclination just as the FTA law does, but doesn't specifically constrain flight time. The minimum fuel law embraces the critical plane solution, the fixed target energy law constrains hyperbolic excess speed at the target and the variable target energy law constrains post-retro speed subject to a prescribed de-boost strategy. The solution for each of these laws, however, corresponds to a particular flight time, so flight time is used as the independent variable in seeking a solution for each law.

The MFG law is targeted by means of a Newton-Raphson-type iteration with flight time as the independent variable. The iteration seeks to null the dot product of the difference of two successive midcourse correction impulses with the impulse itself. That is, it seeks to find the flight time for which the magnitude of the correction velocity doesn't change (i.e. is minimum). The condition for minimizing the magnitude of ΔV is

$$\Delta V \cdot \frac{d(\Delta V)}{dt_f} = 0.$$

We define t_n to be the flight time for the n-th trial and ΔV_n to be the impulse for that trial. Then, approximately,

$$\left(\frac{d(\Delta V)}{dt_f}\right)_n = \frac{\Delta V_n - \Delta V_{n-1}}{t_n - t_{n-1}}$$

and, more approximately,

$$\Delta V_{n+1} = \Delta V_n + (t_{n+1} - t_n)\left(\frac{d(\Delta V)}{dt_f}\right)_n .$$

We look for t_{n+1} such that the following equation holds.

$$\Delta V_{n+1} \cdot \left(\frac{d(\Delta V)}{dt_f}\right)_{n+1} = 0.$$

By making liberal use of the stated approximations, the preceding equation may be solved to render the time-step for the next iteration step.

$$t_{n+1} - t_n = -(t_n - t_{n-1}) \frac{\Delta V_n \cdot (\Delta V_n - \Delta V_{n-1})}{|\Delta V_n - \Delta V_{n-1}|^2}$$

The process converges well for all cases tested, provided that the iteration for $\Delta V_n(t_n)$ converges well. The resultant maneuver changes very little with precise targeting, although the corresponding flight time may shift by an hour or two.

The fixed time of arrival guidance law is pre-targeted to 1.015 times the desired flight time. This empirical factor tends to compensate for the difference between patched-conic and integrated-precise lunar transfer trajectory flight times.

The pre-targeting process for the FTE and VTE guidance laws includes a standard Newton-Raphson iteration to null the third constraint by varying flight time. For the FTE law the third constraint error function is

$$\psi_3 = v_{hed} - \sqrt{C_3}$$

while for the VTE law the function is

$$\psi_3 = \sqrt{\mu/r_{pd}} - \sqrt{C_3 + 2\mu/r_{pd}} + \delta v_r$$

where δv_r is the velocity impulse imparted by burning the retro motor. There are usually two flight times for which $\psi_3 = 0$ for the VTE law. The iteration is constrained to find the solution with positive slope -- which is the solution corresponding to the longer flight time. If the minimum fuel solution is characterized by $\psi_3 > 0$ (the overburn situation), it will not be possible to find any VTE solutions. If this is the case, the precise targeting mode will probably not find any solutions either.

3.1.5 Targeting Methods

In the neighborhood of U, variations in U are related to variations in ψ by

$$\delta\psi = (\nabla_u \psi)\, \delta U = G\delta U$$

The generalized Newton-Raphson method is used in the search for U* such that $\psi(U^*) = 0$. If, at the k-th step of the iteration, we compute

$$U_k = U_{k-1} + \delta U$$

$$= U_{k-1} - G_{k-1}^{-1}\, \psi_{k-1}$$

then U_k will tend toward U*. The gradient, $G = \nabla_u \psi$, is re-computed by finite differences (the Secant Method) at each of the first n iterations (n pre-set), then held fixed. To test convergence, the individual elements of ψ_k are tested against pre-set tolerances.

The straightforward targeting method just described is used with the FTA, FTE and VTE laws, although the convergence of the VTE process is aided by certain modifications to G_{k-1} and "boot-strapping" because ψ is an explicit function of U for this law. The MFG and MTF laws are treated as special cases, but are both formulated to use the Newton-Raphson method to obtain minimum-fuel solutions. In the case of the MFG law,

$$U_k^{min} = \left(I - \frac{CC^T}{C^T C}\right) U_k$$

where C is the third column of G_{k-1}^{-1}. G_{k-1} is made invertible by adjoining a row to $\frac{\partial \psi_1}{\partial U}$ and $\frac{\partial \psi_2}{\partial U}$ which is normal to them both; namely, $\frac{\partial \psi_1}{\partial U} \times \frac{\partial \psi_2}{\partial U}$.

The MTF solution is also a constrained minimum. It is obtained by using flight time, T, as the independent variable in a scalar search for minimum ψ_6. That is, the FTA law is used to find a solution for each T, which renders $\psi_6(T)$, $\psi_1 = \psi_2 = 0$. T is stepped away from the MFG solution time until $\psi_6(T_{n-1}) \leq \psi_6(T_n) \leq \psi_6(T_{n+1})$. A parabolic fit is then used to obtain T* for minimum ψ_6. The MTF solution is then found by targeting FTA to T*.

3.1.6 Retro Maneuvers

The retro or de-boost maneuver of the RAE-B mission is required to transfer from a lunar approach trajectory (which is approximately hyperbolic) to a near-circular capture orbit. The retro motor is a solid rocket whose firing direction and ignition time can be controlled, but whose impulse is fixed. The velocity imparted by firing the retro motor depends on the spacecraft's weight and, therefore, on the midcourse fuel expended. This velocity can be more than sufficient to circularize the capture orbit at the desired radius (overburn), although for the RAE-B weights and specific impulses it is expected to be insufficient (underburn). The retro firing strategy (i.e., specification of firing direction and ignition time) has an influence on the midcourse maneuver strategy as well as on trim strategy. We will proceed to discuss various retro strategies and their impact on midcourse and trim requirements.

The objective of mission control for the RAE-B mission is stated here as achievement of a circular orbit of specified radius, r_d, and inclination, i_d. This objective, particularly the inclination part, can best be achieved with a midcourse maneuver. The midcourse maneuver should be targeted to a radius of closest approach of r_d and inclination of i_d for underburns. For the overburn situation, several different retro strategies can be defined to minimize total correction fuel requirements. Each retro strategy influences the midcourse targeting strategy. We now consider two midcourse targeting procedures which are applicable to overburns and involve the retro strategy.

Variable Target Inclination

The VTI procedure is derived in Appendix D. It amounts to defining desired miss vector components, $B \cdot T$ and $B \cdot R$, in such a way that an out-of-plane retro-burn at periapsis of the approach hyperbola can render a circular orbit of the desired radius and inclination. This procedure is applicable only for overburns. The sketch shows the retro velocity impulse, ΔV_r, in the plane of the approach periapsis velocity, V_p,

and the approach angular momentum vector, H.

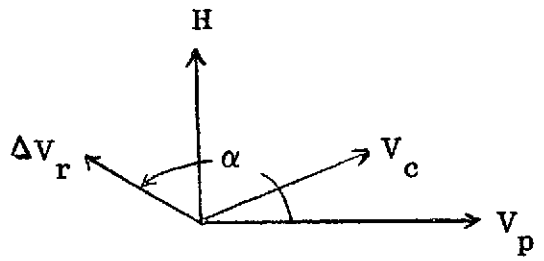

Geometry of the VTI Procedure

The direction of $\hat{\Delta V}_r$ is given by

$$\hat{\Delta V}_r = \hat{V}_p \cos\alpha + \hat{H} \sin\alpha$$

and the new angular momentum vector's direction is

$$\hat{H}' = \hat{H}\cos\beta - \hat{V}_p \sin\beta,$$

The angles, α and β, are defined in the derivation of the VTI procedure as functions of C_3, δ_v, and the desired final orbit radius. The desired miss parameters are computed in such a way that the approach orbit's track differs by β from the desired orbit's track at r_p. If the closest approach and inclination constraint errors are exactly zero, and if the retro-burn is perfect, the post-retro orbit will require no trim.

Variable Approach Distance

The VAD procedure, like the VTI, is applicable only to overburns. The basic idea is to define the desired miss vector magnitude in such a way that if the retro is fired appropriately in-plane at the desired circular orbit radius, r_c, the post-retro orbit will be circular. It is assumed, first of all, that closest approach radius, r_p, of the arrival hyperbola can be varied without significantly changing the arrival energy, C_3, or the retro velocity impulse, δv. Assuming further that r_p is less than the desired circular orbit radius, r_c, we can write

$$V(r_c) = v_r \hat{R}_c + v_\theta \hat{\theta}$$

where v_r is the radial component of velocity and v_θ is the tangential component. The circular post retro velocity is:

$$V_c(r_c) = v_c \hat{\theta}$$

where $v_c = \sqrt{\frac{\mu}{r_c}}$. The required retro impulse, ΔV, is

$$\Delta V = V_c - V = -v_r \hat{R} + (v_c - v_\theta)\hat{\theta}$$

and $$\delta v^2 = v_r^2 + (v_c - v_\theta)^2 = v^2 - 2 v_c v_\theta + v_c^2$$

$$= C_3 + \frac{2\mu}{r_c} - 2\sqrt{\frac{\mu}{r_c}}\ \frac{h}{r_c} + \frac{\mu}{r_c}$$

$$= C_3 + \frac{3\mu}{r_c} - 2\sqrt{\frac{\mu}{r_c}}\ \frac{r_p}{r_c}\ \sqrt{C_3 + \frac{2\mu}{r_p}}$$

The only unknown in the above equation is r_p. We can solve for r_p as follows.

$$C_3 r_p^2 + 2\mu r_p = \left\{\left[\delta v^2 - C_3 - \frac{3\mu}{r_c}\right]\ \frac{r_c}{2 v_c}\right\}^2 = b^2$$

$$r_p = \frac{\sqrt{\mu^2 + C_3 b^2}}{C_3} - \frac{\mu}{C_3}$$

The periapsis constraint error is re-defined for this case as:

PSI (7) = RP - PR.

The desired miss vector magnitude is easily formulated from r_p.

$$BMAG = \left(\frac{\mu}{C_3} + r_p\right) \sin\left(\tan^{-1}\ \frac{v_p v_\infty r_p}{\mu}\right)$$

$$v_p = \sqrt{C_3 + \frac{2\mu}{r_p}}\ , \quad v_\infty = \sqrt{C_3}$$

The true anomaly at which the retro motor is fired is found from

$$\cos\theta = \left(\frac{p}{r_c} - 1\right)/e$$

where the sign of θ is determined by input: if IVTI is positive, θ is negative and vice versa. Defining unit vectors $\hat{P}$ and $\hat{Q}$ along periapsis position and velocity vectors, respectively,

$$\hat{R} = \hat{P} \cos\theta + \hat{Q} \sin\theta$$

$$\hat{\theta} = -\hat{P} \sin\theta + \hat{Q} \cos\theta$$

We define ΔV_r in terms of an out-of-plane angle, α, and a flight path angle, γ.

If the periapsis constraint error is zero, $\alpha = \pi$, and the maneuver will be in-plane. If δv is too large to circularize at r_c for the actual r_p and C_3, the maneuver will be out-of-plane. The direction out-of-plane is chosen to minimize the resultant inclination error. If δv is too small, γ will be chosen so that the radial component of post-retro velocity will be nulled, with the tangential component falling wherever it may as a result.

$$\sin\gamma = -\frac{v_r}{\delta v_r}$$

$$\cos\alpha = \frac{(v_c - v_\theta)}{\delta v_r \cos\gamma}, \text{ or } \alpha = \pi \text{ if } |\cos\alpha| > 1$$

$$\Delta V_r = \delta v_r \left[(\hat{\theta}\cos\alpha + \hat{H}\sin\alpha)\cos\gamma + \hat{R}\sin\gamma\right]$$

It is usually rather inexpensive to change closest approach distance by a few hundred kilometers. In such a change, target-relative energy is also rather invariant. If the final circular orbit radius is not very critical, it may be possible to change the targeted value of closest approach radius so that an in-plane periapsis retro maneuver opposite to the velocity vector can circularize the orbit. This discussion derives the value of r_p to aim for.

Circular Orbit at Arbitrary Radius

Given C_3 and δv, find peri-radius at which periapsis in-plane retro maneuvers render circular orbits.

$$v_c - (v_p - \delta v) = 0 = \sqrt{\frac{\mu}{r_p}} - \sqrt{C_3 + \frac{2\mu}{r_p}} + \delta v = 0$$

$$\left(\sqrt{\frac{\mu}{r_p}} + \delta v\right)^2 = C_3 + \frac{2\mu}{r_p} = \frac{\mu}{r_p} + 2\sqrt{\frac{\mu}{r_p}}\ \delta v + \delta v^2$$

$$2\sqrt{\frac{\mu}{r_p}}\ \delta v = C_3 + \frac{\mu}{r_p} - \delta v^2$$

Finally, after some intermediate algebra,

$$\frac{\mu}{r_p} = \left[\delta v + \sqrt{2\,\delta v^2 - C_3}\right]^2.$$

Approach Retro Strategy

Following the final midcourse maneuver, residual approach errors are expected, due to pre-midcourse navigation errors and midcourse execution errors. Provided that the approach orbit is not expected to impact the Moon, quite a few retro firing options are available. Numerical methods are available within the approach analysis capability of MAESTRO for determining the retro controls to minimize trim requirements, but it is of value to examine and understand certain of the possibilities.

It is believed nearly optimal from trim considerations to correct inclination errors as much as possible with the retro maneuver. The determination of optimal out-of-plane maneuvers is a complicated subject and is not covered here. A retro maneuver to correct residual inclination errors can be easily developed if the maneuver is executed at the node of the approach orbit on the lunar equator. An inclination-correcting maneuver at an arbitrary true anomaly can also be developed quite easily if certain assumptions are made on flight path angle of the maneuver, but will also not be elaborated here.

Retro-maneuvers which are constrained to lie in the plane of the approach trajectory can be much more easily analyzed than are inclination-changing maneuvers. The following discussion treats in-plane circularization at an arbitrary radius using the retro only.

In-plane circularization at an arbitrary radius using the retro only

Given: approach hyperbola (C_3, r_p or equivalently, C_3, h)
retro impulse magnitude, δv

The velocity at radius r is

$$V = v_r \hat{R} + v_\theta \hat{\theta} \qquad (\hat{\theta} \text{ is unit tangential vector})$$

The circular velocity at r is

$$V_c = v_c \hat{\theta}$$

The velocity impulse required to circularize at r is

$$\Delta V_c = V_c - V = -v_r \hat{R} + (v_c - v_\theta)\hat{\theta}$$

$$\delta v_c^2 = v_r^2 + (v_c - v_\theta)^2$$

$$= C_3 + \frac{2\mu}{r} + \frac{\mu}{r} - 2\sqrt{\frac{\mu}{r}}\,\frac{h}{r} \qquad \left(h = r_p\sqrt{C_3 + \frac{2\mu}{r_p}}\right)$$

$$\delta v_c^2 = C_3 + \frac{3\mu}{r} - 2h\sqrt{\frac{\mu}{r^3}}$$

Let us examine the above equation in detail

$$\frac{d\,\delta v_c^2}{dr} = -\frac{3\mu}{r^2} + 3h\sqrt{\frac{\mu}{r^5}} = \frac{3}{r^2}\left(h\sqrt{\frac{\mu}{r}} - \mu\right)$$

$$= \frac{3}{r^2}\left[\sqrt{(r_p^2 C_3 + 2\mu r_p)\left(\frac{\mu}{r}\right)} - \mu\right]$$

At $r = r_p$, the slope is positive, because

$$\sqrt{r_p C_3 \mu + 2\mu^2} - \mu > 0.$$

The slope goes to zero (a maximum of δv_c^2) at

$$r_{max} = \frac{r_p^2 C_3}{\mu} + 2r_p$$

and remains negative (though ever less so) as $r \to \infty$. The limit of δv_c^2 as $r \to \infty$ is C_3. If $r_p C_3 < \frac{\mu}{4}$, the limiting δv_c will be less than $\delta v_c(r_p)$. Otherwise, $\delta v_c(r_p)$ is the lowest value of δv_c. The curve of δv_c^2 vs. r has the general appearance shown in the following sketch.

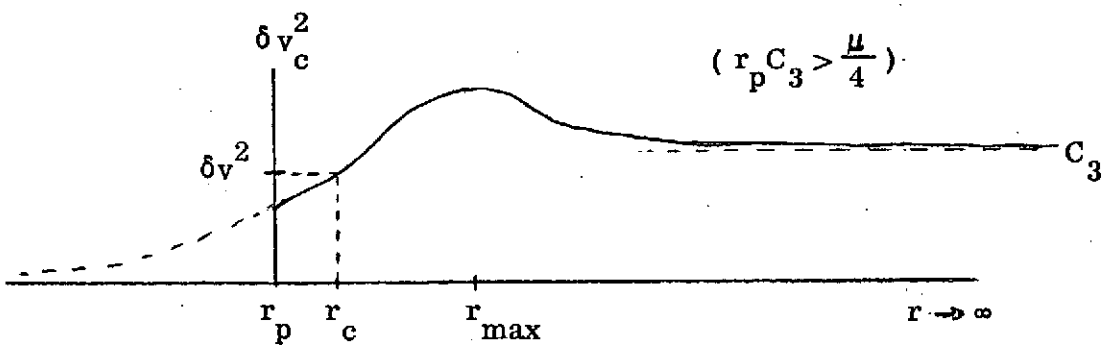

What does all this mean about retro-firing strategy? First of all, it means that if $r_p C_3 > \frac{\mu}{4}$, as is likely for RAE-B following the last midcourse correction, the "cheapest" radius at which to circularize is periapsis. Then, if the available impulse, δv, is greater than $\delta v_c(r_p)$, it is possible to circularize the orbit with the retro alone at some radius, r, $(r > r_p)$. This situation may be called "an overburn at r_p." If δv is also greater than $\sqrt{C_3}$, an additional circular orbit radius may be found $(r > r_{max})$. Of course, either of these circularization situations requires $\delta v < \delta v_c(r_{max})$. If δv is less than $\delta v(r_p)$, the orbit cannot be circularized with the retro alone at any r, but the "most circular" orbit is obtained by firing the retro at periapsis (unproven, but inferred). Even if the orbit can be circularized with retro-fire alone, the radius of the orbit may not be acceptable. Let us denote a desired circular orbit radius by r_d. Let us also consider several cases which might arise. $(C_3 r_p > \frac{\mu}{4})$.

Case 1: $r_p > r_d$

No circularization is possible at r_d.

1a: $\delta v < \delta v_c(r_p)$

No circularization is possible at r_p, but the maneuver at r_p will minimize the required trim.

1b: $\delta v_c(r_p) \le \delta v \le \delta v_c(r_{max})$ (overburn at r_p)

A circular orbit can be obtained at r_c, where $\delta v_c(r_c) = \delta v$. Now, r_c can be

compared with r_d - it may be an acceptable radius. At $r > r_c$, δv represents an underburn at r, while at r in the range $r_p \leq r < r_c$, δv can provide an overburn at r. In the latter case, r is the apoapsis radius of the post-retro orbit and it may be possible to lower post-retro periapsis to r_d; a minimum-trim strategy. It is not possible to lower post-retro periapsis below that which would result from overburning at r_p. These recent statements assume that the post-retro velocity lies entirely in the tangential direction, i.e., along $\hat{\theta}$. It is also possible to give the post-retro velocity an out-of-plane angle and/or a flight path angle, thereby using δv less efficiently and changing the post-retro orbit's shape and orientation.

1c: $\delta v > \delta v_c(r_{max})$

Not likely to occur.

Case 2: $r_p \leq r_d$

Three regions can be identified. The first is when δv is greater than necessary to circularize at r_p. In this case the retro can circularize the orbit at r_c ($r_p < r_c < r_d$). If $\delta v < \delta v_c(r_p)$, the "most circular" place to fire the retro is at r_p. The best place to fire from the criterion of minimizing trim to r_d depends on the opposite apsidal radius, r_a, which is achieved by firing the retro at r_p.

2a: $r_a > r_d$

The best place to fire to minimize trim is r_p since the change of r_a with r has a slope of about 7 for likely RAE-B ranges of C_3, r_p and δv. This slope implies a trim fuel penalty for firing before or after approach periapsis.

2b: $r_a < r_d$

Fire the retro at r such that $r_a = r_d$. This will minimize the trim.

See section 3.3 for more information on retro strategy.

3. 1.7 Lunar Orbit Trim

Once the retro motor has fired, the spacecraft is in lunar orbit. Assuming this orbit to be elliptical with energy C_{3e} and angular momentum h_e, we will proceed to define the trim sequence and the trim fuel cost. The in-plane trim is accomplished with a 2-impulse Hohmann transfer to circular at the desired radius, r_d.

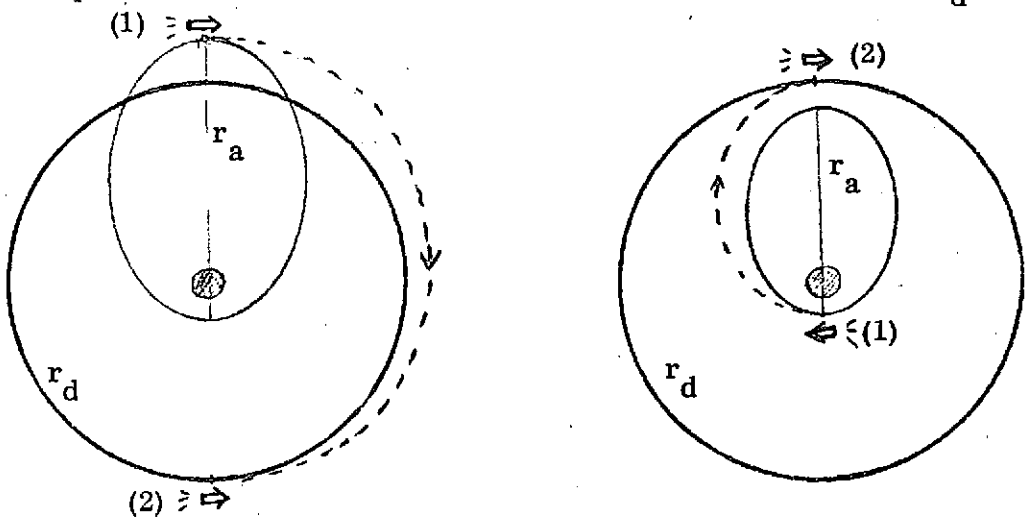

Case 1: $r_a > r_d$ Case 2: $r_a < r_d$

Two-Impulse Hohmann Transfers

The periapsis radius, r_p, and apoapsis radius, r_a, can be defined from C_{3e} and h_e.

$$p = \frac{h^2}{\mu} \qquad \text{semi-latus rectum}$$

$$e = \sqrt{1 + \frac{C_{3e} p}{\mu}} \qquad \text{eccentricity}$$

$$r_p = \frac{p}{1 + e} \qquad \text{periapsis radius}$$

$$r_a = \frac{p}{1 - e} \qquad \text{apoapsis radius}$$

$$a = \frac{r_p + r_a}{2} = -\frac{\mu}{C_{3e}} \qquad \text{semi-major axis}$$

Case 1: $r_a > r_d$

The semi-major axis, a_i, and energy, C_{3i}, of the intermediate orbit must be

$$a_i = \frac{r_a + r_d}{2}$$

and $$C_{3i} = -\frac{\mu}{a_i} = -\frac{2\mu}{r_a + r_d} .$$

The velocity at r_a before the first impulse is

$$v_a^- = \sqrt{C_{3e} + \frac{2\mu}{r_a}} = \sqrt{\frac{2\mu r_p}{r_a(r_a+r_p)}}$$

and after the impulse,

$$v_a^+ = \sqrt{C_{3i} + \frac{2\mu}{r_a}} = \sqrt{\frac{2\mu r_d}{r_a(r_a + r_d)}}$$

so that the first maneuver requires an impulsive velocity

$$\delta v_1 = \sqrt{\frac{2\mu}{r_a}} \left| \sqrt{\frac{r_d}{r_a+r_d}} - \sqrt{\frac{r_p}{r_a + r_p}} \right| .$$

The velocity on the intermediate orbit at r_d is

$$v_d^- = \sqrt{C_{3i} + \frac{2\mu}{r_d}} = \sqrt{\frac{2\mu r_a}{r_d(r_a+r_d)}}$$

while the desired circular velocity is

$$v_d^+ = \sqrt{\frac{\mu}{r_d}}$$

so that the second impulse is

$$\delta v_2 = \sqrt{\frac{\mu}{r_d}} \left| \sqrt{\frac{2 r_a}{r_a + r_d}} - 1 \right|$$

and the total in-plane trim velocity is

$$\delta v = \delta v_1 + \delta v_2 .$$

Case 2: $r_a < r_d$. In this case, it is slightly cheaper to transfer first from r_p to r_d. By a derivation similar to that for case 1, we obtain

$$\delta v_1 = \sqrt{\frac{2\mu}{r_p}} \left| \sqrt{\frac{r_d}{r_p+r_d}} - \sqrt{\frac{r_a}{r_a + r_p}} \right|$$

$$\delta v_2 = \sqrt{\frac{\mu}{r_d}} \left| \sqrt{\frac{2r_p}{r_p+r_d}} - 1 \right|$$

It should be noted that the two cases can be computed with the same equations by interchanging roles between r_a and r_p.

Inclination Change

The inclination is changed by a third impulse executed at the node of the orbit on the equator. The impulse is applied on the intermediate orbit of the in-plane adjustment at the nodal crossing of larger radius. Although this strategy is not usually optimal, it is convenient, it leaves the node invariant, it always permits a solution and it separates out the in-plane and out-of-plane trim costs. Let the larger nodal radius vector (of either the pre-trim or intermediate orbit, actually) be R and its corresponding velocity be V^-. If the inclination is to be changed by δi, the rotated post-impulse velocity, V^+, will be

$$V^+ = \cos \delta i \, V^- + (1-\cos \delta i) \, \hat{R} \cdot V^- \hat{R} + \sin \delta i \, \hat{R} \times V^-$$

and $\delta V_3 = V^+ - V^-$

$$= (\cos \delta i - 1) V^- + (1-\cos \delta i) \, \hat{R} \cdot V^- \hat{R} + \sin \delta i \, \hat{R} \times V^-$$

$$\delta v_3^2 = \left[(1-\cos \delta i)^2 + \sin^2 \delta i\right] \left[V^- \cdot V^- - (\hat{R} \cdot V^-)^2\right]$$

$$= 2 (1-\cos \delta i) \left|\hat{R} \times V^-\right|^2$$

$$= 4 \sin^2 \left(\frac{\delta i}{2}\right) \left|\hat{R} \times V^-\right|^2$$

$$\delta v_3 = 2 \sin \frac{|\delta i|}{2} \left|R \times V^-\right|$$

To roughly estimate the cost of correcting inclination, assume $\left|\hat{R} \times V^-\right| = \sqrt{\frac{\mu}{r_d}}$ and $\sin \frac{\delta i}{2} = \frac{\delta i}{2}$.

$$\delta v \approx \sqrt{\frac{\mu}{r_d}} \, \delta i = 22.94 \left(\frac{m}{sec} / \text{deg}\right) \delta i^o$$

The fuel cost is computed with the rocket equation

$$\delta v = \delta v_1 + \delta v_2 + \delta v_3$$

$$\delta w = w_0 \left(1 - e^{-\frac{\delta v}{c}}\right)$$

The weight before trim is w_0 and the characteristic velocity (gI_{sp}) of the trim motor is c.

3.2 Operational Strategy

The capability of MAESTRO's midcourse guidance package enables the Flight Director to design maneuvers enhancing the probability of mission success. This section is intended to describe how one might best use the program to answer the midcourse correction questions.

3.2.1 Mission Success Criteria

The primary criterion for mission success (from a guidance point of view) is whether enough correction fuel is available to place the spacecraft in a circular lunar orbit at the right altitude and inclination. The solution is constrained to a specific range of allowable angles between the Sun-direction and the spin-axis direction at any maneuver time and is also constrained to insure tracking visibility everywhere in the vicinity of the maneuvers.

3.2.2 Operational Procedures

The procedures for real-time selection and determination of RAE-B's midcourse correction maneuvers will now be described. Figure 3.1 illustrates the order in which the program's various operational modes can be utilized to select a suitable maneuver. The first step shown in the figure is propagation of the anchor vector to closest approach to the Moon and determination of trim requirements. This can be done by invoking the trajectory propagation (MODE = 0) and approach analysis (MODE = 2) modes. Alternatively, this step can be taken by running the midcourse analysis (MODE = 3) mode, since the first printout from the midcourse analysis describes arrival conditions and approximate trim requirements for the no-midcourse trajectory. The second step is to run a minimum-fuel guidance (MFG) scan for a range of allowable midcourse ignition times. This scan will determine total correction fuel requirements, spin-axis/Sun angle and visibility for midcourse and retro maneuvers for the MFG law. The maneuver will probably be selected from the FTA-law scan, presuming that arrival time was selected for best visibility, but the MFG scan is useful in ascertaining primary mission success attainability. The primary criterion for mission success is required-vs.-available correction fuel, and if the mission objectives cannot be achieved under the MFG law, there is little chance they could be achieved under a different law. The midcourse analysis capability does not include a facility for studying alternate mission possibilities, although marginal opportunities may be enhanced by varying targeting and retro-strategy parameters which are specified by input. Assuming that the available correction fuel supply is more than sufficient to achieve the desired orbit under the MFG law in an attainable range of midcourse ignition times, the next step (3a in the figure) can be taken.

Scanning runs under the fixed-time-of-arrival (FTA) and variable-target-energy (VTE) laws will obtain the penalties in fuel and penalties or advantages in Sun angle and maneuver visibility of imposing arrival constraints. If the fuel cost is acceptable and the Sun angle constraint is not violated, the FTA law would seem to render the most likely candidate maneuver from visibility considerations, assuming the correction is targeted to the nominal arrival time. If a fairly-large midcourse maneuver is

Figure 3.1

Operational Strategy Diagram

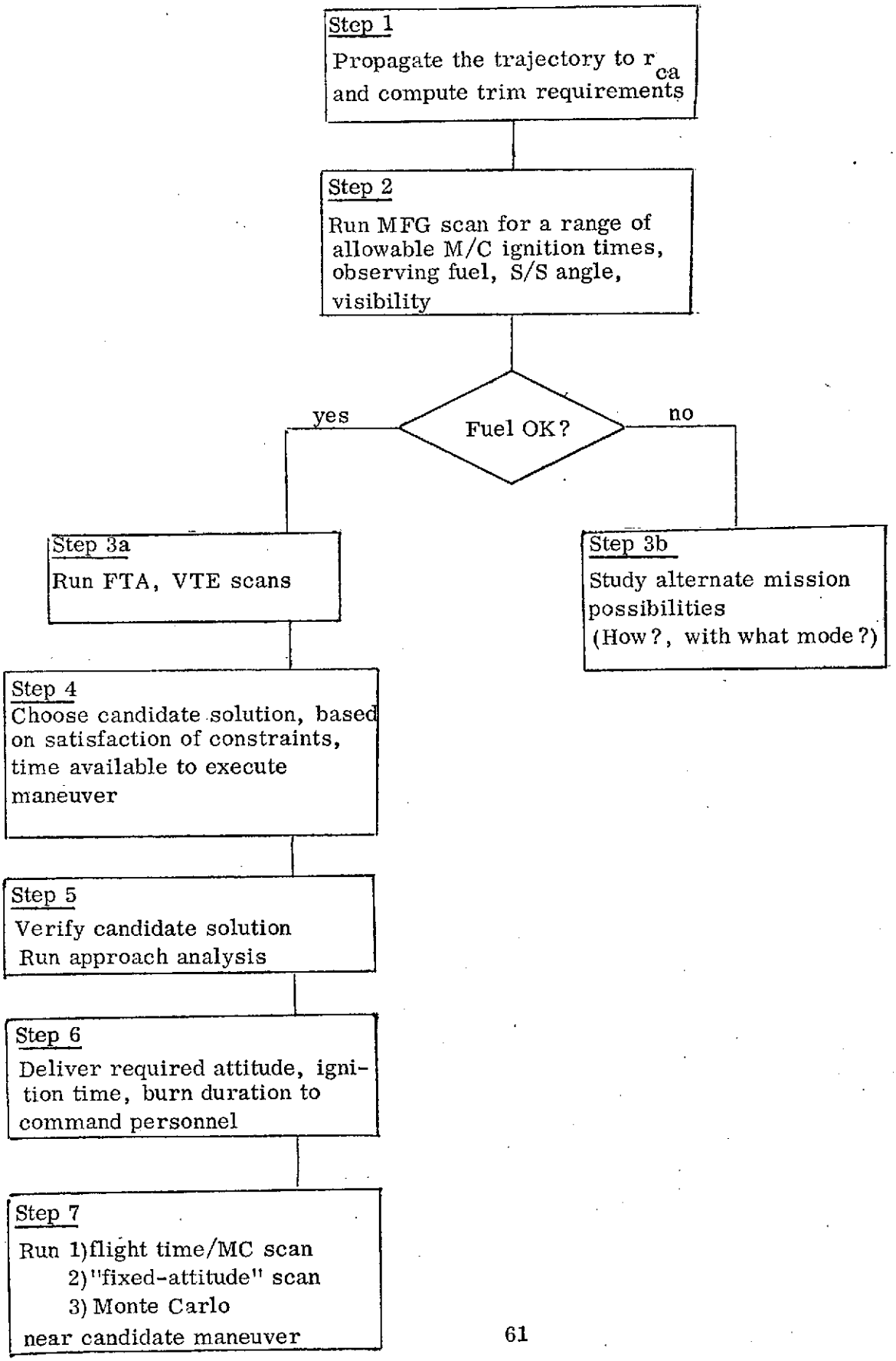

required for the MFG and FTA solutions, the VTE solution can be obtained without much penalty in fuel or visibility. This solution has the advantage of circularizing the lunar orbit with the retro-burn alone if the midcourse and retro burns are accurate enough. By eliminating a major trim maneuver, greater reliability should be achieved. There seems to be no advantage to scanning the requirements for the fixed-target-energy (FTE) law and very little advantage in the minimum-total-fuel (MTF) law for the real-time midcourse analysis of the RAE-B mission.

The choice of a suitable midcourse correction maneuver must be made by the Flight Director, who makes his decision based on the information provided him. If only a small correction is required, he may somewhat arbitrarily choose a late maneuver and perform more analysis in the ample time left before the maneuver is to be executed. If a marginally-large correction is required, it will usually be advantageous to execute the first midcourse correction as early as possible. In this case, extensive analysis may have to coincide with or follow transmission of the maneuver command.

The selected maneuver should be re-targeted with as much precision as is available in trajectory propagation to ascertain the specific values of burn time and attitude to be commanded. Once a suitable maneuver has been selected, the midcourse verification (MODE = 5) and approach analysis (MODE = 1) modes may be invoked to study the solution. Further midcourse guidance analysis (MODE = 3) capabilities are available, also, for illuminating characteristics of the solution. By scanning flight times (FTA) as well as midcourse ignition times, the Flight Director can gain an understanding of how the selected maneuver fits into the set of possible maneuvers and how variations in flight time or ignition time influence fuel requirements and Sun angle behavior. The "fixed-attitude" scan enables the effects of execution errors to be determined. Under this option, the program automatically varies midcourse correction velocity and/or right ascension and declination of the thrusting axis over specified ranges at each midcourse ignition time. The output includes radius of closest approach, inclination, flight time and total correction fuel, enabling a determination of execution error effects on these quantities. This option also enables an understanding of penalties for incomplete attitude control which may drive the spin-axis to an attitude near-but-not-at the attitude required for a perfect correction.

The Monte Carlo (MODE = 4) capability can be utilized to assure the Flight Director that if he can believe the input tracking and execution error statistics, the success of the mission is assured. If the Monte Carlo run indicates low success probability, the assumed error statistics must be reduced.

3.2.3 Run Setups

A great many of the program option keys can be set up before the flight and run in blocks according to the operational procedure being followed. The launch epoch, anchor epoch and anchor vector must be provided in any case, as must also the attitude, weight and thrusting information. As for the remaining inputs, many of the inputs peculiar to midcourse guidance analysis are invariant with chosen procedure or guidance law and will be provided in Block Data. Library files containing the inputs peculiar to each procedure step should be set up before launch to enable rapid turn around of midcourse guidance information. It is the purpose of this paragraph to define such files.

File 1: Epochs, anchor vector, attitude, weights, thrust tables

File 2: Standard midcourse settings

File 3: Settings for a step of the midcourse procedure

Figure 3.2 Input data stack

Standard settings for midcourse analysis

Table 3.1. contains those settings for midcourse analysis which would be invariant between procedure steps.

Table 3.1

Standard Midcourse Settings

410-419	OBSLON	***	Tracker longitudes (deg)
420	PSID(1)	2838.	Radius of closest approach for targeting (km)
421	PSID(2)	121.	Selenographic inclination for targeting (km)
422	PSID(3)	414000.	Nominal flight time from launch (sec)
423	PSID(4)	.62	Nominal C_3 at lunar arrival (km^2/ sec^2)
424	PSID(5)	0.	Desired circular excess speed (km/sec)
435	SIGATM	.5	Expected midcourse attitude error (deg)
436	SIGDVM	.01	Expected midcourse proportional error (fraction)

440	TMC2	259200.	Second midcourse time from launch (sec)
444	RO	2838.	Desired lunar orbit radius (km)
446	CIO	121.	Desired selenocentric orbit radius (deg)
449	TRINC	0.	Inclination trim tolerance (deg)
475	TRUE	20.	True anomaly range for retro firing (deg)
480-89	OBSLAT	***	Tracker latitudes (deg)
490	TOL(1)	10.	Tolerance on B·T (km)
491	TOL(2)	10.	Tolerance on B·R (km)
492	TOL(3)	10.	Tolerance on flight time (sec)
493	TOL(4)	.0001	Tolerance on hyperbolic excess speed (km/sec)
494	TOL(5)	.0001	Tolerance on circular excess speed (km/sec)
495	TOL(6)	.02	Tolerance on total fuel (kg)
496	TOL(7)	5.	Tolerance on closest approach radius (km)
497	TOL(8)	.2	Tolerance on approach inclination (deg)
1036	KMETH	6	Trajectory computation method for analysis
1044	MODE	3	Midcourse analysis mode key
1050	MCOUT	0	Extra output key for midcourse analysis
1058	KOUT9	9	Auxiliary unit number (logical for scope)
1061	MCUNIT	11	Auxiliary unit number for temporary storage
1062	IBTR	2	Selector for targeting to radius and inclination
1064	NGROPT	1	Number of trials to re-compute the gradient
1065	NT	10	Maximum trials for targeting
1066	JET	1	Preliminary targeting key
1067	MCLIM	100	Limit on step-size for targeting
1070	IPROB	0	Probability for linear propagation (%)
1071	IBURN	6	Midcourse burn method key
1075	KMETHP	6	Initial integration method for targeting
1077	KTF	0	Scan procedure key
1078	IVTI	2	Variable target approach key (set for in-plane)
1080	NORMIN	0	Retro maneuver optimization key
1093	KPLOT	0	Plot key for scanning modes

Minimum Fuel Guidance Scan

The first run should be a broad scan of MFG requirements near anchor epoch to establish the general scope of midcourse and retro requirements. Table 3.2 presents the parameters which must be considered for this step, together with appropriate values for them.

Table 3.2

Minimum Fuel Scan Step Inputs

434	DELTMC	18000.	Step-size for scanning ignition times (sec)
478	TMC	18000.	First midcourse ignition time (sec)
1051	JMC	9	Number of ignition times to consider
1063	KGLAW	1	Guidance law indicator (MFG)

The results of this scanning run will be total correction fuel, spin-axis/Sun angle and tracking station visibility versus midcourse ignition time for the minimum midcourse fuel solution. Answers will be computed with the multi-conic trajectory propagator and other simplifying assumptions, but will indicate the midcourse guidance requirements and choices. The first trial midcourse time of 5 hours may be too early to be achievable, considering anchor epoch and attitude-change and attitude determination time requirements. This run will hopefully reveal one or more ignition time regions in which a properly executed midcourse correction burn will render a good trajectory for total achievement of mission objectives. Violation of Sun angle constraints can usually be averted and poor visibility can be corrected or even accepted if necessary, but total fuel requirements are really the indicator of mission success achievability. If every ignition time of the scan required (for the MFG law) more than the available fuel, an evaluation of alternate mission possibilities should be immediately undertaken.

The standard setting for overburn retro-strategy (IVTI, location 1078) is 2. This setting obtains the in-plane pre-pericynthion firing strategy which circularizes the orbit with the retro-burn at the final desired radius. Other values for retro Sun angle and visibility can be obtained with settings of -2., 1. and -1. Required midcourse fuel will vary only slightly with changes in the setting of IVTI and there is no difference in the solution unless the overburn situation is encountered (midcourse correction fuel

requirement is greater than about 16 kilograms). It is not known at this time which of the overburn retro firing strategies is preferable.

Other Guidance Law Scans

If the MFG scan indicates satisfactory fuel requirements for a range of ignition times, that range should then be scanned for FTA and VTE solutions. The fixed time of arrival run should be targeted to the nominal flight time to satisfy visibility constraints. The VTE law should be targeted only in the range for which the MFG solution is an underburn (δv less than about 16 kg). The following tables are set up for a case in which the MFG solution has a small δv over the entire range of ignition times. The simplifying assumptions of the MFG scan are retained through this step. The FTA and VTE cases can be stacked.

Table 3.3a

Fixed Time of Arrival Scan Step Inputs

422	PSID(3)	414000.	Desired flight time (seconds from launch)
434	DELTMC	18000.	Step-size for scanning ignition times (sec)
478	TMC	18000.	First midcourse ignition time (sec)
1051	JMC	9	Number of ignition times to consider
1063	KGLAW	2	Guidance law indicator (FTA)

Table 3.3b

Variable Target Energy Scan Step Inputs

424	PSID(5)	0.	Desired circular excess speed (km/sec)
434	DELTMC	18000.	Step-size for scanning ignition time, (sec)
478	TMC	18000.	First midcourse ignition time (sec)
1051	JMC	9	Number of ignition times to consider
1063	KGLAW	4	Guidance law indicator (VTE)

Verification of Candidate Maneuver

After the Flight Director has chosen a candidate ignition time range, guidance law and retro firing strategy from the MFG, FTA and VTE scanning steps, he should scan ignition times in a smaller localized range and then re-target the particular solution without the simplifying assumptions used in the broader scan.
This run defines the ignition time, burn duration and spin-axis attitude for commanding the maneuver.

Table 3.4

Verification Targeting Step Inputs

422	PSID(3)	414000.*	Desired flight time (sec)
434	DELTMC	3600.	Step-size for scanning ignition times (sec)
478	TMC	50400.*	First midcourse ignition time (sec)
492	TOL(3)	1.	Flight time tolerance (sec)
496	TOL(7)	1.	Closest approach tolerance (km)
497	TOL(8)	.01	Inclination tolerance (deg)
1014	KINT	5	Numerical integration scheme key
1029	KOBL	1	Lunar oblateness key
1036	KMETH	4	Trajectory propagation method
1051	JMC	3	Number of ignition times to consider
1063	KGLAW	2*	Guidance law indicator
1070	KPROB	99	Probability level for linear error propagation (%)
1071	IBURN	1	Midcourse burn method

* assumed characteristics of the selected maneuver

The linear error propagation should really be run with the multiconic trajectory generator rather than in this step, but should not be run in a broad scanning step either. The selected maneuver should be used to initiate a run in the midcourse verification and approach analysis modes.

Flight Time Scan

The flight time scan step will illuminate the nature of the solution relative to neighboring solutions. It would be better to run this scan before selecting the candidate solution if there is time to study the results before having to supply commands. An auxiliary data tape will be written as a step in generation of hard-copy plots of the scan results.

Table 3.5

Flight Time Scan Step Inputs

422	PSID(3)	396000.*	Initial desired flight time (sec)
434	DELTMC	3600.	Step-size for scanning ignition times (sec)
478	TMC	50400.*	First midcourse time (sec)
1050	MCOUT	1	Extra output key
1051	JMC	3	Number of ignition times to consider
1063	KGLAW	2	Guidance law indicator (FTA)
1077	KTF	10	Number of one-hour flight time steps
1093	NPLOT	21	Plot indicator and tape unit number

* assumed characteristics of the selected maneuver

This case will scan flight times from 110^h to 120^h in one-hour steps while varying ignition times between 14^h and 16^h in one-hour steps. Submittal of the plot-run should follow examination of the data.

Execution Variation Scan

The execution variation scan can provide bounds on performance by perturbing the midcourse maneuver about its commanded value. The varied parameters (in order of most-rapid variation) are: 1. declination, 2. right ascension, 3. velocity impulse and 4. ignition time.

Table 3.6

Execution Variation Scan Step Inputs

47	RAI	50.68*	Desired right ascension of spin-axis (deg)
48	DECI	43.34*	Desired declination of spin-axis (deg)
426	PSID(7)	.03807*	Initial velocity impulse (km/sec)
434	DELTMC	36.	Ignition time scan-step (sec)
474	CONE	1.	Attitude scan-step (deg)
478	TMC	53964.*	Initial ignition time (sec)
479	DINK	.001	Velocity impulse step-size (km/sec)
1041	JRA	3	Number of right ascension steps
1042	JDEC	3	Number of declination steps
1051	JMC	3	Number of ignition times to scan
1077	KTF	-3	Number of velocity impulse steps (negative)
1080	NORMIN	2	Inclination-trim option key

The variations shown in this table ($.01^h$, 1^o, $1\ ^m$/sec) are set to convenient values for interpolation, but could be set to 3σ values to examine worst-case performance. After examination of the results of this run, the Monte Carlo option can be invoked to investigate statistically the effects of navigation errors as well as errors in the velocity impulse and attitude.

3.3 Experimental Results

MAESTRO's midcourse guidance capability has been tested relative to two launch opportunities (April 14, 1973 and June 10, 1973) using simulated anchor epochs and anchor vectors. The results of these tests are presented here to illustrate trends and are not to be regarded as quantitative results.

3.3.1 Flight/Ignition Time Scans

The option for scanning flight times with the fixed time of arrival (FTA) guidance law was used to generate midcourse maneuver requirements at each of several midcourse ignition times. Each maneuver is targeted to the same radius of closest approach and inclination.

Figure 3.2 shows total fuel (i.e., midcourse plus trim) requirements for the nominal April 14 trajectory. This figure shows 9 v-shaped curves. The uppermost of these curves describes total fuel for a midcourse maneuver executed two hours after epoch, with the other curves spaced at two-hour intervals thereafter. These curves focus toward a point at 115.3^{h} flight time and 6.3 kg total fuel. This total fuel requirement is used entirely for trim, since no midcourse maneuver is needed for any candidate maneuver time when guiding FTA to the nominal arrival time. The minimum fuel guidance (MFG) law solutions for these same maneuver ignition times are all characterized by negligible midcourse maneuvers, 115.3^{h} flight times and 6.3 kg total fuel. The figure shows the total fuel penalty for midcourse targeting to flight times away from the nominal.

Figure 3.3 shows the total fuel requirements for the April 14 opportunity when injection velocity is $10^{m}/s$ "hotter" than the nominal. The two-hour correction is represented by the curve with the lowest minimum. The minimum total fuel for this ignition time is about 8.4 kg and the minimum fuel increases with ignition time to about 13.8 kg for the 18-hour correction. It may also be observed that the minima occur at flight

Figure 3.2

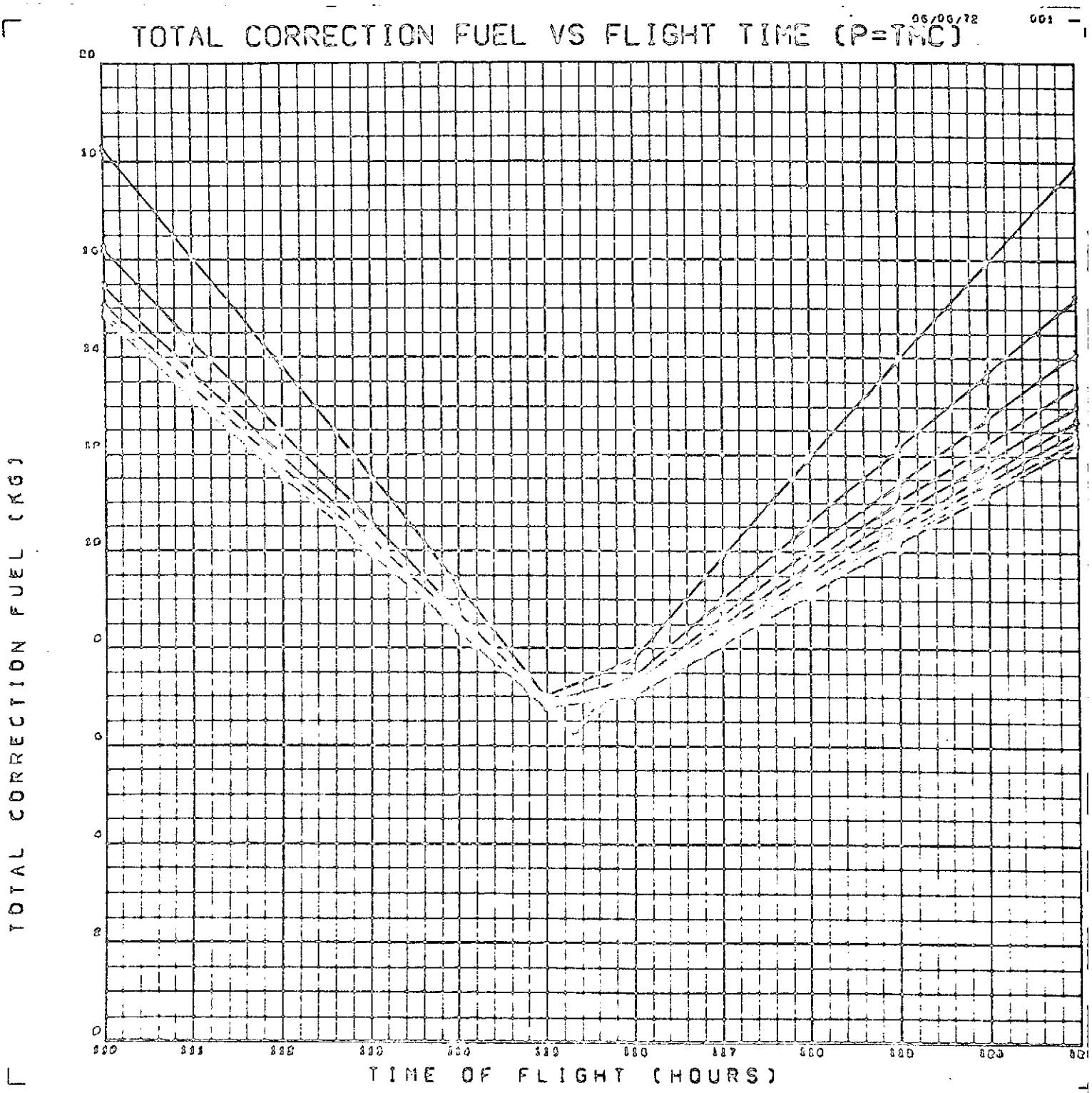
TOTAL CORRECTION FUEL VS FLIGHT TIME (P=TMC)
06/06/72
001
TOTAL CORRECTION FUEL (KG)
TIME OF FLIGHT (HOURS)

Figure 3.3

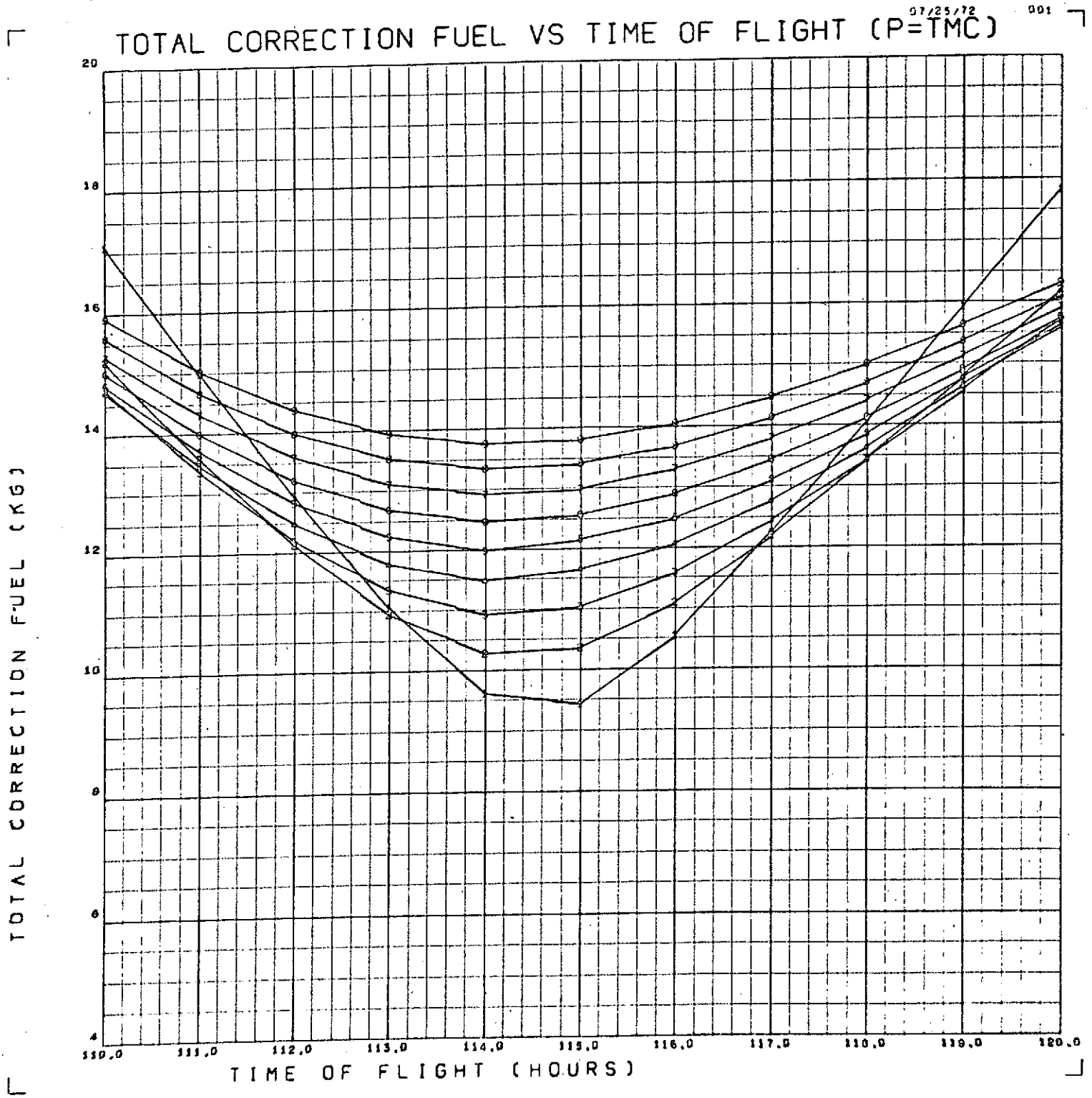
TOTAL CORRECTION FUEL VS TIME OF FLIGHT (P=TMC)
07/25/72
001
TOTAL CORRECTION FUEL (KG)
20
18
16
14
12
10
8
6
4
110.0
111.0
112.0
113.0
114.0
115.0
116.0
117.0
118.0
119.0
120.0
TIME OF FLIGHT (HOURS)

times slightly shorter than the nominal, a fact which correlates well with the fact of a "hot" trajectory.

Figure 3.4 displays the same data as figure 3.3, although the two figures have vastly different appearances. Figure 3.4 is a contour plot which presents contours of equal total fuel in the plane of flight time and midcourse ignition time. The contour of least total fuel shown in the figure is the one at the bottom. This is the contour of 10 kg total fuel. Its irregularity is due to granularity of the data and to shortcomings of the contouring and plotting algorithms. The contour lines are separated by 1 kg in total fuel. The region of allowable flight times and midcourse ignition times would be bounded by the contour of maximum-allowable total fuel.

Figure 3.5 shows still another way of presenting the data of figure 3.3 . In this figure, total fuel is plotted against midcourse ignition time. Each curve represents the fuel requirements for a particular flight time, targeted with the FTA law. The uppermost curve is for 120^h flight time, the next highest for 110^h. The lowest two curves are for 114^h and 115^h. These lowest curves indicate the total fuel penalty for delaying the minimum-fuel midcourse maneuver.

Figure 3.6 displays the required spin-axis orientations for midcourse maneuvers on the "hot" April 14 trajectory. Each curve is for a single midcourse maneuver time and is generated by connecting points of different flight times. The obviously out-of-place lines from the uppermost curve are plotting errors and should be ignored. The uppermost curve is for the two-hour correction. The curves begin at the upper-right corner of the plot, where flight time is 110^h, and proceed toward the lower-left, where flight time is 120^h. Curvature of the curves is exaggerated, due to plotting declination versus right ascension, but the path on the celestial sphere still differs somewhat from a great circle. The dot at about (20^o, 10^o) is the direction of the Sun at midcourse time (it moves only about $.5^o$ over the 16-hour span of midcourse times). The line drawn nearly perpendicular to the family of curves shows how midcourse spin-axis orientation varies with midcourse time for a 115^h FTA correction (which is nearly the MFG correction for this trajectory).

Figure 3.4

07/25/72 002

TOTAL CORRECTION FUEL CONTOURS

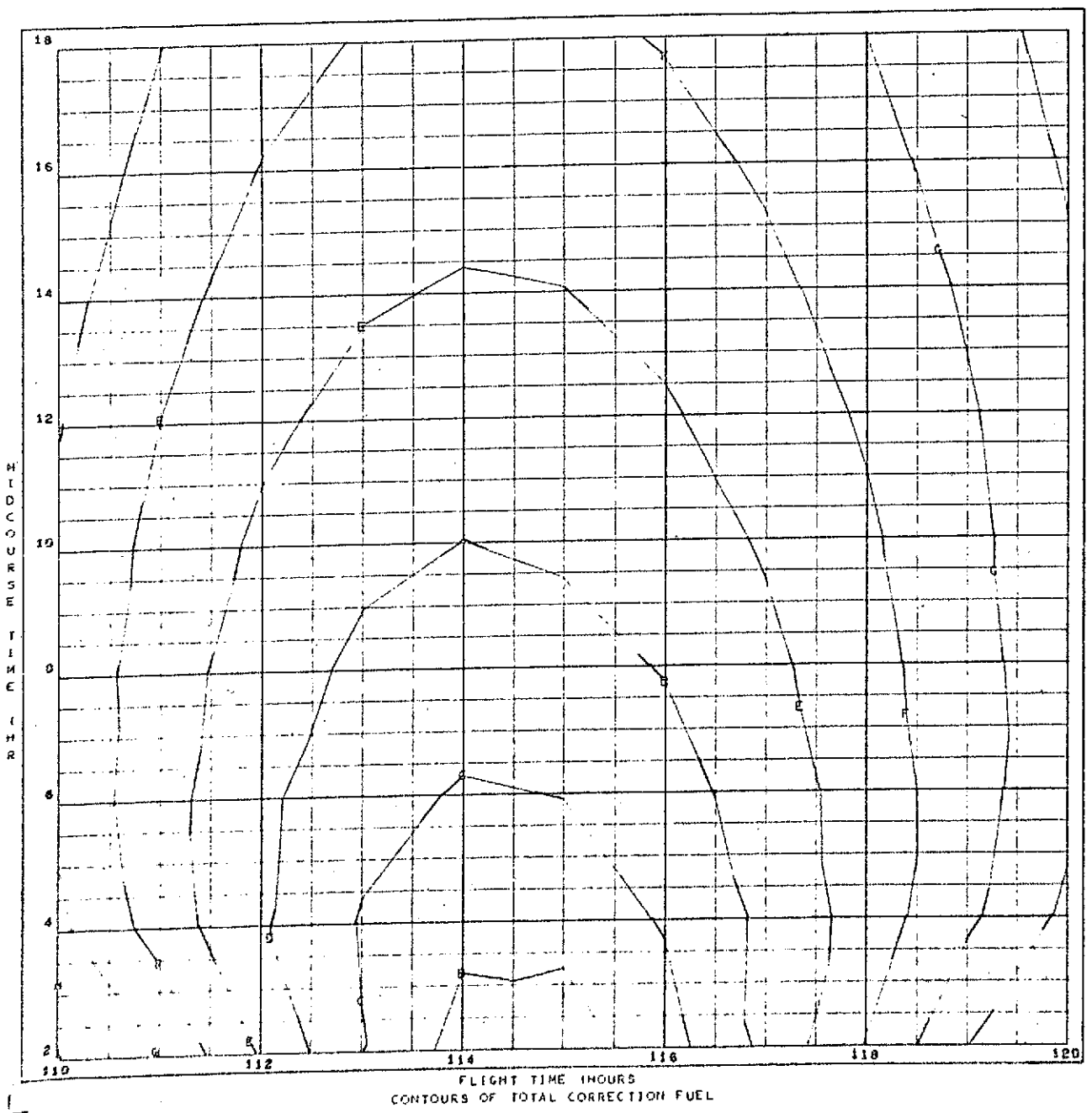

CONTOUR IDENT.	
1	0.00000x10**00
2	1.00000
3	2.00000
4	3.00000
5	4.00000
6	5.00000
7	6.00000
8	7.00000
9	8.00000
A	9.00000
B	10.00000
C	11.00000
D	12.00000
E	13.00000
F	14.00000
G	15.00000
H	16.00000
I	17.00000
J	18.00000
K	19.00000
L	20.00000
M	21.00000
N	22.00000
O	23.00000
P	24.00000
Q	25.00000
R	26.00000
S	27.00000
T	28.00000
U	29.00000
V	30.00000
W	31.00000
X	32.00000
Y	33.00000
Z	34.00000
*	35.00000

Figure 3.5

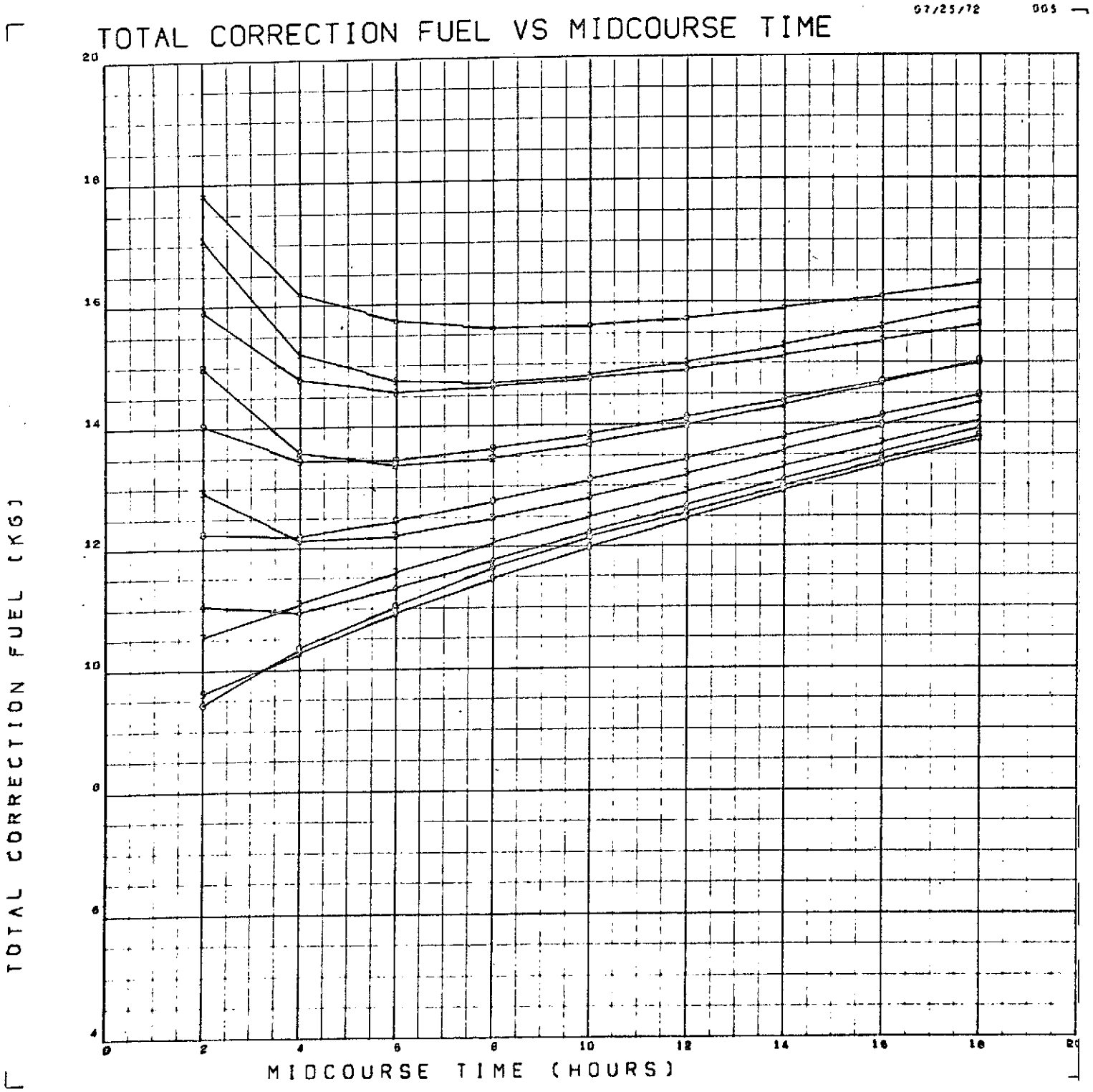
07/25/72 005
TOTAL CORRECTION FUEL VS MIDCOURSE TIME
TOTAL CORRECTION FUEL (KG)
MIDCOURSE TIME (HOURS)
20
18
16
14
12
10
8
6
4
0
2
4
6
8
10
12
14
16
18

Figure 3.6

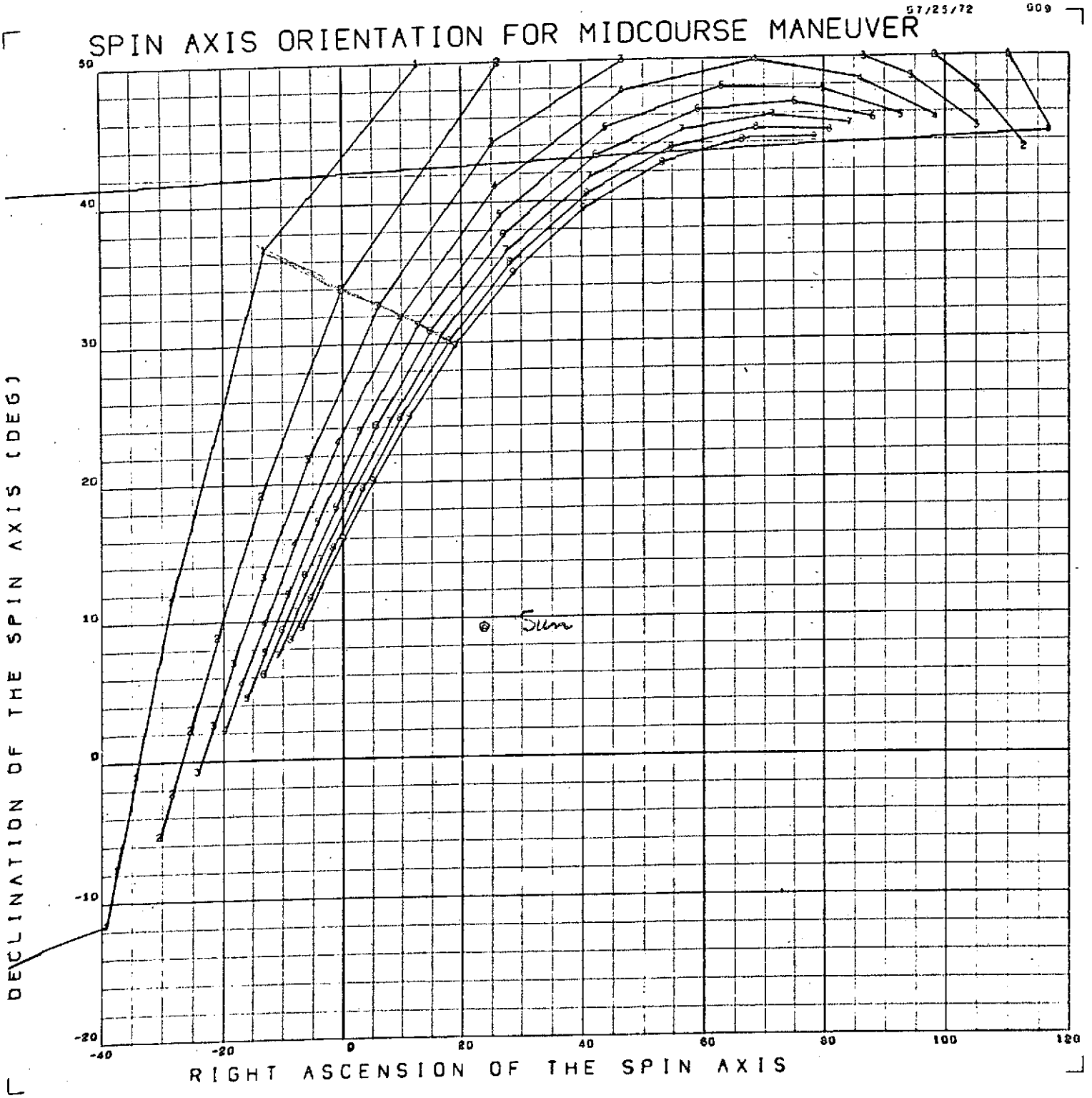
SPIN AXIS ORIENTATION FOR MIDCOURSE MANEUVER
07/25/72
009
DECLINATION OF THE SPIN AXIS (DEG)
50
40
30
20
10
0
-10
-20
-40
-20
0
20
40
60
80
100
120
RIGHT ASCENSION OF THE SPIN AXIS

Figure 3.7 shows spin-axis/Sun angle plotted against flight time, again for each of a span of midcourse ignition times. The figure shows the distance of the points of the curves of figure 3.6 from the Sun-direction in that figure. The uppermost curve is for the 2-hour correction maneuver.

Figure 3.8 shows contours of constant spin-axis/Sun angle in the plane of flight time and midcourse ignition time. This is another way of presenting the data shown in figure 3.7. The lowest contour shown is the small v-shaped one at the top of the figure. It represents a spin-axis/Sun angle of 20^{o}. Successive contours are separated by 5^{o}.

Figure 3.9 presents the spin-axis/Sun angle information of the previous two figures, but plots it against midcourse time in curves of constant flight time. The uppermost curve is for a 110^{h} flight time and the next-highest for a 111^{h} flight time. The curves get generally lower to the 115^{h} flight time curve and then climb again. The lowness of the 115^{h} curve shows that the minimum fuel correction has about the smallest spin-axis/Sun angle and especially so for later midcourse ignition times (for this case).

Figure 3.10 is the same type of plot as figure 3.6, but presents spin-axis orientation requirements for the April 14 "cold" trajectory whose injection velocity is 10 $^{m}/s$ below nominal. The curves are almost reflections of the curves of figure 3.6 about the 0^{o}-declination axis. The orientations of short flight times appear at the lower-right part of the figure and the curves focus toward the upper left as flight time increases. The lowest curve is for the 2^{h} correction time.

Figure 3.11 is plot of total fuel versus midcourse fuel for the April 14 "hot" trajectory. Each sloping v-shaped curve is generated by scanning flight times for a particular midcourse execution time. The upper-left point of each curve is for 110^{h} flight time and the right-most point is for 120^{h}. The skinniest and longest curve in the center of the bunch is for the 2^{h} midcourse time. The plot shows that the slope of total fuel to midcourse fuel changes on either side of the minimum fuel solution. It also shows that the minimum total fuel solution is very nearly the same as the minimum midcourse fuel solution. Other test results (see Progress Report for June, 1972), show that these curves focus into a straight line at the overburn point which begins at about 16 kg of midcourse fuel expenditure. If a circularizing-retro overburn procedure such as

Figure 3.7

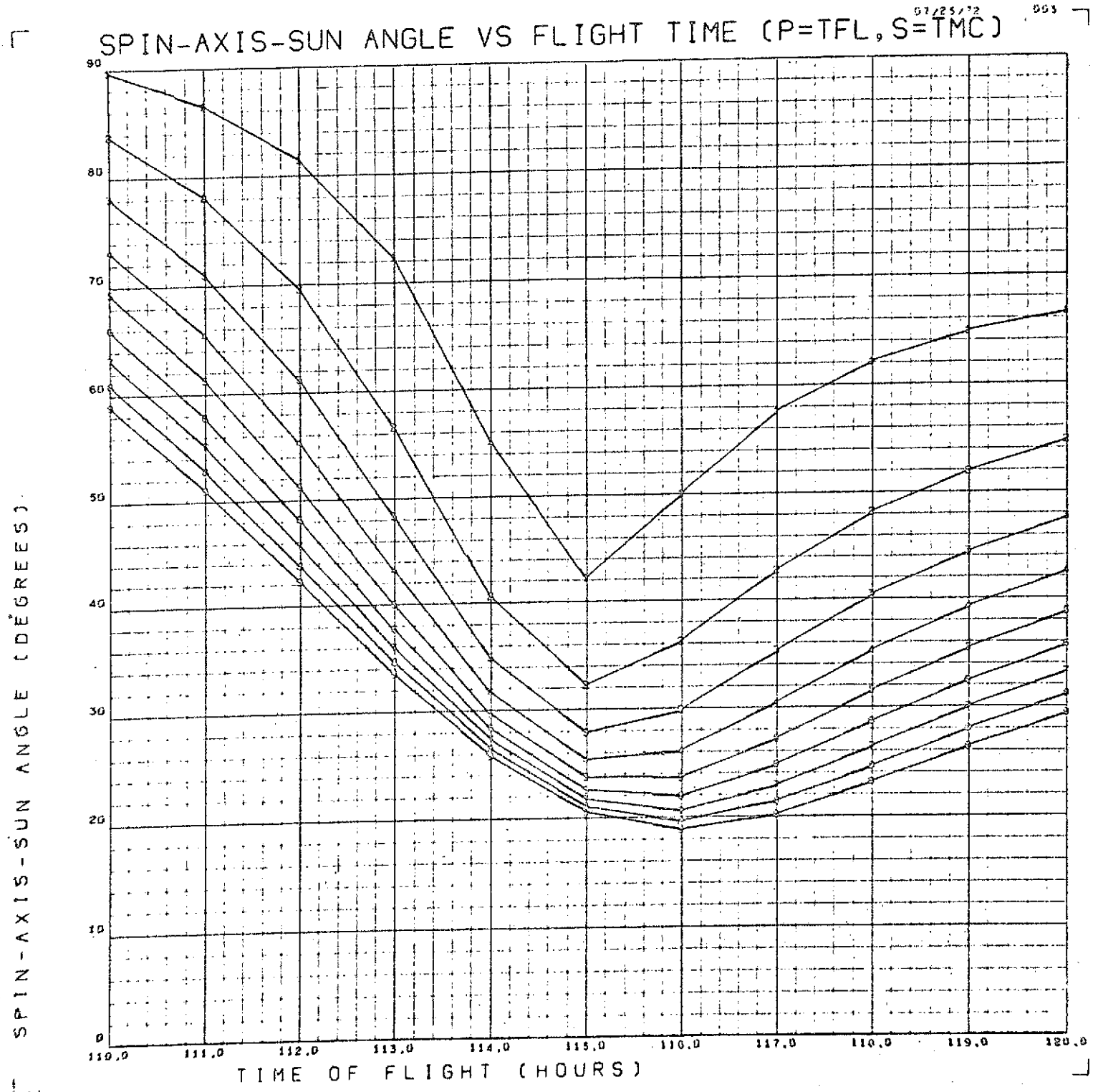
SPIN-AXIS-SUN ANGLE VS FLIGHT TIME (P=TFL, S=TMC)
07/25/72
003
SPIN-AXIS-SUN ANGLE (DEGREES)
90
80
70
60
50
40
30
20
10
0
110.0
111.0
112.0
113.0
114.0
115.0
116.0
117.0
118.0
119.0
120.0
TIME OF FLIGHT (HOURS)

Figure 3.8

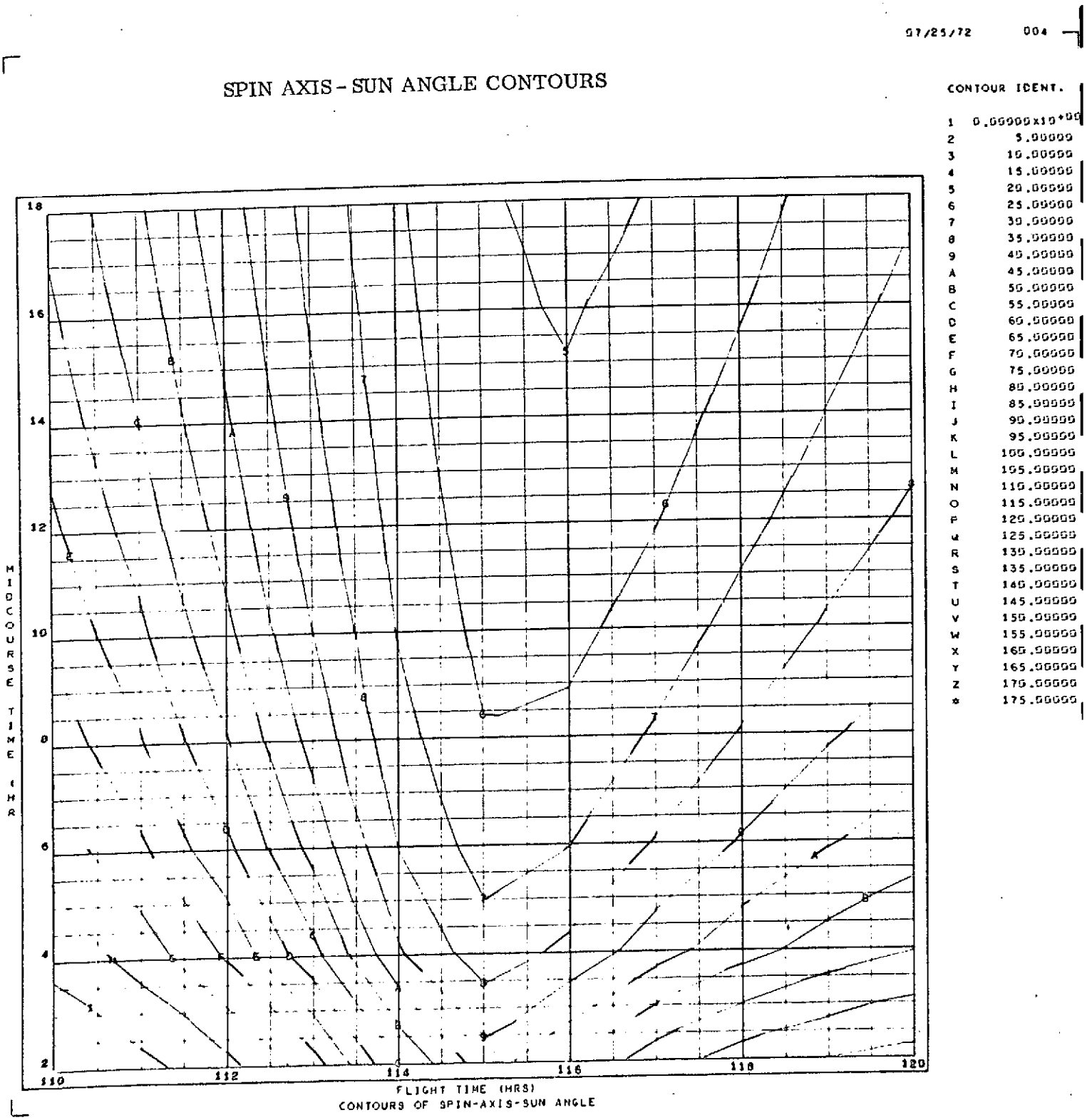
07/25/72 004
SPIN AXIS - SUN ANGLE CONTOURS
CONTOUR IDENT.
1 0.00000x10**00
2 5.00000
3 10.00000
4 15.00000
5 20.00000
6 25.00000
7 30.00000
8 35.00000
9 40.00000
A 45.00000
B 50.00000
C 55.00000
D 60.00000
E 65.00000
F 70.00000
G 75.00000
H 80.00000
I 85.00000
J 90.00000
K 95.00000
L 100.00000
M 105.00000
N 110.00000
O 115.00000
P 120.00000
Q 125.00000
R 130.00000
S 135.00000
T 140.00000
U 145.00000
V 150.00000
W 155.00000
X 160.00000
Y 165.00000
Z 170.00000
* 175.00000
MIDCOURSE TIME (HR
18
16
14
12
10
8
6
4
2
110
112
114
116
118
120
FLIGHT TIME (HRS)
CONTOURS OF SPIN-AXIS-SUN ANGLE

Figure 3.9

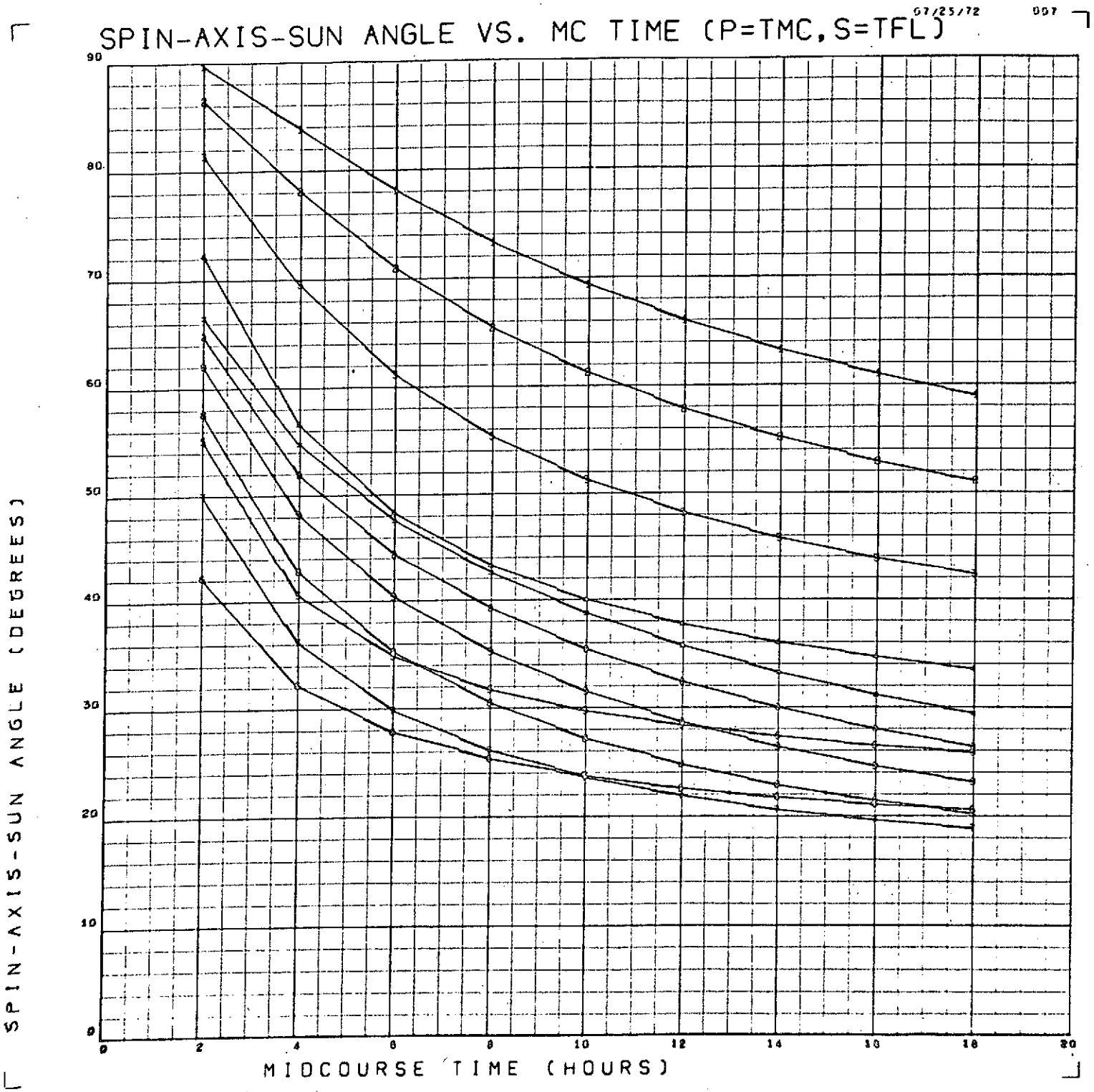
SPIN-AXIS-SUN ANGLE VS. MC TIME (P=TMC, S=TFL)
07/25/72
007
SPIN-AXIS-SUN ANGLE (DEGREES)
0
10
20
30
40
50
60
70
80
90
0
2
4
6
8
10
12
14
16
18
20
MIDCOURSE TIME (HOURS)

Figure 3.10

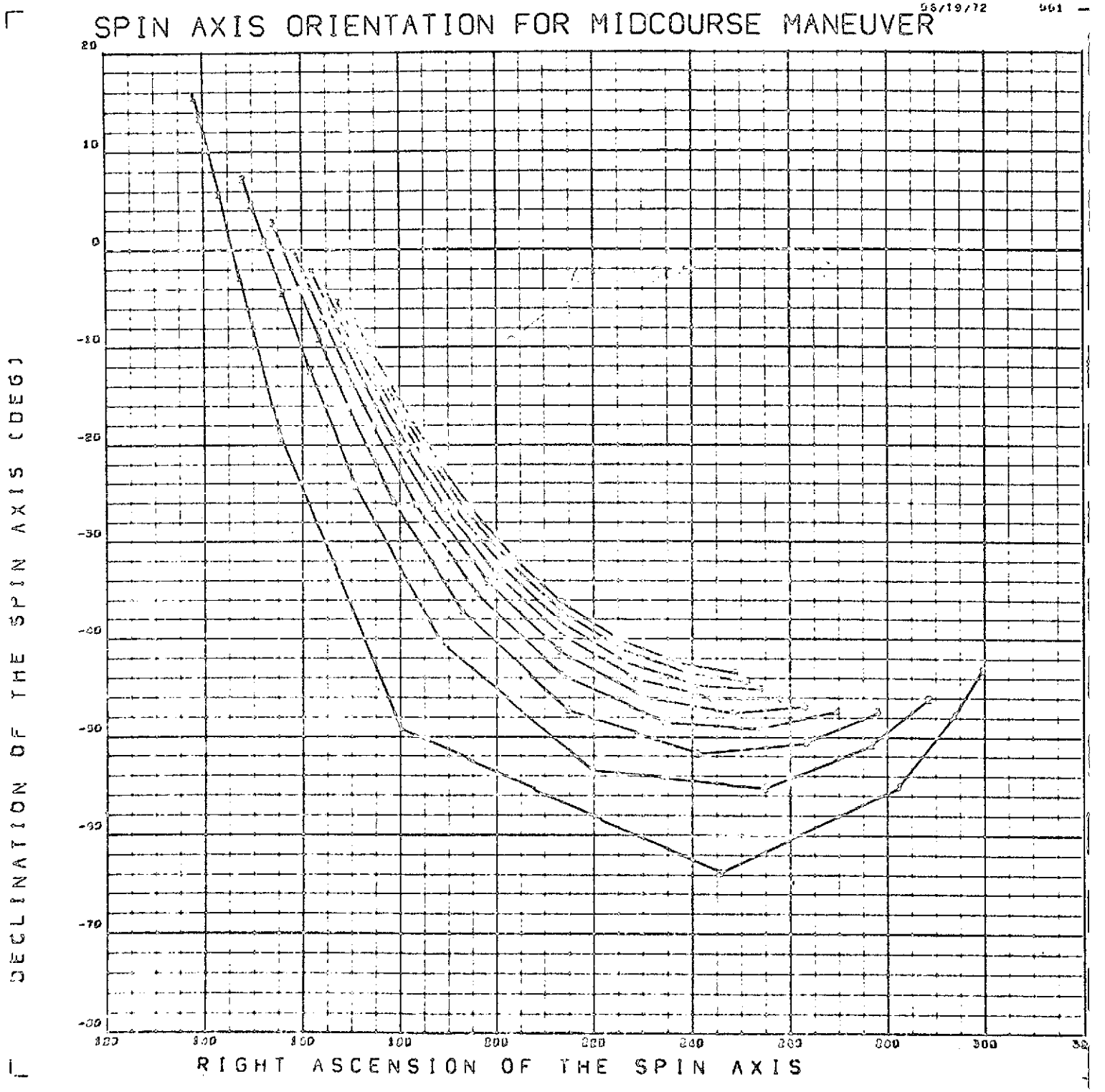
SPIN AXIS ORIENTATION FOR MIDCOURSE MANEUVER
06/19/72
961
20
10
0
-10
-20
-30
-40
-50
-60
-70
-80
DECLINATION OF THE SPIN AXIS (DEG)
RIGHT ASCENSION OF THE SPIN AXIS

Figure 3.11

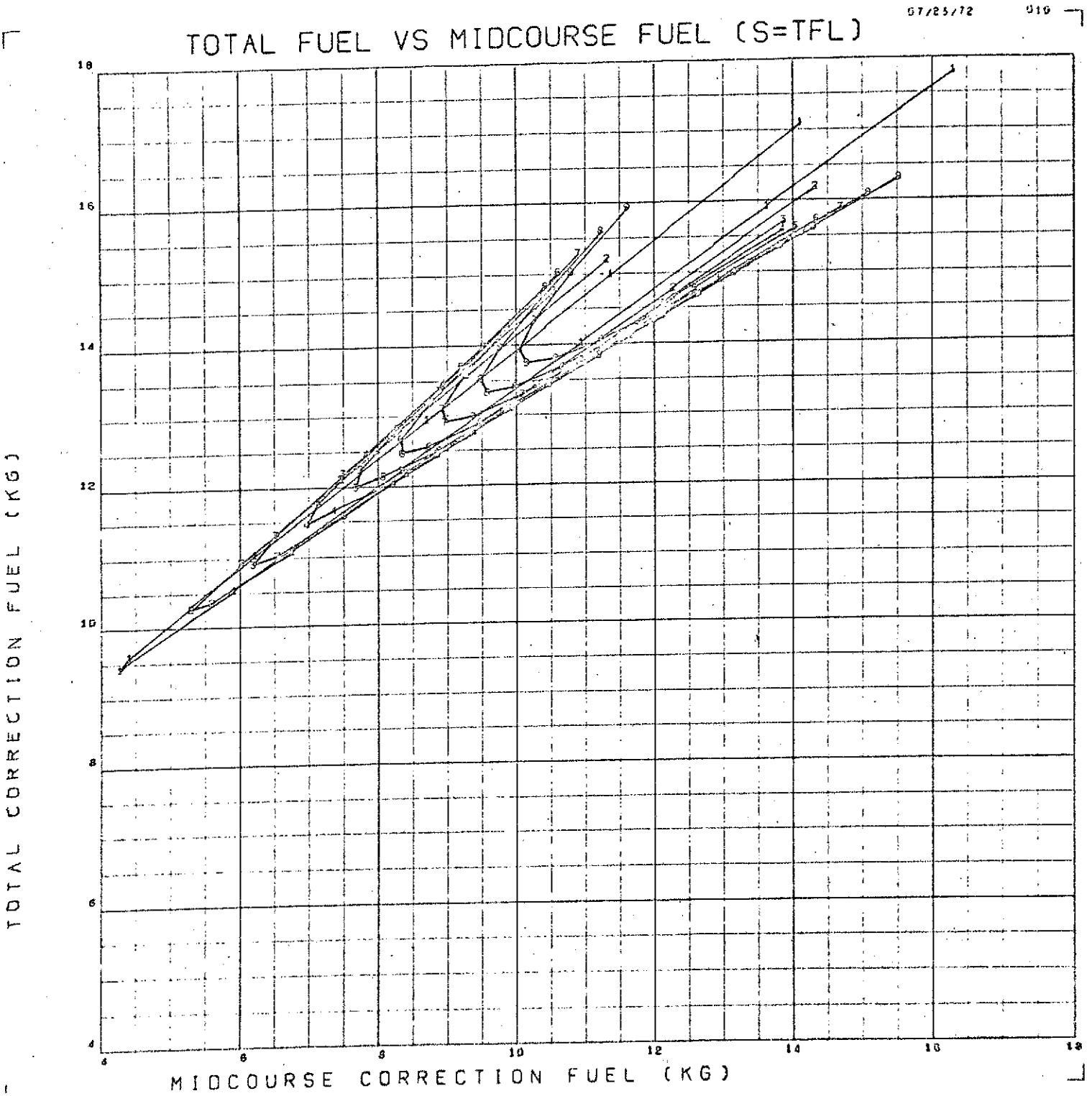
07/25/72 010
TOTAL FUEL VS MIDCOURSE FUEL (S=TFL)
TOTAL CORRECTION FUEL (KG)
MIDCOURSE CORRECTION FUEL (KG)
4
6
8
10
12
14
16
18

variable target inclination is used, the slope of this line is 45^{o}, otherwise the slope is greater than 45^{o}.

Figure 3.12 was generated for a "hot" June 10 trajectory. It presents trim fuel versus midcourse correction fuel for that trajectory. This figure presents the same type of information as figure 3.11. Each curve is generated by scanning flight times for a particular midcourse maneuver time. The curve containing the upper-leftmost point is for a 2^{h} correction. Each curve focuses to zero-trim at about 16 kg of midcourse fuel expenditure and then bounces upward along a focused beam. If a circularizing-retro overburn procedure had been assumed, the post-retro trim fuel would have been zero and the curves would have followed the lower edge of the plot after about 16 kg of midcourse fuel expenditure.

Figure 3.13 presents the same data as figure 3.12., but plots trim fuel against flight time. By extrapolating each of these curves to the flight time of zero trim requirement, it is possible to obtain the flight time of the variable target energy (VTE) solution for each midcourse execution time.

Figure 3.14 is a contour plot of trim fuel in the plane of flight time and midcourse time. The minimum contours shown are the third and fourth lines down from the upper right-hand corner of the plot. These lines of .5 kg trim fuel bound a valley whose minimum is the zero-trim or VTE solution for this case. This contour plot also shows a maximum trim region in the lower left-hand corner, should a maximum be of any interest.

Figures 3.15 and 3.16 present the relationships between midcourse fuel and velocity (delta-v) and between burn time and midcourse fuel expenditure. These curves are based on initial spacecraft weight of 333.39 kg, an I_{sp} of 226, an initial weight flow rate of .02404 kg/sec and a weight flow rate at 900 seconds of .01202 kg/sec. One might use these curves as quick-and-dirty cross references. For instance, a 100 m/s correction could be translated into about 14.7 kg of expended fuel and then into a midcourse burn duration of about 13 minutes.

Figure 3.12

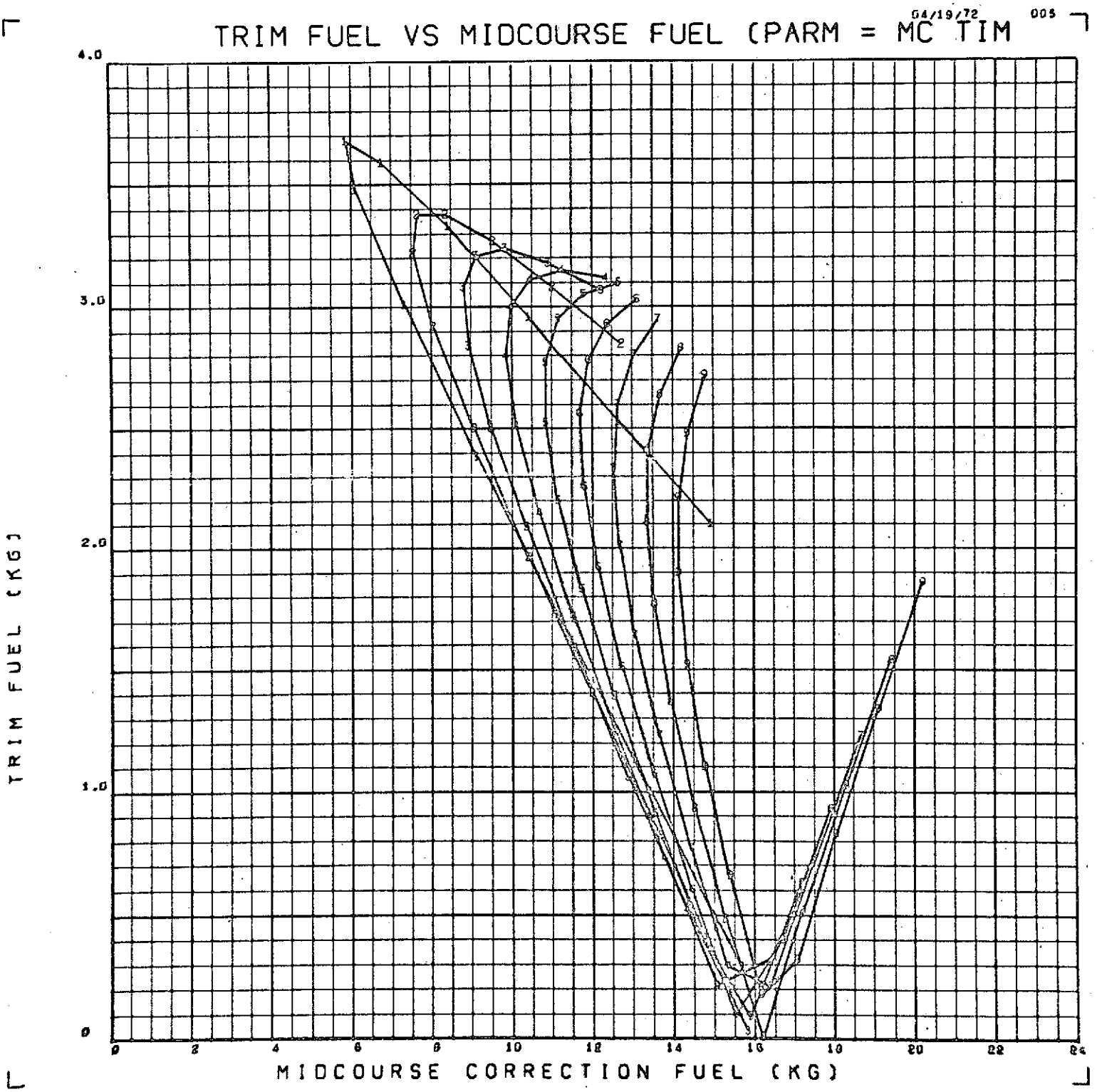
TRIM FUEL VS MIDCOURSE FUEL (PARM = MC TIM
04/19/72
005
TRIM FUEL (KG)
4.0
3.0
2.0
1.0
0
0
2
4
6
8
10
12
14
16
18
20
22
24
MIDCOURSE CORRECTION FUEL (KG)

Figure 3.13

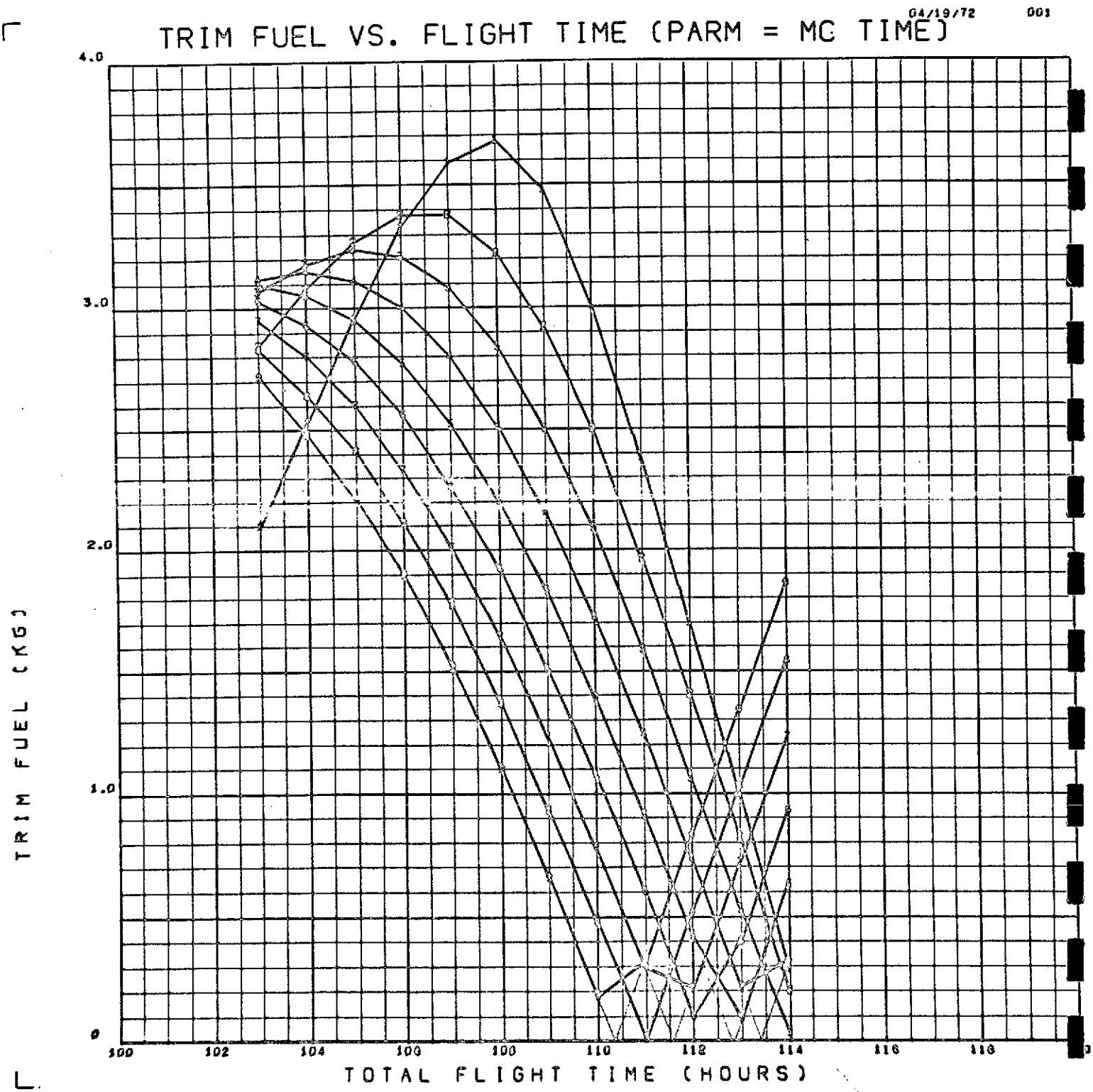
TRIM FUEL VS. FLIGHT TIME (PARM = MC TIME)
04/19/72
001
4.0
3.0
2.0
1.0
0
TRIM FUEL (KG)
100
102
104
106
108
110
112
114
116
118
TOTAL FLIGHT TIME (HOURS)

Figure 3.14

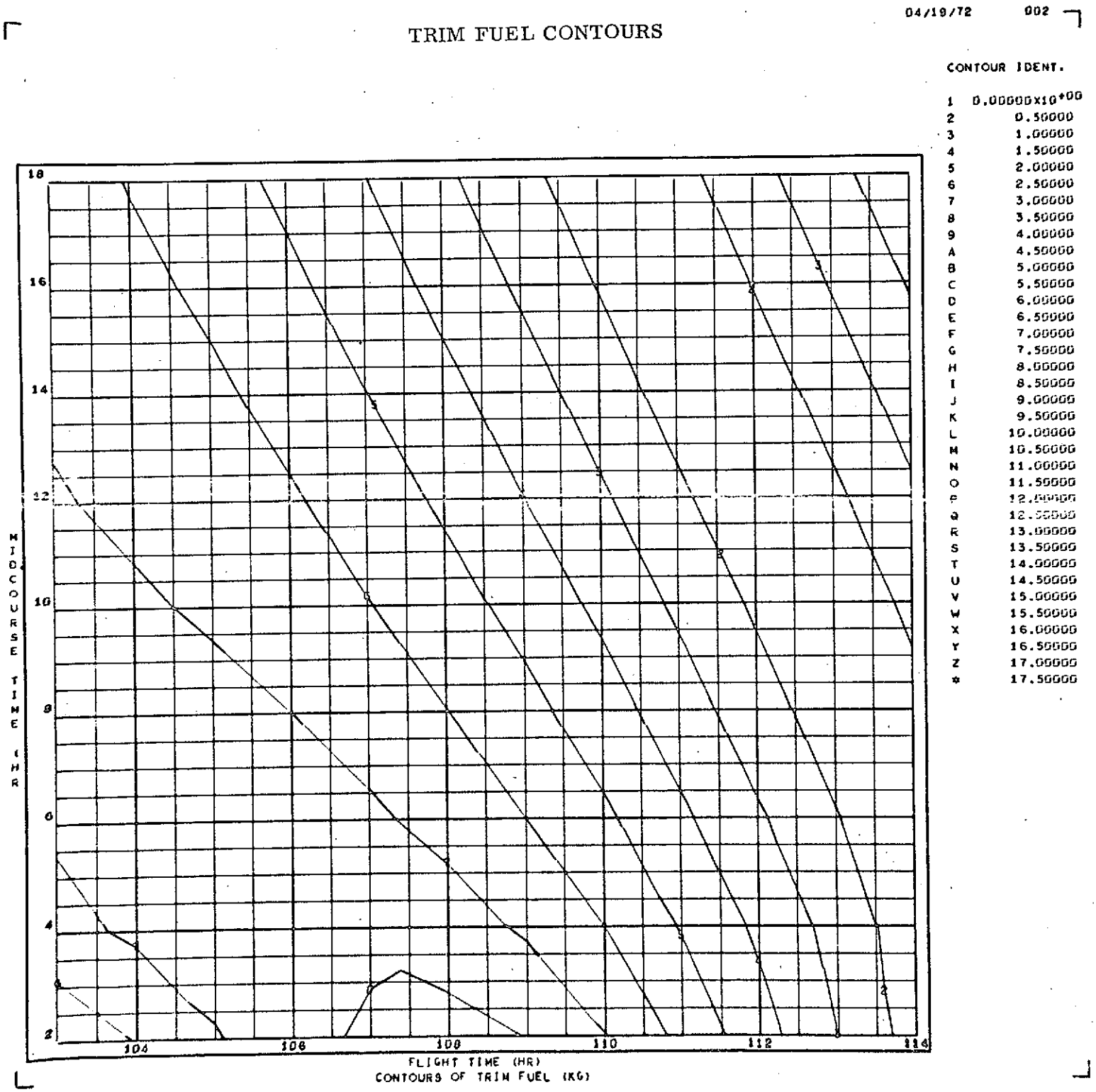
TRIM FUEL CONTOURS
04/19/72 002
CONTOUR IDENT.
1 0.00000x10**00
2 0.50000
3 1.00000
4 1.50000
5 2.00000
6 2.50000
7 3.00000
8 3.50000
9 4.00000
A 4.50000
B 5.00000
C 5.50000
D 6.00000
E 6.50000
F 7.00000
G 7.50000
H 8.00000
I 8.50000
J 9.00000
K 9.50000
L 10.00000
M 10.50000
N 11.00000
O 11.50000
P 12.00000
Q 12.50000
R 13.00000
S 13.50000
T 14.00000
U 14.50000
V 15.00000
W 15.50000
X 16.00000
Y 16.50000
Z 17.00000
* 17.50000
MIDCOURSE TIME (HR
18
16
14
12
10
8
6
4
2
104
106
108
110
112
114
FLIGHT TIME (HR)
CONTOURS OF TRIM FUEL (KG)

Figure 3.15

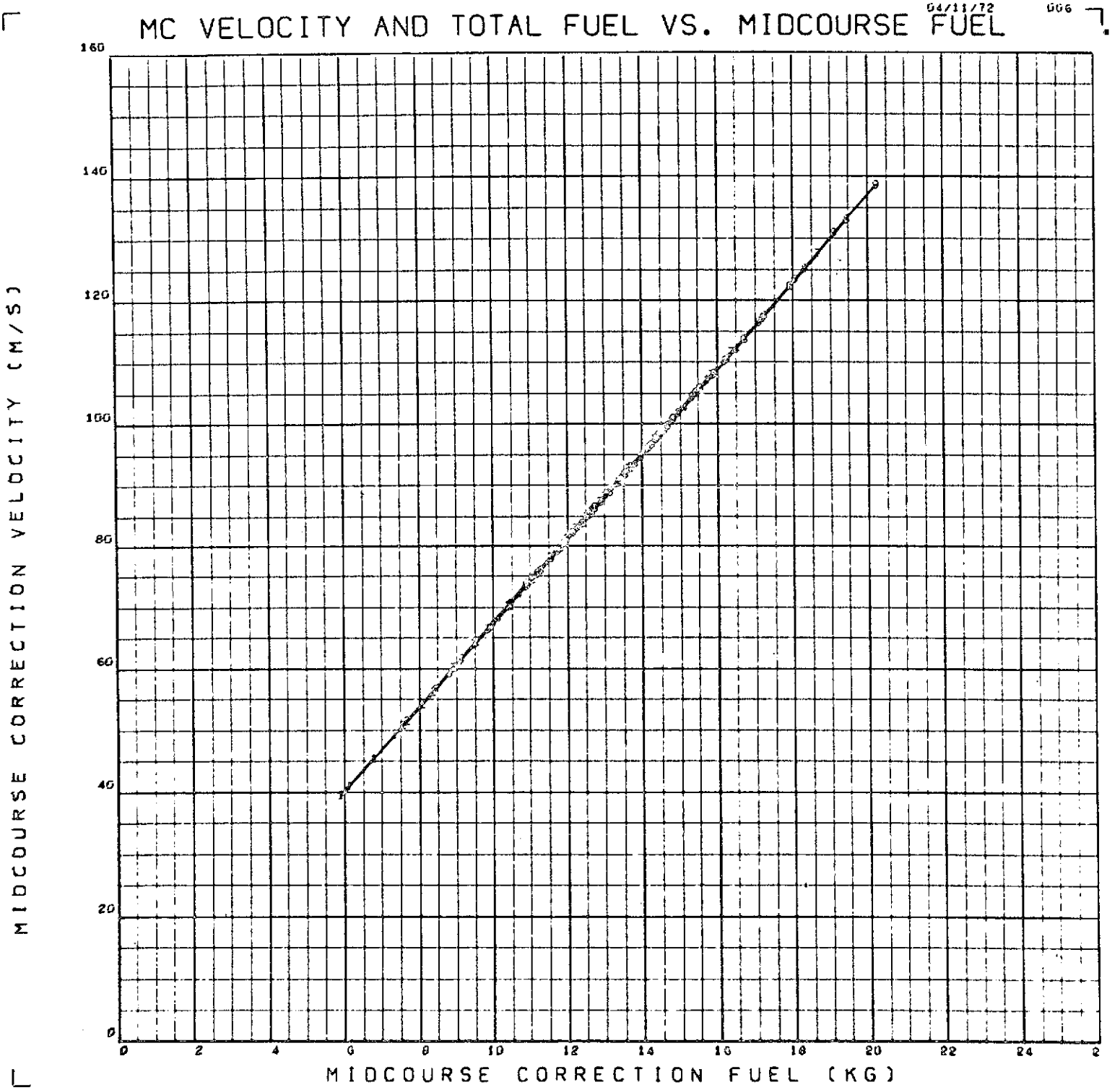
MC VELOCITY AND TOTAL FUEL VS. MIDCOURSE FUEL
04/11/72
006
MIDCOURSE CORRECTION VELOCITY (M/S)
160
140
120
100
80
60
40
20
0
0
2
4
6
8
10
12
14
16
18
20
22
24
MIDCOURSE CORRECTION FUEL (KG)

Figure 3.16

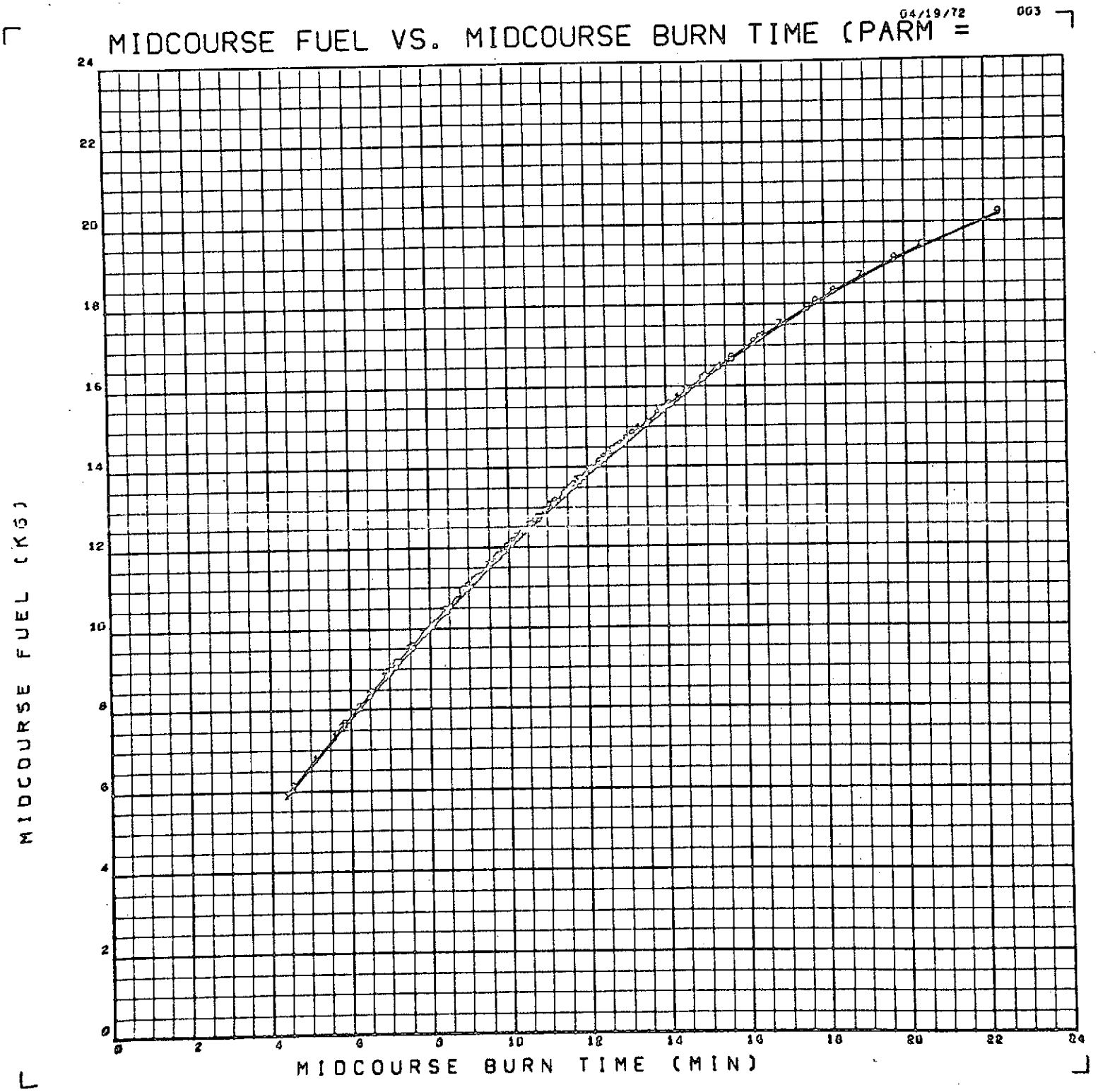
MIDCOURSE FUEL VS. MIDCOURSE BURN TIME (PARM =
04/19/72
003
MIDCOURSE FUEL (KG)
MIDCOURSE BURN TIME (MIN)
0
2
4
6
8
10
12
14
16
18
20
22
24

3.3.2 "Fixed-Attitude" Scans

The "fixed-attitude guidance" capability is simply an automated procedure for varying the midcourse command parameters:

1. ignition time
2. burn duration (ΔV)
3. right ascension of the spin axis
4. declination of the spin axis.

Two situations have been investigated using this capability. The first of these is that the execution of the midcourse maneuver is imperfect relative to that determined by midcourse targeting. The automated procedure can be made to compute and display the consequences of such imperfections. The second situation which has been investigated is that the attitude control system is inoperative. The question of interest is then of what can be done with control of only ignition time and burn duration.

Figures 3.17 and 3.18 show total fuel (midcourse plus trim) for variations of ±6 minutes in ignition time, ±1 m/s in velocity impulse and ±1 degree in each angle relative to a 2-hour MFG-targeted correction. The fuel values are in kilograms and primarily reflect trim variations, since the midcourse fuel is nearly constant at about 6 kilograms. In computing the data shown in Figure 3.17, the retro motor was fired in-plane at periapsis and inclination errors were not trimmed out. For Figure 3.18, the firing time and retro attitude were optimized to minimize trim velocity while trimming out inclination errors. Inclination of the post-retro, pre-trim orbit was printed out on the run and varied only occasionally and slightly from the desired orbital inclination of 116.5°. This result confirms the suspicion that it is nearly optimal to remove inclination errors with the retro burn rather than even partly with trim maneuvers. Figure 3.19 shows the variations in radius of closest approach and inclination which result from command errors of the 2-hour MFG correction. An initially-surprising result shown by this figure is that attitude errors in right ascension and declination map into the same straight line on the figure. Appendix D explains why this result is generally true for attitude variations from a minimum fuel correction. Each arrow in the figure is the result of attitude variations at a particular ignition time and burn duration. The central arrow

Figure 3.17

				1.90^h					
		- 1 m/s		0			+ 1 m/s		
	$+1^o$	12.67	12.22	11.82	10.10	10.28	10.44	11.15	11.29	11.43
-6^m	dec	10.48	10.00	9.58	10.91	11.09	11.26	11.78	11.93	12.06
	-1^o	9.78	9.97	10.15	11.72	11.90	12.07	12.39	12.53	12.66
		-1^o	r.a.	$+1^o$						
				2.00^h						
		18.02	17.55	17.15	12.20	11.72	11.29	10.19	10.37	10.54
0		15.93	15.44	15.01	10.00	9.50	9.63	10.99	11.17	11.34
		13.83	13.32	12.86	10.10	10.31	10.51	11.78	11.96	12.14
				2.10^h						
		23.05	22.60	22.21	17.14	16.64	16.19	11.78	11.28	10.81
$+6^m$		21.17	20.70	20.28	15.01	14.48	14.01	9.58	9.76	9.95
		19.28	18.77	18.31	12.86	12.31	11.80	10.40	10.62	10.82
			-1 m/s			δ v			+ 1 m/s	

Total Fuel for a Command Error Scan

(no inclination trim)

			1.90^h					
	- 1 m/s			0 m/s			+ 1 m/s	
14.03	13.41	12.95	14.25	14.78	15.31	33.90	34.74	35.42
11.10	10.48	10.03	17.63	18.36	19.02	38,02	38.85	39.53
9.94	10.05	10.20	21.43	22.37	23.09	41.83	42.65	43.33
			2.00^h					
24.49	24.09	23.48	12.56	11.97	11.46	17.17	18.23	18.66
21.51	21.08	20.44	10.02	9.50	9.65	21.09	22.04	22.97
19.13	18.11	17.83	10.25	10.59	10.84	25.29	26.34	27.21
			2.10^h					
36.70	36.03	35.48	21.52	20.75	20.15	11.81	11.33	10.94
34.08	33.35	32.73	18.69	17.95	17.38	9.97	10.32	10.71
31.44	30.63	29.96	15.86	15.15	14.52	11.69	12.18	12.80

Total Fuel for a Command Error Scan

(with inclination errors trimmed out)

FIG. 3.19

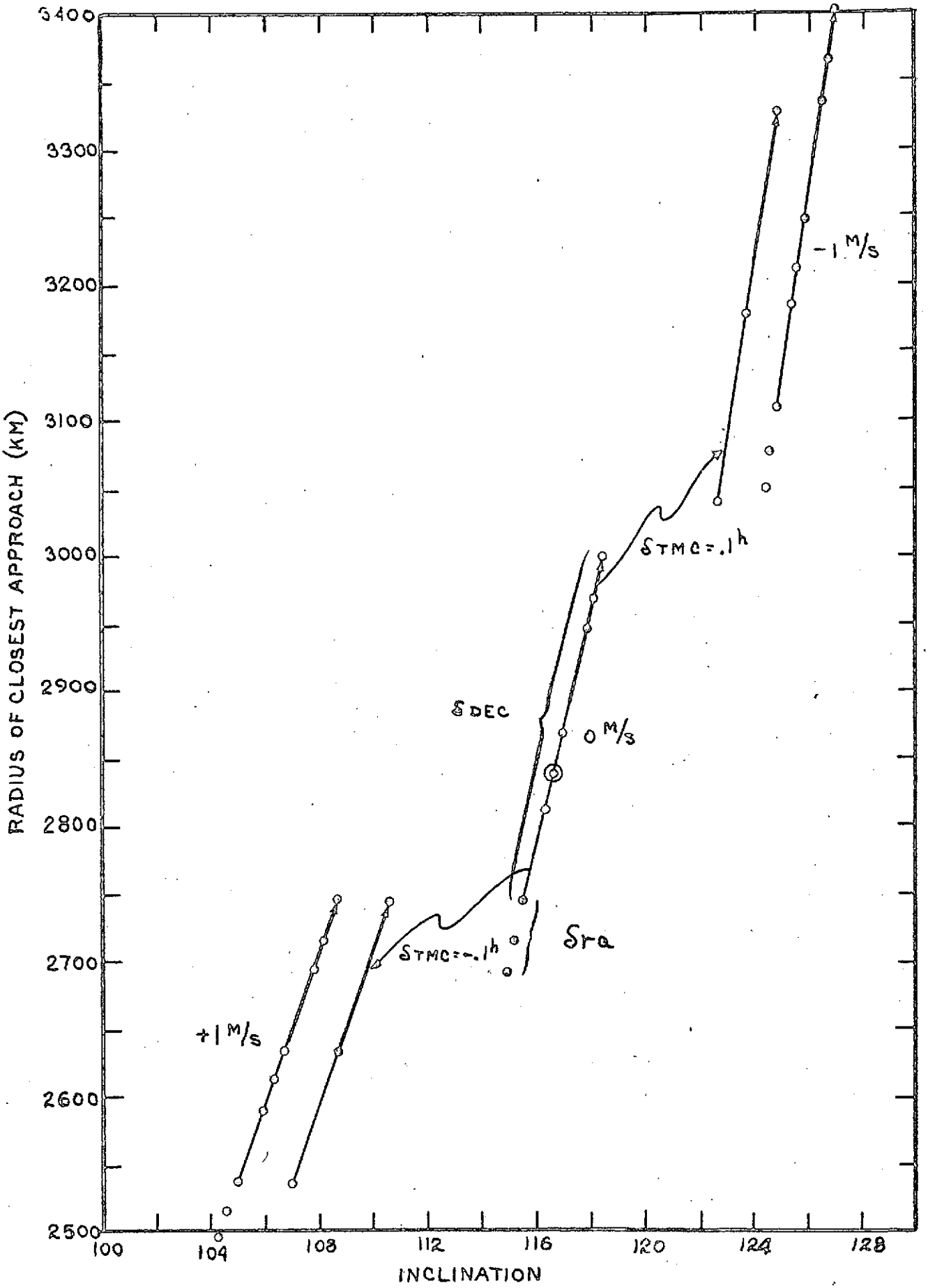

CLOSEST APPROACH AND INCLINATION VARIATIONS

is for the nominal ignition time and burn duration, while the extreme arrows are for ±1 m/s deviations in velocity impulse from the nominal of 39.07 m/s. The other arrows are for ignition time variations of ±6 minutes from the nominal, holding the velocity impulse constant at its nominal value. An earlier-than-nominal ignition time is seen to have the same effect as a "hot" burn and vice versa.

Figures 3.20., 3.21., 3.22 and 3.23 describe the end conditions which could be achieved with the midcourse spin-axis attitude fixed at that of the injection velocity vector. The trajectory is the April 14 nominal 115-hour trajectory which requires no midcourse correction. The figures show separate curves for each midcourse ignition time under consideration. These are from 2 hours to 18 hours after launch. The top curve in each figure corresponds to the 2-hour correction. The abscissa in each figure is midcourse velocity magnitude in meters per second. Figure 3.20 shows radius of closest approach, figure 3.21 shows inclination and figure 3.22 shows flight time to closest approach. Figure 3.23 shows total correction fuel (midcourse plus trim) for in-plane trim of the orbit to circular. The calculations used in generating this figure assume that attitude control becomes operable prior to the retro maneuver and that the retro maneuver occurs at periapsis and opposite to the velocity there. It may be noted that the variations are nearly all due to trim fuel requirements since the curve of midcourse fuel vs. midcourse velocity is very nearly a straight line through the origin.

3.3.3 Retro and Trim Results

Very few presentable results have been obtained concerning the retro maneuver. Solutions for retro direction and firing time are determined either by numerical optimization to minimize trim fuel or by an assigned retro strategy such as

1. firing the retro at perilune to give an impulse opposite to the velocity there.
2. firing the retro at perilune to impart an out-of-plane impulse required by the variable target inclination procedure, or
3. firing the retro in-plane to circularize the orbit at the desired final radius in accordance with the variable approach guidance procedure.

Figure 3.24 is a contour plot which shows the path of the retro direction during the numerical optimization procedure.

April 14 - nominal/ATT=INJ

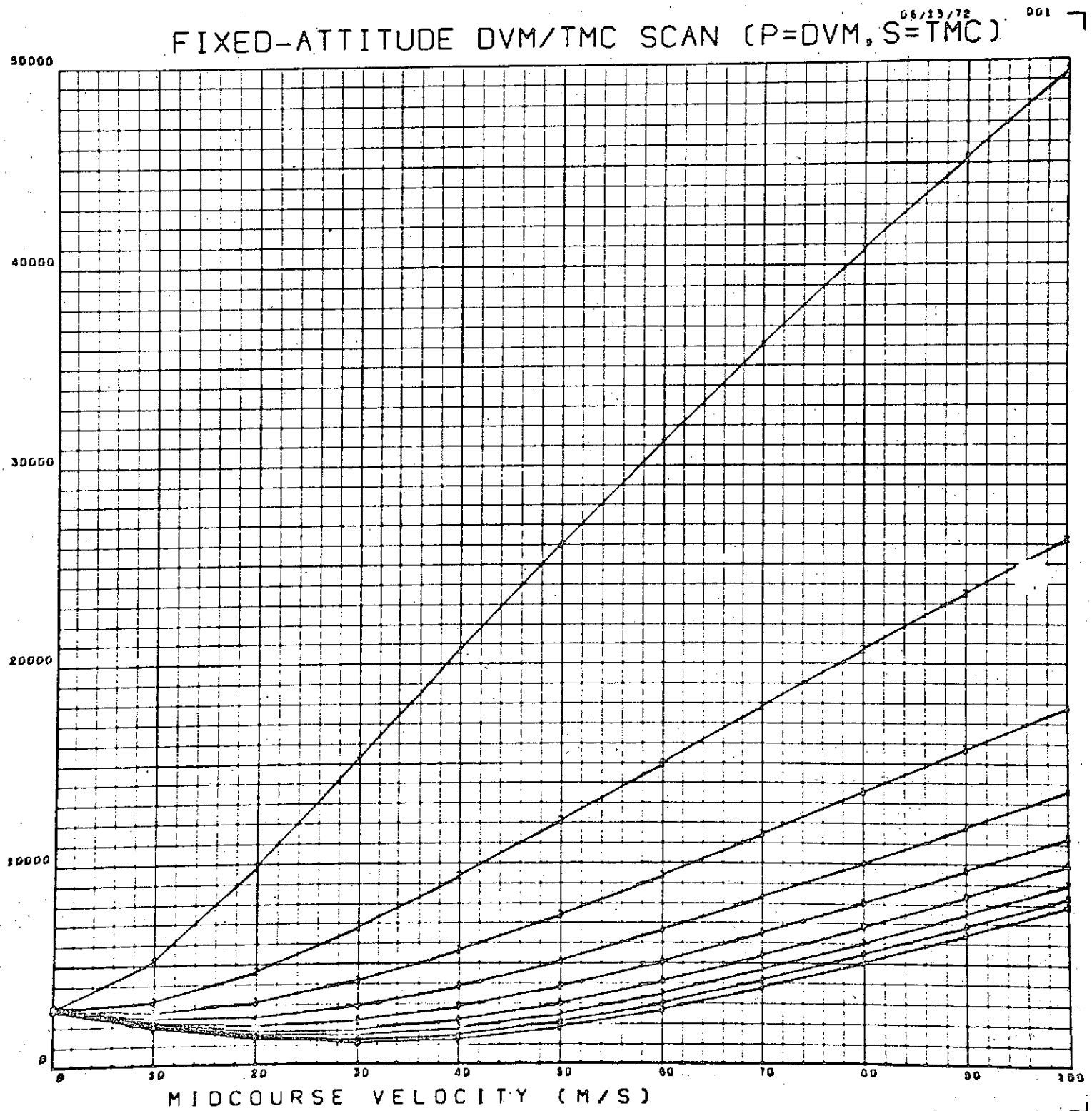

Figure 3.2 1

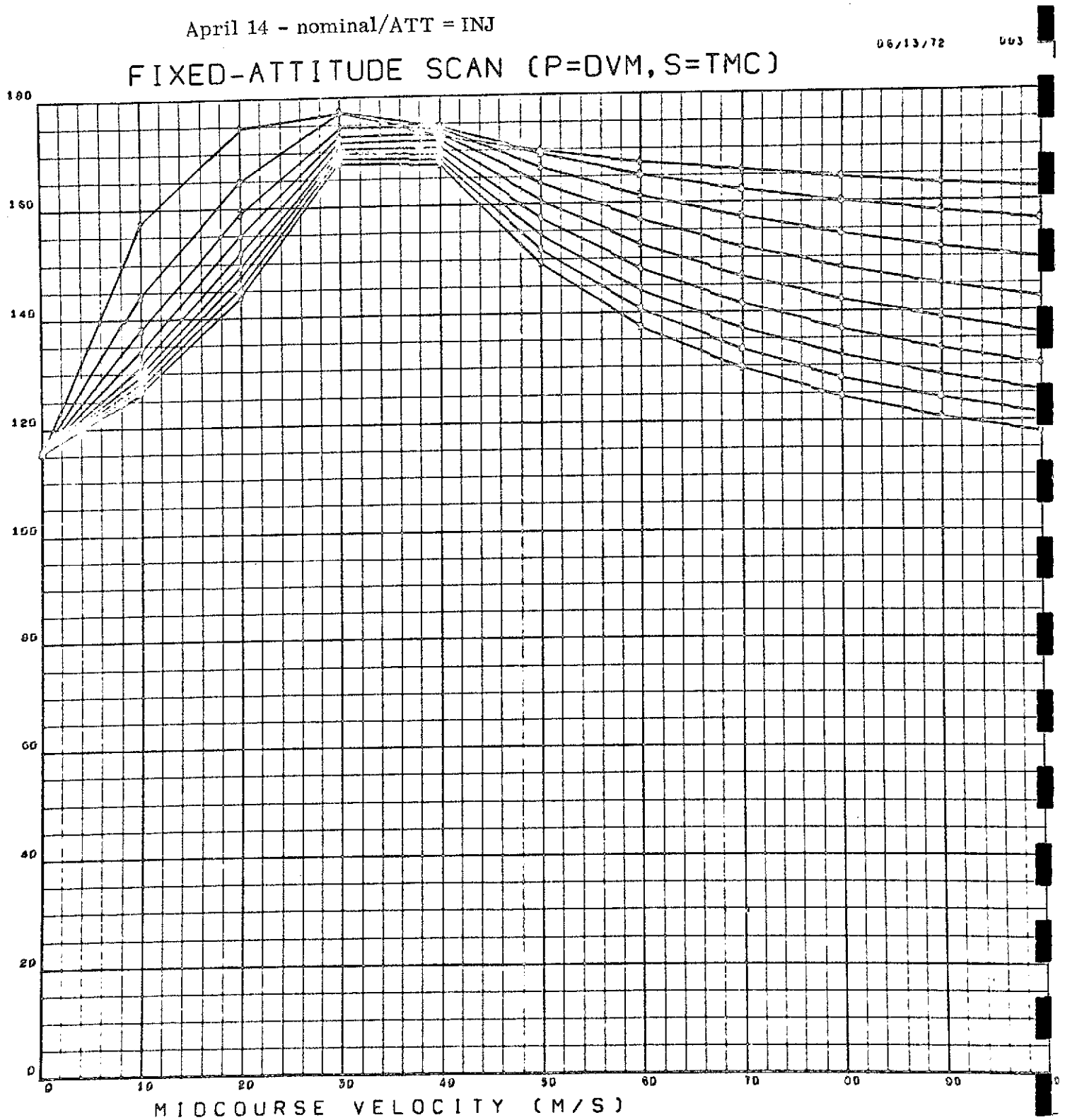
April 14 - nominal/ATT = INJ
06/13/72
003
FIXED-ATTITUDE SCAN (P=DVM, S=TMC)
180
160
140
120
100
80
60
40
20
0
0
10
20
30
40
50
60
70
80
90
INCLINATION (DEGREES)
MIDCOURSE VELOCITY (M/S)

Figure 3.22

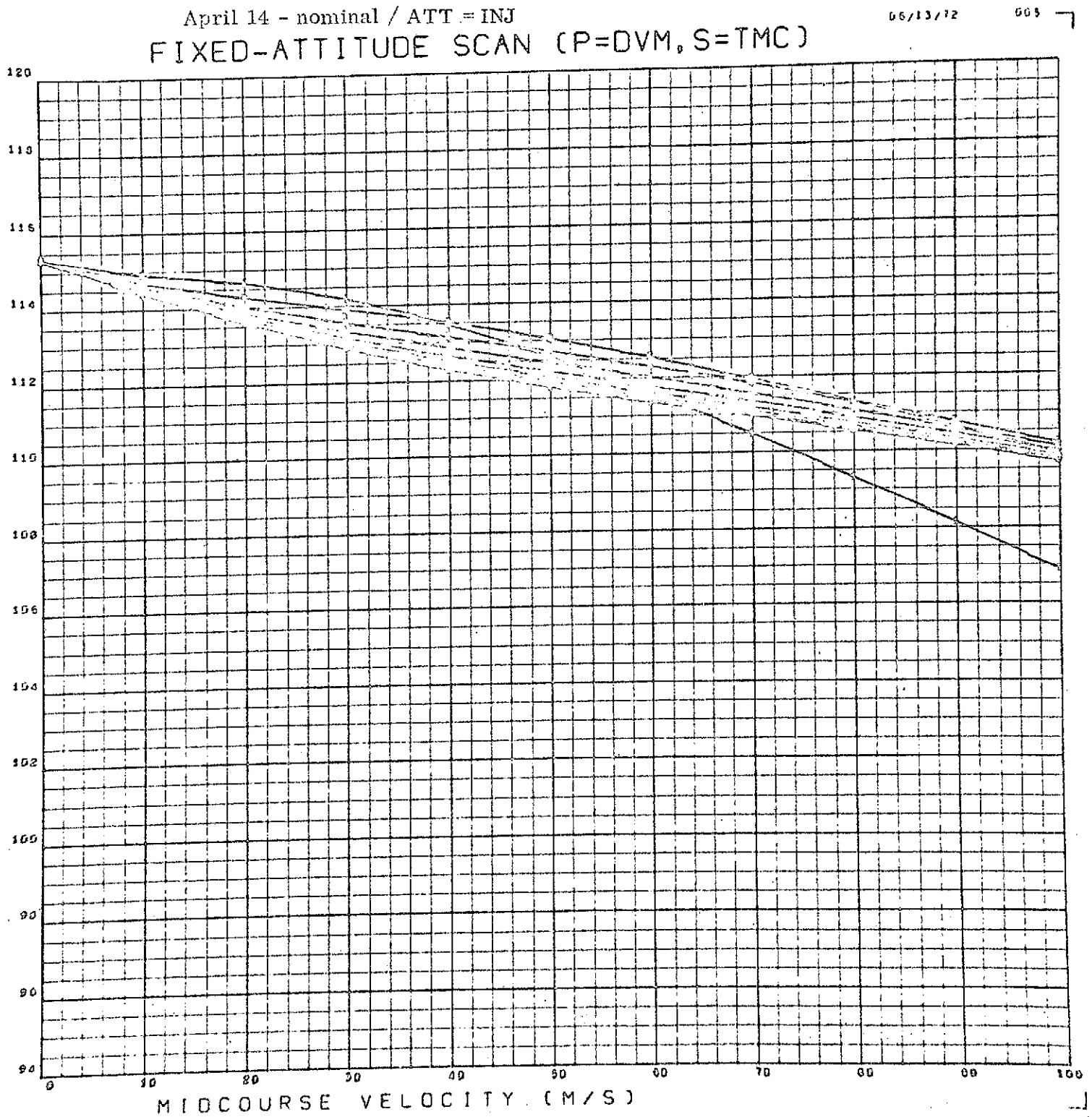
April 14 - nominal / ATT = INJ
06/13/72
005
FIXED-ATTITUDE SCAN (P=DVM, S=TMC)
120
118
116
114
112
110
108
106
104
102
100
98
96
94
0
10
20
30
40
50
60
70
80
90
100
MIDCOURSE VELOCITY (M/S)

Figure 3.2 3

April 14 - nominal / ATT=INJ

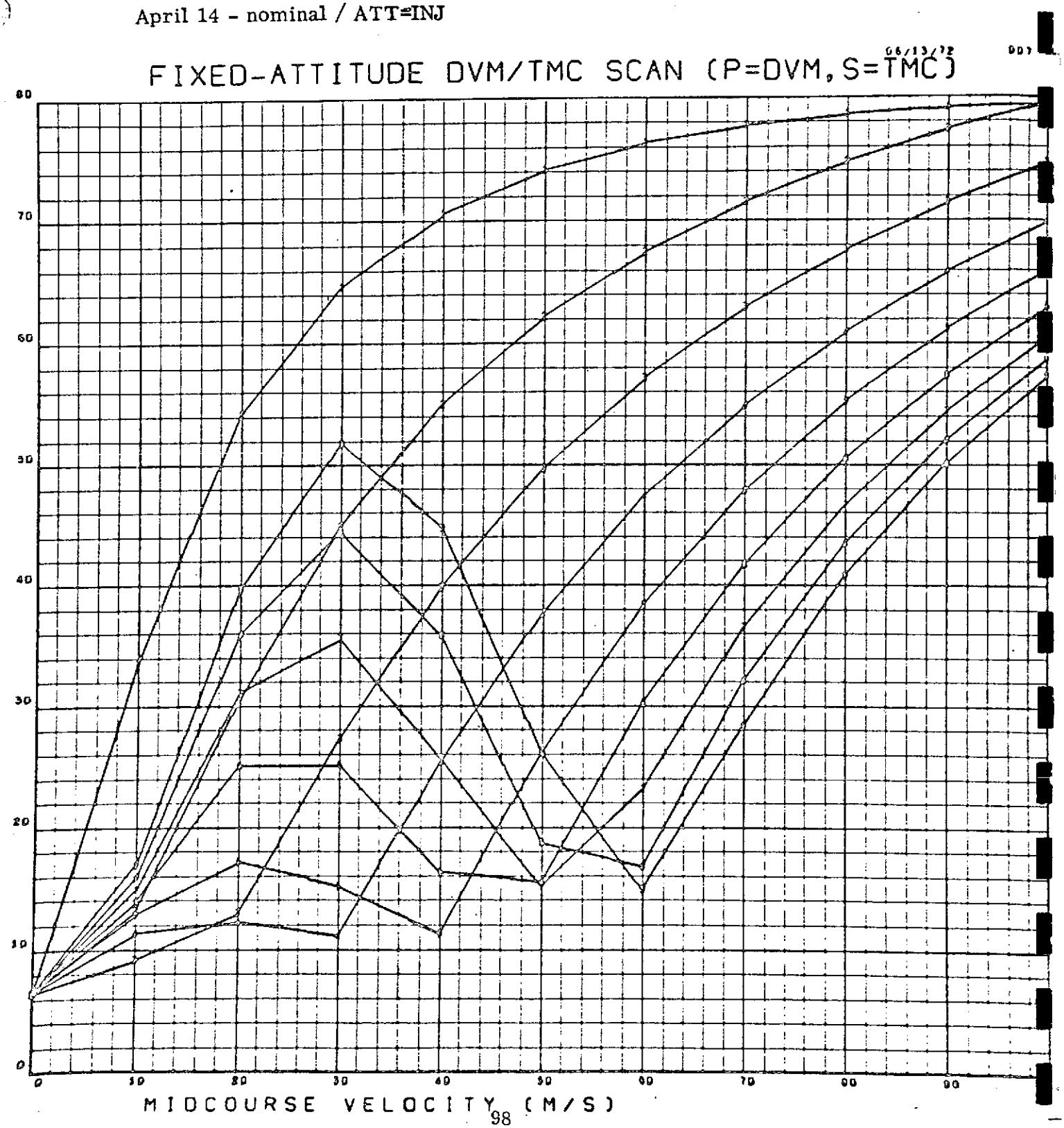

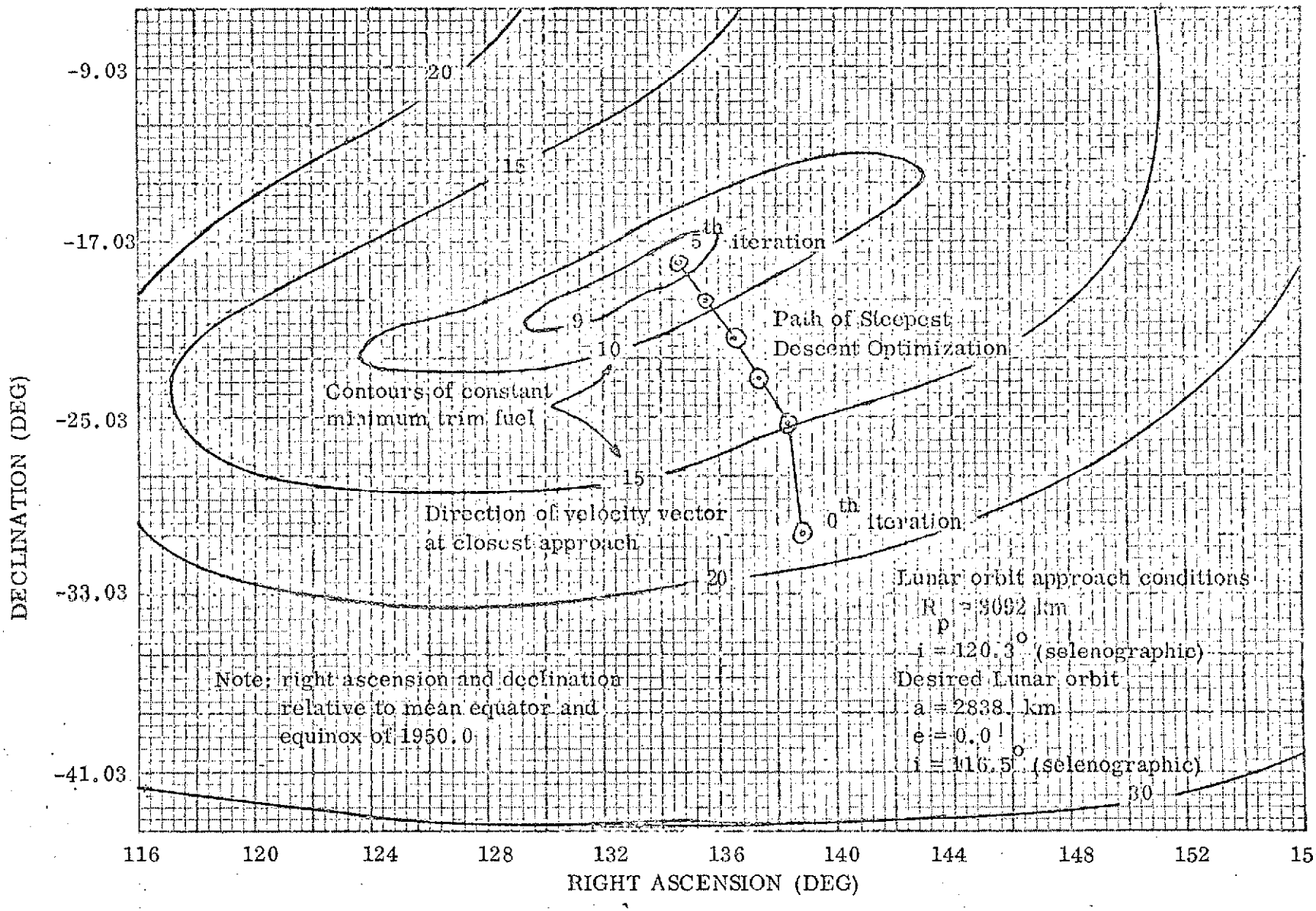

RAE-B RETRO ATTITUDE OPTIMIZATION

Figure 3.24

The numerical procedure for obtaining retro direction and firing time includes, for each candidate retro direction, a minimization of trim fuel by varying firing true anomaly. Figure 3.25 is a plot of trim velocity vs. firing true anomaly for two neighboring candidate directions and the same approach trajectory. The occurrence of double minima for this case may be noted.

Figure 3.26 shows the fuel penalties for aim-point variations from the desired r_{pd} = 2838 km and $i_d = 116.5^o$. The lower-right number at each intersection point of the grid is the midcourse fuel required to target to that intersection, using the MFG law. The upper-left number at each intersection is the total correction fuel (midcourse plus trim) to trim the orbit to r_{pd} and i_d. The values shown relate to a 2^h midcourse correction to a slightly errant trajectory. The trim fuel values were determined with the numerical procedure for optimizing retro direction and firing time. It is apparent that the trajectory should be targeted to r_{pd} and i_d at the midcourse correction. It may also be observed that the midcourse fuel cost for targeting to other grid points is very small. The fuel for trimming the trajectory targeted to r_{pd} and i_d is seen to be about 3.65 kg. It does not appear possible to separate trim costs due to inclination variations from trim costs due to radius of closest approach variations, since radius-correcting costs differ at different inclinations. Figure 3.27 differs from 3.25 only in that the midcourse maneuver is executed at 18^h rather than at 2^h. Trim fuel costs differ somewhat between the two figures due to differing characteristics of the approach trajectory for the two maneuver times. Extra printout from one of the trajectories targeted to $i = 106.5^o$ revealed that the optimal firing true anomaly (for that trajectory) was about $+16^o$, which would probably put the firing point closer to the equator than periapsis was. The retro direction and required trim fuel changed during the numerical optimization process as shown.

	True Anomaly	Right Ascension	Declination	Trim Velocity
First Guess	0.	82.81	-41.77	254.67
Optimal Solution	16.34	117.19	-48.41	157.96

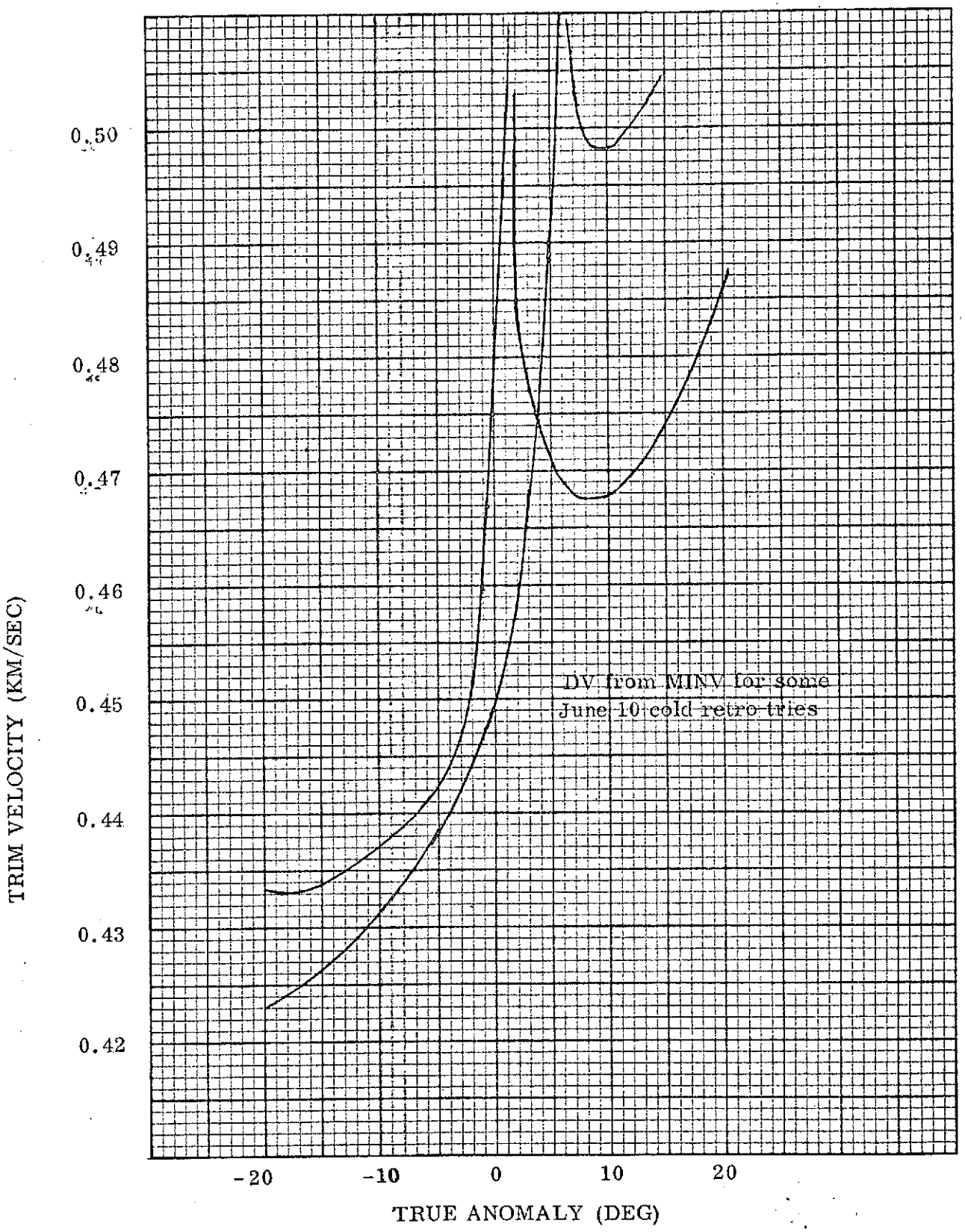

TRIM VELOCITY VS. TRUE ANOMALY

Fuel Penalties for Aim-Point Variations

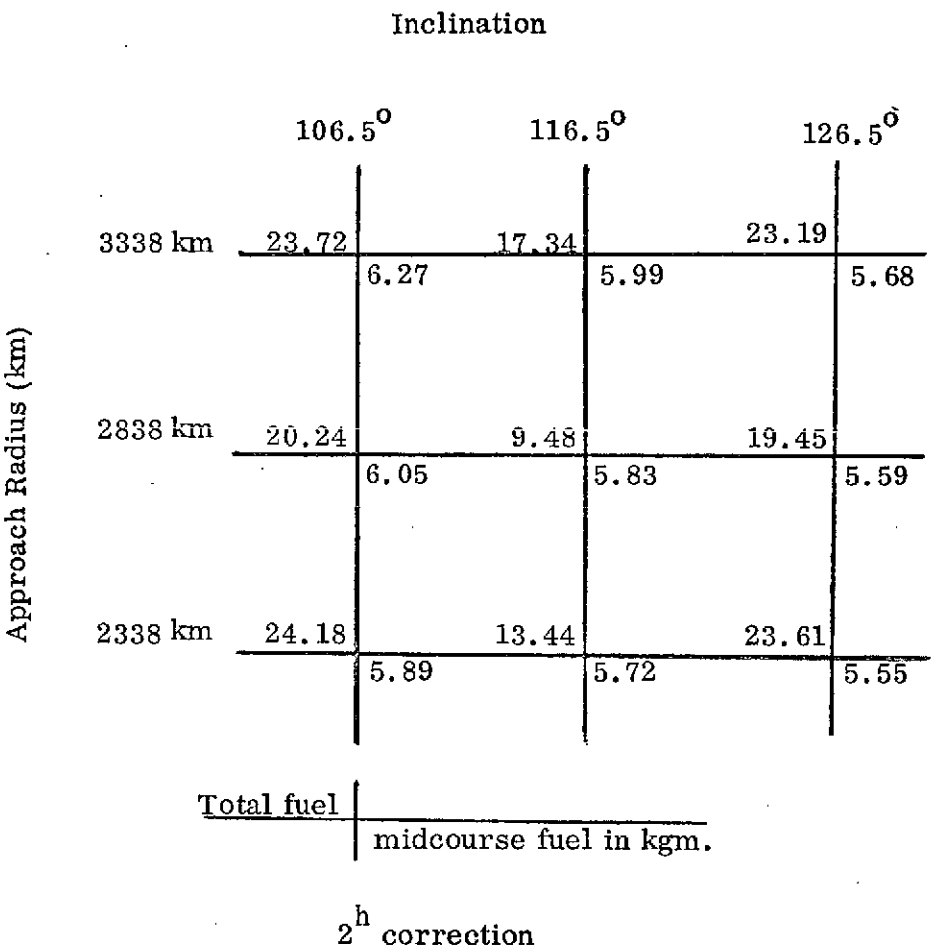

Figure 3.27

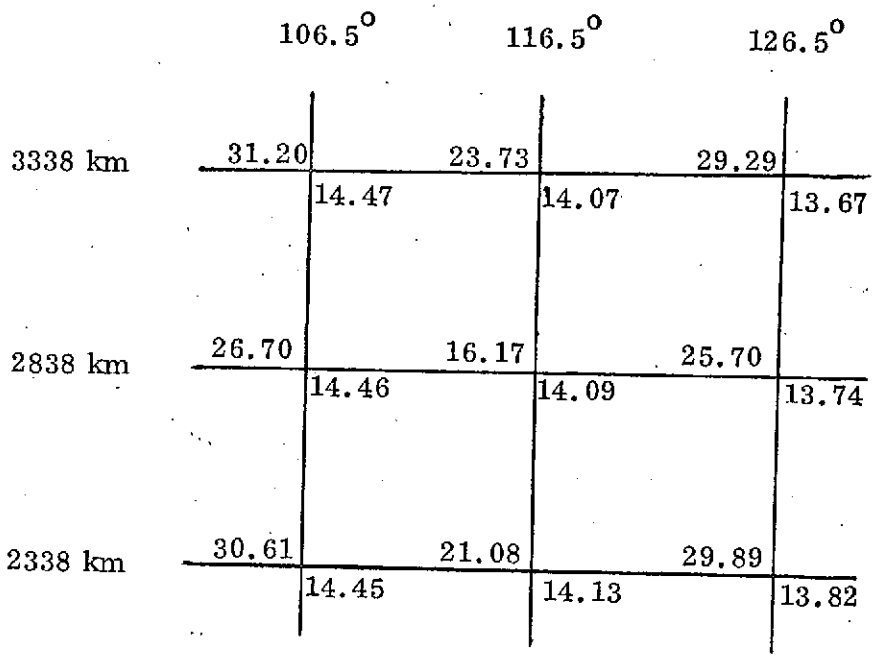

Fuel Requirements / Aim Point

Total fuel	
	midcourse fuel in kgm.

18^h correction

Analysis of in-plane retro and trim requirements is much simpler that for non-coplanar trims. Whatever the retro maneuver is, it usually results in an elliptical orbit about the Moon. If inclination errors are ignored, the optimal strategy for trimming to circular at a given radius is a two-impulse Hohmann transfer. Characteristics of such a transfer have been extensively studied. Figure 3.28 shows curves of trim velocity (sum of the two impulses) versus one apsis radius, called approach pericynthion. Each curve represents a different value of the opposite apsidal radius. The top curve is for 2338 km and the bottom curve is for 2838 km. Some of the middle curves are for opposite apsidal radii greater than 2838 km and some for smaller. Notice that the minimum of each curve occurs at no deviation from 2838 km in approach pericynthion and that the lowest curve also characterizes "correct" apsidal radius. Each of these cases requires only one impulse. Figure 3.29 was generated by contour-plotting the data of 3.28 . The x-axis of the plot is deviation of approach pericynthion from 2838 km and the y-axis is deviation of the opposite apsidal radius. The contour lines are separated by 10 m/s in trim velocity to circularize to 2838 km. The plot may be imagined to be an inverted pyramid. The value of such a plot in analysis of in-plane trim will be seen later.

Trim and Retro Strategies

Figure 3.30 is basically a contour plot of trim velocity in the plane of apsidal altitude errors. That is, the x-axis represents first-apsis altitude relative to 1100 km and the y-axis represents second-apsis altitude relative to 1100 km. The rectangles are lines of constant trim velocity to trim the orbit in-plane to 1100 km. They are spaced 10 m/s apart.

Line L_1 is the locus of circular orbits. Points P_i represent possible pairs of first-apsis, second-apsis errors following a (hyperbolic) periapsis anti-velocity maneuver. Points located to the upper-left of L_1 represent results of underburning with respect to circular at r and those to the lower-right of L_1, overburning with respect to circular at r. The vectors emanating from P_i represent loci of points attainable by firing the retro at some radius greater than periapsis radius, always nulling the post-retro radial velocity with the retro maneuver. These loci are drawn as straight lines of slope 7. They closely approximate actual loci in the area of $C_3 = .6\ km^2/sec^2$,

Figure 3.23

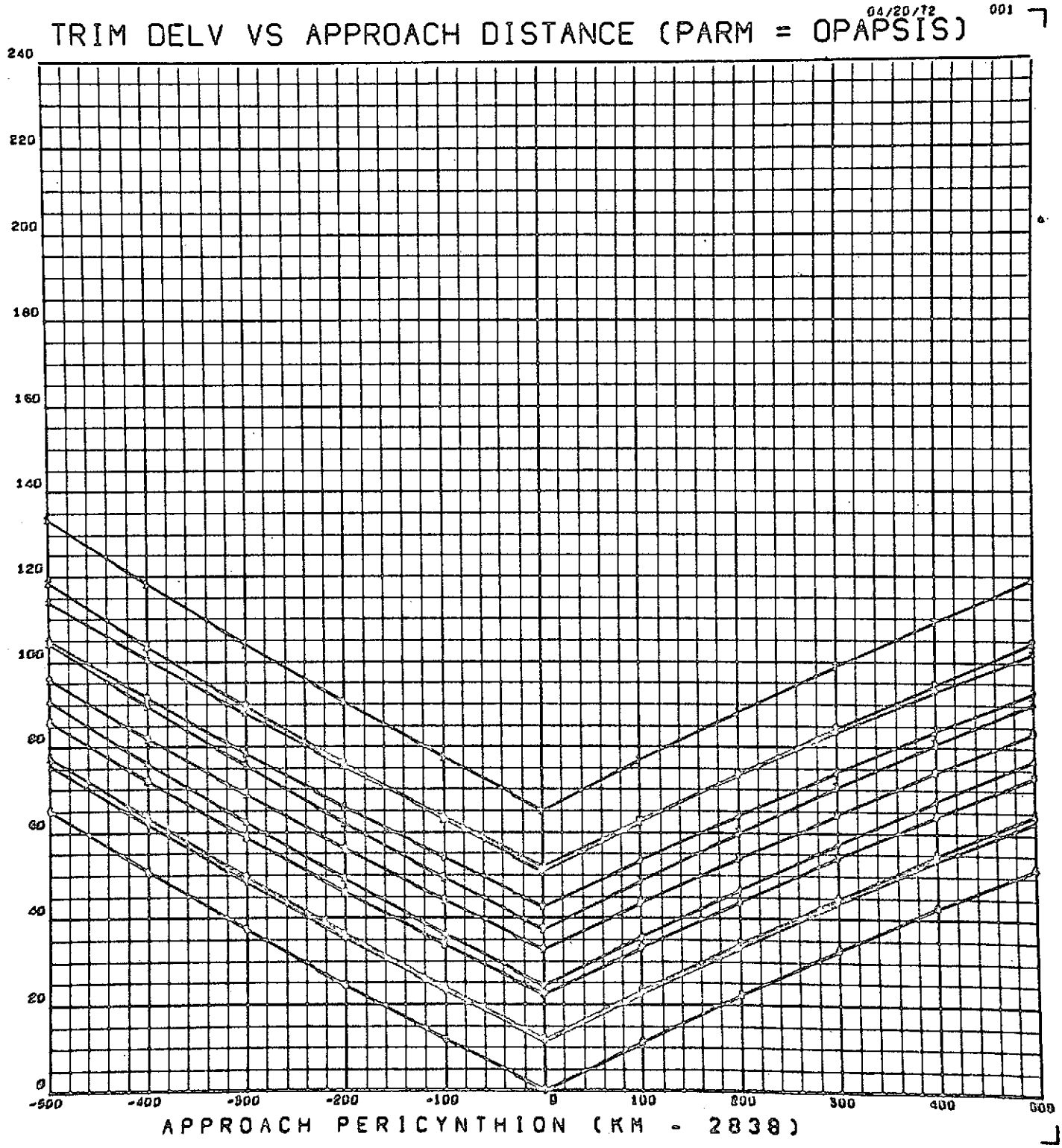
TRIM DELV VS APPROACH DISTANCE (PARM = OPAPSIS)
04/20/72
001
240
220
200
180
160
140
120
100
80
60
40
20
0
-500
-400
-300
-200
-100
0
100
200
300
400
500
APPROACH PERICYNTHION (KM - 2838)

04/20/72 002

TRIM VELOCITY CONTOURS

CONTOUR IDENT.	
1	0.00000x10+00
2	10.00000
3	20.00000
4	30.00000
5	40.00000
6	50.00000
7	60.00000
8	70.00000
9	80.00000
A	90.00000
B	100.00000
C	110.00000
D	120.00000
E	130.00000
F	140.00000
G	150.00000
H	160.00000
I	170.00000
J	180.00000
K	190.00000
L	200.00000
M	210.00000
N	220.00000
O	230.00000
P	240.00000
Q	250.00000
R	260.00000
S	270.00000
T	280.00000
U	290.00000
V	300.00000
W	310.00000
X	320.00000
Y	330.00000
Z	340.00000
*	350.00000

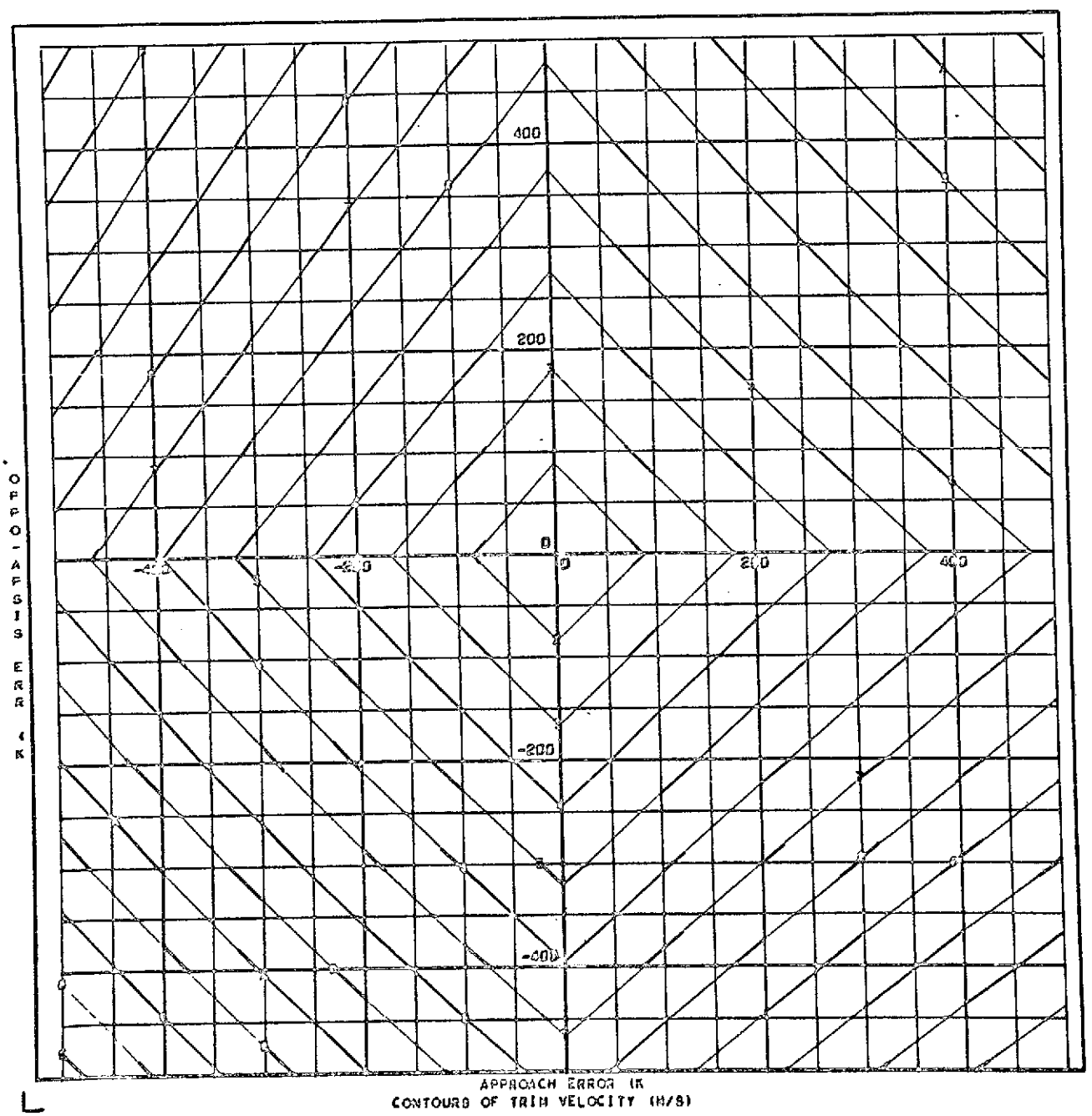

APPROACH ERROR (K

CONTOURS OF TRIM VELOCITY (M/S)

Figure 3.30

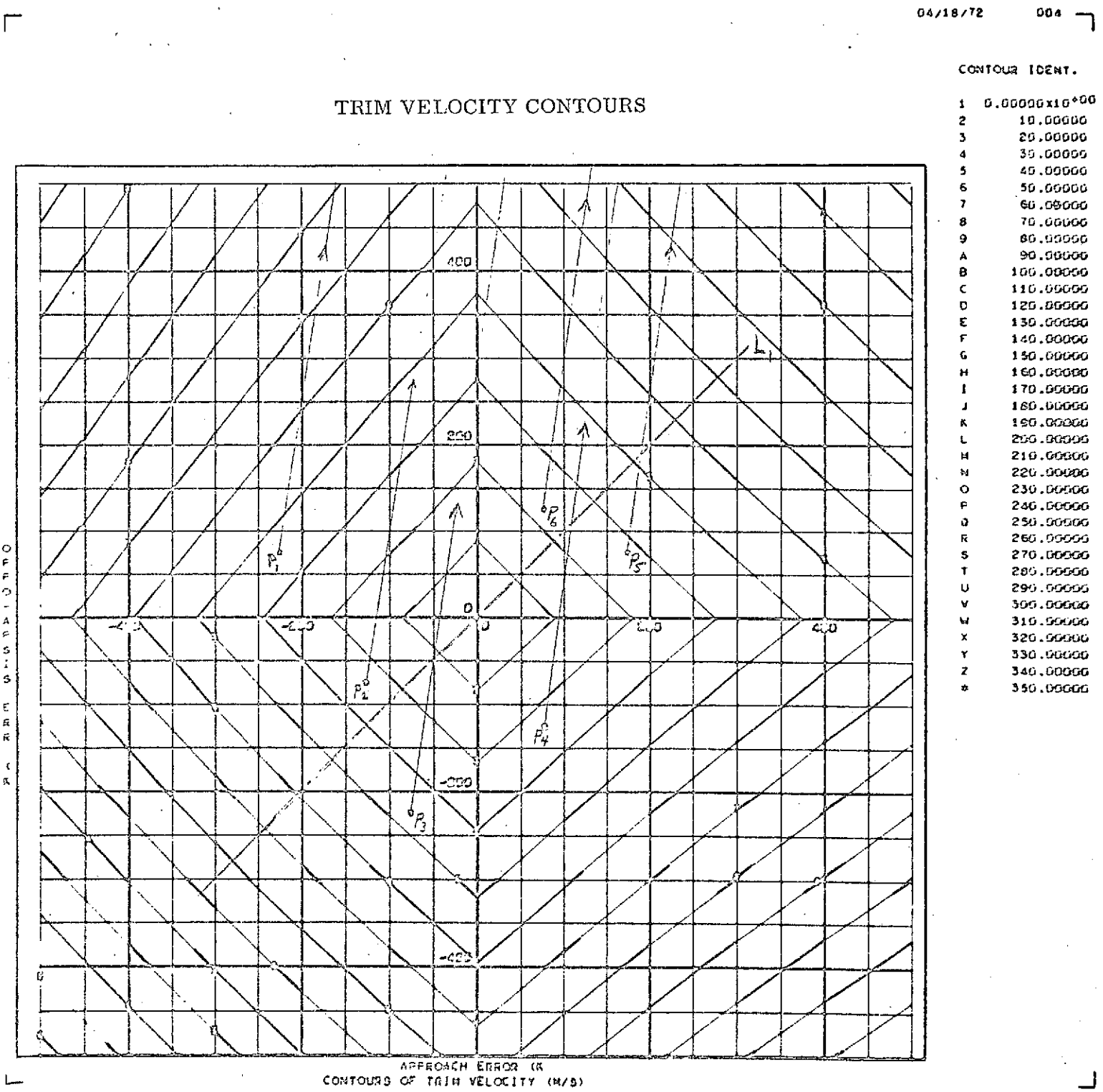
04/18/72 004
TRIM VELOCITY CONTOURS
CONTOUR IDENT.
1 0.00000x10**00
2 10.00000
3 20.00000
4 30.00000
5 40.00000
6 50.00000
7 60.00000
8 70.00000
9 80.00000
A 90.00000
B 100.00000
C 110.00000
D 120.00000
E 130.00000
F 140.00000
G 150.00000
H 160.00000
I 170.00000
J 180.00000
K 190.00000
L 200.00000
M 210.00000
N 220.00000
O 230.00000
P 240.00000
Q 250.00000
R 260.00000
S 270.00000
T 280.00000
U 290.00000
V 300.00000
W 310.00000
X 320.00000
Y 330.00000
Z 340.00000
* 350.00000
100
200
-200
-400
0
-4.0
-2.0
2.0
4.0
L1
P1
P2
P3
P4
P5
P6
OFFSET ERR (R
APPROACH ERROR (R
CONTOURS OF TRIM VELOCITY (M/S)

r_p = 2838 km and δv = .7 km/sec. Let us investigate each point.

P_1 and P_6	The best strategy is to fire at periapsis.
P_2	Fire at periapsis for best circularization but at the radius where the attainable locus crosses the y-axis for minimum trim.
P_3 and P_4	Better firing radii can be found for retro-fire for either circularization or trimming to r_d.
P_5	The trim-minimum retro-fire location is periapsis, but the orbit could be circularized further out.

Final Midcourse Strategies

Figure 3.31 shows the same trim contours as figure 3.30, but has some different loci drawn over the contours. L_2 and the two lines parallel to it are loci of points attainable for fixed C_3, δv pairs by moving periapsis radius, r_p. It is reasonable to assume that r_p can be changed by a midcourse correction with relatively little change in C_3 or δv.

Any point in the half-plane above L_2 corresponds to an underburn at r_d while any point below L_2 corresponds to an overburn at r_d. The figure shows that above L_2 it is best to make $r_p = r_d$ so that the x-axis error is zero to minimize trim velocity (with no energy change). Below L_2, the midcourse maneuver should be targeted to the intersection of the r_p-locus and L_3. L_3 is the locus of periapsis points (at various C_3's and δv's) for which it is possible to circularize with an in-plane retro maneuver at r_d. This intersection is always to the left of x = 0. L_3 is the slope = 7 line passing through (0, 0). If the last midcourse correction is targeted to $r_p = r_d$ while the resulting energy and δv correspond to a point below L_2, the trim velocity will be minimized by retro-firing at a radius greater than r_d where y = 0 (second apsis is r_d).

3.3.4 Pre-Targeting Results

The pre-targeting capability of MAESTRO's midcourse guidance mode has been investigated. The results are quite satisfactory. Table 3.7 is presented to illustrate the accuracy of the pre-targeting capability in predicting midcourse maneuvers. Minimum fuel guidance maneuvers were simulated in 10^h steps beginning 10^h after launch of a "hot" June 10, 1973 trajectory. The uncorrected trajectory is characterized by

Figure 3.31

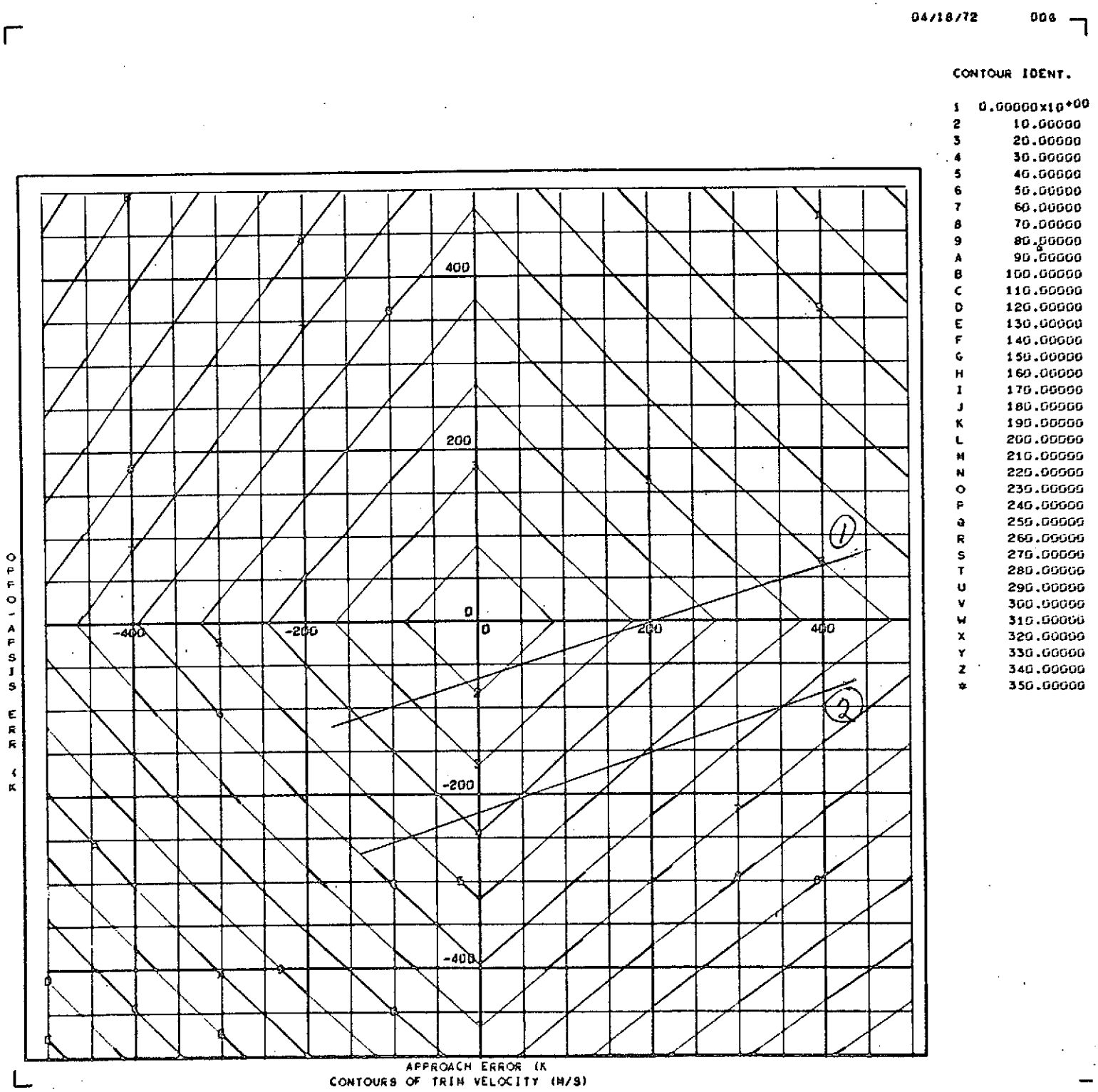

Trim Velocity Contours and Midcourse Partials

$r_p = 40014$ km

$i = 175.77^o$

$t_f = 103.10^h$

$C_3 = .7682$ km^2/sec^2

The first line shown for each midcourse maneuver describes the pre-targeted (P) results. The second line represents the results obtained when the pre-targeted maneuver is applied impulsively to a multi-conic transfer. The third line shows the targeted results (still impulsive, multiconic). The constraint tolerances are 5 km in r_p and $.2^o$ in i. The maneuver is described by impulsive velocity (m/s), right ascension (deg) and declination (deg). ΔRP is kilometers less than 2838 in closest approach radius. ΔI is degrees less than 116.5 in inclination. ΔTF is seconds less than 396000 (110 hours) in time of flight. The energy, C_3, is in km^2/sec^2. The first thing to notice from the table is how little the maneuver parameters and the flight time change during targeting.

Table 3.7

Pre-Targeting Comparisons with Multi-Conic Minimum Fuel Guidance

MC	IT	DVMG	RAS	DEC	ΔRP	ΔI	ΔTF	C3
10^h	P	73.31	72.88	34.60	-	-	6450.	.630
	0	73.31	72.88	34.60	441.4	2.70	12670.	.636
	1	72.82	73.02	36.23	.3	.01	12557.	.637
20^h	P	102.23	77.85	32.79	-	-	10933.	.643
	0	102.23	77.85	32.79	484.5	4.85	16455.	.647
	1	100.77	79.46	33.94	1.8	.03	16931.	.652
30^h	P	129.92	80.91	31.87	-	-	14501.	.656
	0	129.92	80.91	31.87	525.6	6.72	19217.	.657
	1	127.38	82.35	32.81	2.3	.04	19665.	.662
40^h	P	160.13	82.60	31.34	-	-	17279.	.669
	0	160.13	82.60	31.34	506.1*	6.65	21041.	.666
	1	156.99	83.47	32.12	1.7	.03	21206.	.670
50^h	P	197.35	81.58	30.91	-	-	18317.	.675
	0	197.35	81.58	30.91	493.1*	6.63	21087.	.665
	1	193.44	83.12	31.64	3.3	.05	21635.	.673

* represents deviation from the desired radius of the variable approach guidance procedure

Another item of interest in the table is the small size of the closest approach and inclination errors when the pre-targeted solution is propagated to closest approach with the multiconic method. The flight time for the pre-targeted (patched-conic) minimum fuel solution is seen to be about one or two hours longer than the targeted solution. The pre-targeted maneuver is compensated for this time difference by introducing a factor on the transfer time used in solution of Lambert's problem. A final item of interest in the table is the closeness of C_3 (Jacobian energy) for the pre-targeted solution and C_3 for the multiconic trajectory. The Jacobian energy is computed as the square of the Moon-relative velocity at patch to the sphere of influence minus a constant term of about .025 km^2/sec^2. The potential energy term, $\frac{2\mu}{r_{soi}}$ (which is omitted from the energy computation in pre-targeting) has, by contrast, a value of about -.148 km^2/sec^2.

Tables 3.8 and 3.9 are similar to 3.7 in that they show the progression of maneuver and end conditions during targeting. They describe FTA and VTE maneuvers at the same times as the MFG maneuvers of table 3.7, and for the same errant trajectory.

DVMG	midcourse velocity (m/s)
BTE	error in B·T (km)
BRE	error in B·R (km)
FTE	flight time error (seconds less than 396000)
VIE	hyperbolic excess velocity error (km/sec less than $\sqrt{.62}$)
VCE	circular excess velocity error (km/sec less than $\sqrt{\mu/r_{pd}}$)
TFE	total fuel for in-plane trim to r_{pd}(kg)
RPE	radius of closest approach error (km less than r_{pd}= 2838)
INE	inclination error (deg less than 116.5)

3.3.5 Finite Burn Results

Some comparisons have been made between the various methods for simulation of the midcourse burn phase. Of particular interest is how good an approximation the impulsive burn is to the carefully-integrated finite burn. Table 3.10 presents data

Table 3.8

IT	DVMG	BTE	BRE	FTE	VIE	VCE	TFE	RPE	INE
0	77.36	707.	545.	5845.	0.001	-0.019	19.63	519.7	3.43
1	84.92	-25.	-4.	-81.	0.008	-0.013	14.09	-9.8	-0.16
2	84.80	1.	0.	3.	0.008	-0.013	13.92	0.4	0.01

IT	DVMG	BTE	BRE	FTE	VIE	VCE	TFE	RPE	INE
0	109.41	392.	426.	5077.	0.007	-0.005	22.29	365.6	1.35
1	115.57	-7.	-7.	-62.	0.016	0.001	17.14	-6.1	-0.03
2	115.88	0.	0.	2.	0.016	0.001	17.01	0.3	0.00

IT	DVMG	BTE	BRE	FTE	VIE	VCE	TFE	RPE	INE
0	141.60	640.	453.	4176.	0.017	0.011	66.79	490.3	4.74
1	146.04	-15.	-6.	-70.	0.026	0.016	21.59	-7.8	2.73
2	145.96	0.	0.	2.	0.026	0.016	21.27	0.3	0.00

IT	DVMG	BTE	BRE	FTE	VIE	VCE	TFE	RPE	INE
0	176.89	814.	406.	2738.	0.032	0.030	70.67	449.5	4.63
1	179.15	-10.	-4.	-44.	0.039	0.033	26.11	-5.5	2.08
2	179.10	0.	0.	1.	0.039	0.033	25.90	0.2	0.00

IT	DVMG	BTE	BRE	FTE	VIE	VCE	TFE	RPE	INE
0	219.59	512.	346.	593.	0.056	0.055	77.05	333.4	2.45
1	218.77	-1.	-1.	-7.	0.057	0.055	31.36	-0.6	-0.65
2	218.76	-0.	0.	0.	0.057	0.055	31.34	0.1	-0.00

NO-MIDCOURSE APPROACH CONDITIONS

RCA (KM)	INC (DEG)	TCA (HRS)	C3 (K2/S2)	TRACKING
40014.	175.77	103.10	0.7682	86100002

Table 3.9

IT	DVMG	BTE	BRE	FTE	VIE	VCE	TFE	RPE	INE
0	103.06	14.	506.	-8586.	0.020	-0.002	20.35	298.1	-1.75
1	106.58	-1.	-1.	-10256.	0.022	-0.000	15.67	-0.8	-0.00

IT	DVMG	BTE	BRE	FTE	VIE	VCE	TFE	RPE	INE
0	114.05	365.	454.	1692.	0.013	-0.001	23.49	372.5	1.04
1	114.73	-1.	-1.	727.	0.014	-0.000	16.83	-0.8	-0.01

IT	DVMG	BTE	BRE	FTE	VIE	VCE	TFE	RPE	INE
0	132.88	917.	433.	12052.	-0.004	-0.000	28.86	505.1	5.54
1	131.73	-4.	-2.	10712.	-0.002	-0.000	19.27	-2.1	-0.02

IT	DVMG	BTE	BRE	FTE	VIE	VCE	TFE	RPE	INE
0	159.98	925.	373.	20000.	-0.025	0.001	70.59	478.0	5.94
1	157.19	-0.	-1.	19480.	-0.025	0.000	22.83	-0.4	0.00

IT	DVMG	BTE	BRE	FTE	VIE	VCE	TFE	RPE	INE
0	199.03	973.	338.	27082.	-0.057	0.003	75.57	477.5	6.69
1	195.57	5.	1.	27321.	-0.060	-0.000	28.19	2.0	0.03

NO-MIDCOURSE APPROACH CONDITIONS

RCA (KM)	INC (DEG)	TCA (HRS)	C3 (K2/S2)	TRACKING
40014.	175.77	103.10	0.7682	86100002

Table 3.10

Finite Burn Method Comparisons

10^h correction

Method	IT	DVMG	RAS	DEC	RPE	INE	FTE	VIE	TBURN
0	0	73.30	72.52	34.58	436.4	2.57	12565.	-.010	
	1	72.82	73.06	36.23	.4	.01	12569.	-.011	8.75
1	0	73.30	72.52	34.58	419.5	2.09	12588.	-.010	
	1	72.90	73.15	36.21	.4	.01	12612.	-.011	8.76
4	0	73.30	72.52	34.58	419.5	2.09	12588.	-.010	
	1	72.90	73.15	36.21	.4	.01	12612.	-.011	8.76
6	0	73.30	72.52	34.58	400.5	1.33	12601.	-.010	
	1	73.03	73.16	36.21	.3	.01	12616.	-.011	8.78

50^h correction

Method	IT	DVMG	RAS	DEC	RPE	INE	FTE	VIE	TBURN
0	0	196.95	81.68	30.98	447.9	5.88	21119.	-.028	
	1	193.44	83.16	31.64	2.8	.04	21657.	-.033	31.14
1	0	196.95	81.68	30.98	337.2	.88	21081.	-.029	
	1	195.97	83.18	31.63	2.4	.02	21684.	-.033	31.62
4	0	196.95	81.68	30.98	343.1	1.53	21082.	-.029	
	1	195.66	83.62	31.60	3.0	.01	21928.	-.034	31.56
6	0	196.95	81.68	30.98	373.7	2.50	21104.	-.029	
	1	195.04	83.28	31.62	2.3	.02	21744.	-.033	31.44

for four methods of simulating the midcourse burn phase.

IBURN	Method
0	Impulsive burn
1	Cowell integration of the burn
4	NICE/Mean integration of the burn
6	Closed-form/Multiconic burn approximation

The trajectory represented in Table 3.10 was a June 10, 1973 "hot" trajectory. Ignition times of 10^h and 50^h were considered. The 10^h correction required a burn duration of about 8.75^m while the 50^h correction required a burn of about 31.5^m (too long, considering available fuel) for the minimum fuel maneuver. The zero-th iteration for each method was primed with the same impulsive ΔV from pre-targeting. The pre-burn and post-burn trajectory method was multiconic in each case. The column headings have the following meanings.

IT	Iteration number
DVMG	Impulsive velocity magnitude (m/s)
RAS	Right ascension of thrust (deg)
DEC	Declination of thrust (deg)
RPE	Radius of closest approach error (km less than 2838)
INE	Inclination error (deg less than 116.5)
FTE	Flight time error (seconds less than 396000)
VIE	Hyperbolic excess velocity error (km/sec less than $\sqrt{.62}$)
TBURN	Midcourse burn duration (minutes)

Each midcourse burn is targeted to RPE and INE tolerances of 5 km and .2 deg, respectively while constraining the maneuver ΔV to lie in the critical plane. Several observations can be made about the data presented in Table 3.10.

1. The impulsive approximation errors are only about the size of expected resolution and pointing errors for the earlier correction and are still almost negligible for the later correction.

2. The variation of the Method 6 solution from the impulsive solution is greater than that of Methods 1 and 4 for the 10^h correction, but less for the 50^h correction.

3. Flight time for the MFG solution does not change very much between methods. The change in FTE between impulsive and other methods is much less than the burn duration, indicating suitability of applying the impulse at ignition time.

4. Methods 1 and 4 give exactly the same results for the 10^h correction, but differ for the 50^h correction. The difference may be due to the integration step size being too large (it is the burn duration) for one method or the other.

SECTION 4

ON-LINE CONTROL AND DISPLAYS

This section will describe the methods for communication between the Flight Director and the mission control program. The Flight Director must have a means of controling the scope of the analysis. He will determine which analysis will be performed at which times. The Flight Director must also be provided with displays which present the information in a concise, easy-to-read format. The first section describes the method which will enable the Flight Director to control the analysis. The second section describes the displays which are generated for the Flight Director.

4.1 CONTROL

Figure 4.1 is an overall block diagram of the mission control system. The system is controlled by the Flight Director. He is in charge of all mission analysis operations and is responsible only to the Mission Director. The Flight Director will control the analyses through the 2250 console using the Graphic Terminal System. GTS is a system executive which controls the submittal of jobs to the 360/75 computer. This system also has the capability to retrieve and edit data files with the use of the 2250 light pen and typewriter. By using this system, inputs which determine the type of analysis performed by MAESTRO can easily be controlled by the Flight Director. GTS has been used during several simulations and has functioned satisfactorily. The use of GTS will not degrade the reliability of MAESTRO because the card input capability of MAESTRO is still retained. Thus, MAESTRO can still be used in the event of a failure of the 2250 or on another computer if scheduling conflicts exist with the orbit determination or attitude determination programs on the 360/75.

The Flight Director has the responsibility for all operations of MAESTRO and he will decide which analyses are required at which times. A team of spacecraft experts and the mission scientist are available for consultation with the Flight Director. This team will help evaluate the effects of mission analysis decisions on the basic scientific objectives of the mission and operational characteristics of the spacecraft.

Mission Control System Block Diagram

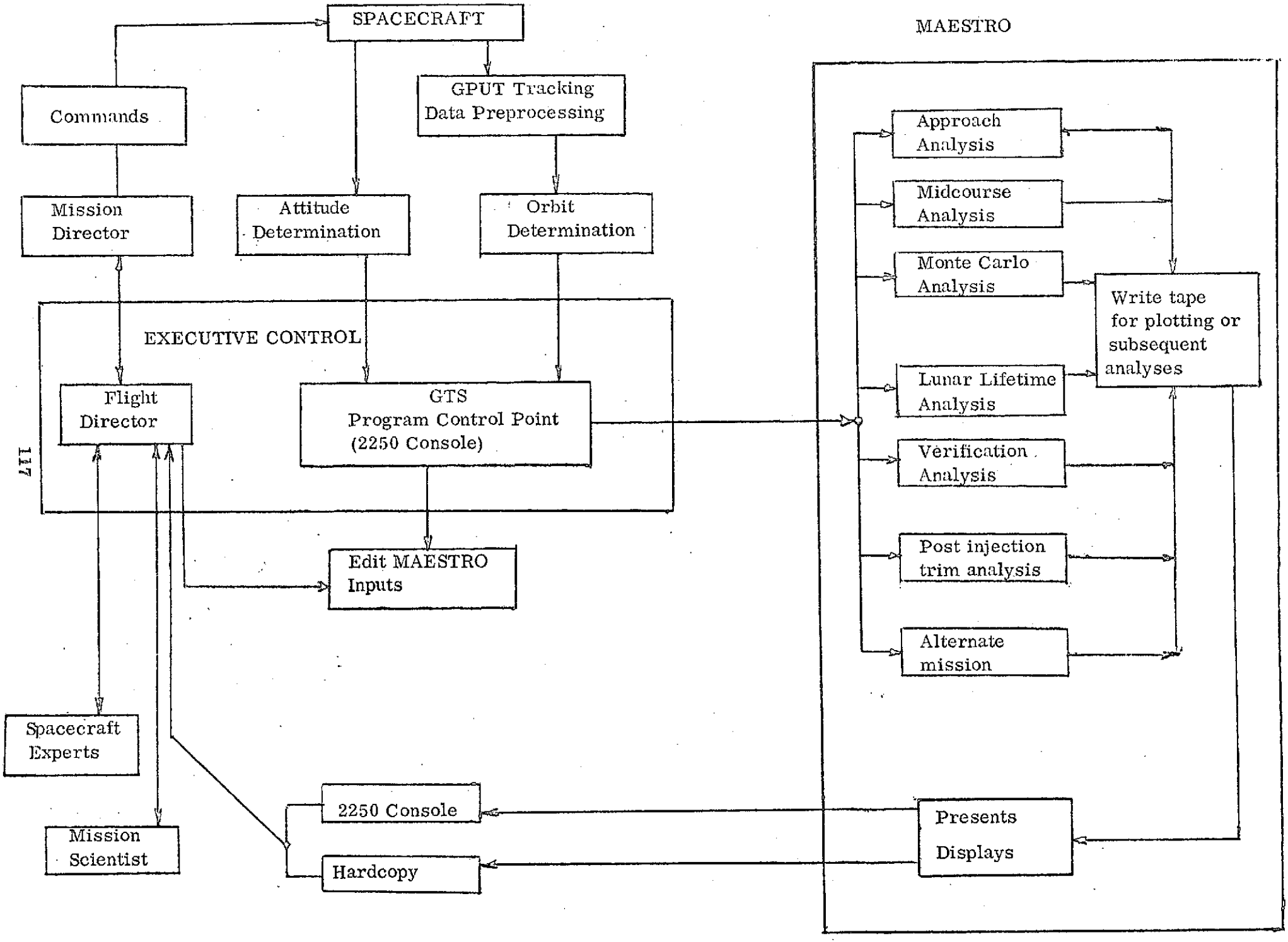

Figure 4.1

MAESTRO was designed with many operational modes to provide the Flight Director with the capability of performing the necessary mission analysis tasks as rapidly as possible. The operational modes of MAESTRO were defined in Section 2. Here they will be described according to their roles in the decision-making process.

A. Preliminary GO/NOGO analysis

As soon as a preliminary state is available from the orbit determination program, midcourse analysis runs will be made to determine the amount of fuel required and approximate execution time for the first MC maneuver. This data provides the Flight Director with the information to determine whether the primary mission is achievable and the amount of analysis time available until the first command decision must be made.

B. Refined Midcourse Analysis

Many midcourse analysis runs will be made with different guidance laws and execution times to determine the final midcourse velocity and attitude.

C. Verification of the Midcourse Decision

Precise midcourse and approach analysis runs will be made to verify the decision made in B. Monte Carlo runs will be made to verify that the decision will provide a high probability of mission success.

D. Lunar Approach Analysis

Approach analysis runs will be made to determine the retro firing time and attitude.

E. Lunar Approach Verification

Precise approach analysis runs will be made to verify the decision made in D. Monte Carlo runs will be made to verify that the decision will result in a high probability of mission success.

F. Post Injection Trim

The post injection trim analysis will be used to determine the firing times and attitude of the impulse(s). This analysis will be used in both an approximate and precise modes.

G. Alternate Mission

In the event of a launch vehicle of spacecraft failure it may be possible to achieve an orbit which will still yield valuable scientific data. The midcourse or approach analysis modes can be used to determine the maneuver to achieve an acceptable alternate mission. These analyses can be performed in both approximate and precise modes.

4.2 DISPLAYS

MAESTRO will have the capability of presenting displays via the 2250 console, on hardcopy or as the output from a plotting processor. These displays will have levels of complexity that will range from an easy to read outline form to a comprehensive presentation of the analysis performed. The current displays available in MAESTRO are shown in the uses guide, reference 2. These displays are obtained on the 2250 console under GTS and hardcopies are also printed. It was found that the 2250 screen is hard to read because the images were constantly blinking. Thus, hardcopies of the 2250 displays should be provided to the Flight Director as soon as possible.

The displays contained in MAESTRO provide the Flight Director with a means for rapidly accessing the spacecraft's capability under various in-flight mission situations. The basic ground rule used in designing the MAESTRO displays was to provide the Flight Director with all of the information he needs without clouding the problem with too much information. In some cases this necessitated more than one display for an analysis mode. For example, the approach analysis displays have two levels of complexity. One display provides the Flight Director with a rapid estimate of the retro motor's attitude which results in a minimum post injection trim requirement. A second display provides comprehensive information about each trial firing at the desired attitudes. All of the displays available in MAESTRO are discussed in the following paragraphs.

RETRO FIRE ANALYSIS

There are two different displays presented in this analysis. One display is a summary type of display presenting minimum eccentricity and post injection trim fuel requirement at the retro attitudes tried. This display is actually a contour map printed by the computer and depicts the attitudes which result in the minimum trim fuel requirement.

The Flight Director can use this display to isolate the desired range of attitude.

A second display presents, detailed information about each trial retro firing. This display contains the mission constraints and post retro orbital elements as a function of firing time for each attitude. The display is set up so that a page is devoted to each retro attitude. Thus, it is easy to see that the Flight Director could easily be snowed under by the output from this mode. The first display is included to eliminate the undesirable attitudes so that the Flight Director will not have to waste his time sifting through a large stack of output searching for good attitude angles.

The information from the retro firings can also be saved on a tape. This tape can later be used with some type of post processor or a plotting program.

MIDCOURSE ANALYSIS

The displays presented by the midcourse analysis provide the Flight Director a means of accessing the spacecraft's capabilities as a function of the available control variables. Logic is included to automatically scan the execution time and flight time so that a display presenting the fuel requirement and constraints as the above quantities are varied can be presented. The display also contains information about execution errors and retro conditions. The execution error portion of the display contains the error elipse at the target planet of the quantities targeted. It also contains the expected second midcourse requirement. The retro portion of the display presents the retro firing time, attitude, mission constraints and post injection trim requirement after retro for each midcourse correction. The quantities derived for this display assume an errorless midcourse correction.

A second display is also available from the midcourse analysis mode. This display presents the target planet conditions as a function of firing time, midcourse velocity and attitude. This display was included for two reasons. First, as a failure mode analysis tool in case of attitude control failure. The midcourse requirement can be determined for any fixed attitude or range of attitudes if the spacecraft's attitude is constrained for some reason.

This display can also be used to determine the stability of some predetermined midcourse maneuver. The execution time, velocity and attitude can be scanned about

some selected maneuver to determine the affects of errors of one of the above quantities on the conditions at the target planet.

A tape is also written from this analysis for use in a plotting program.

MONTE CARLO ANALYSIS

The Monte Carlo analysis display contains information about each sample and a statistical summary at the end of the analysis. The information printed for each sample is the fuel, its mean value of the past samples for the first and second midcourse, first second and third trim maneuver and fuel remaining. The spin axis-sun angle, its mean and standard deviation is also presented for the maneuvers mentioned above along with the retro spin axis sun angle. The pre-trim orbital elements, their mean and standard deviations are also presented. These elements include the apo and periapsis radius, argument of perigee, inclination, longitude of the ascending node, true anamoly and retro firing time. The information presented for each sample provides the Flight Director with the specific details of each sample and indicates when enough samples are run. As an option, the Flight Director can also obtain information to restart any sample which he thinks might require more analysis.

A statistical summary is printed at the end of the display. This summary presents the mean, maximum value encountered and standard deviation of all the quantities mentioned above. This includes the fuel and spin axis-sun angle of all the maneuvers and the pre-trim orbital elements.

VERIFICATION ANALYSIS

The display contained in the verification analysis can be divided into three parts, real-time thrusting analysis, station coverage and target planet conditions. The real-time thrusting display is used to obtain information that can be used while the midcourse motor is burning. This display presents the spacecraft thrust, weight and velocities away from the visible tracking stations as a function of time since ignition assuming a nominal engine burn. The thrust data can be converted to chamber pressure data and an expected doppler shift determined from the velocities away from the visible tracking stations. This data can then be compared to the real-time telemetry data and corrective action initiated if the telemetry data wildly differed from the predicted data.

The tracking coverage display presents the local time, elevation angle and azimuth angle of the spacecraft for each of the tracking sites at the time of midcourse engine ignition.

The last part of the verification display presents a summary of the motor firing conditions and the conditions at the target planet. The motor conditions include the burn time, attitude and spin axis-sun angle at ignition. The conditions at closest approach to the target planet are presented. These are the time of closest approach, radius and inclination with respect to the target planet's equator.

POST INJECTION TRIM ANALYSIS

The post injection trim display available presents the elements of the initial orbit, transfer orbit and final orbit. The firing time, magnitude, direction and spin axis-sun angle of each trim maneuver is also output. This display is automatically presented for two types of trim maneuvers. First, a two impulse plane-change maneuver. The other type of maneuver is a two impulse Hohmann transfer maneuver with no plane change.

SECTION 5

OPERATIONAL LOGISTICS AND TESTING

This section contains a description of important factors concerning the decision-making processes. The first subsection presents a typical sequence of events for this mission and emphasizes the necessity for a smooth man-machine interaction. The second section describes possible failure modes and presents contigency plans in case some of these failures should occur. The last section shows how tests have been conducted on the MAESTRO system to insure its reliability.

5.1 FLIGHT PROFILE OUTLINE

In Reference(1) a fairly detailed outline of the probable sequence of events was presented but there was little said about the timing of events. Some preliminary estimates on the timing for the key elements of the system are now available and it is important to consider the sequence in which these elements will be used.

Suppose, for clarity, that the launch is initiated at Cape Kennedy on June 10, 1973, 12:00 hours GMT. Suppose further that the nominal third stage burnout time is 15 minutes after liftoff.

At the time of liftoff, or before, the entire mission control system should begin a test exercise to verify that all elements of the system are operational at that time. All data channels, storage devices, and operational modes of the system should be briefly tested in a way that will show up any possible problem.

Let us now suppose that the third stage injects the spacecraft into its translunar trajectory at 12:15 GMT and that tracking data begins coming in a 12:30. This possible delay is trajectory dependent but we assume for illustration that the time between translunar injection (TLI) and first acquisition by one of the

tracking stations is 15 minutes. Assume that it requires 15 more minutes of tracking, data processing, and differential correction to obtain a reasonably accurate but unrefined state vector. This vector may now be entered into the mission control program for a preliminary midcourse sweep 1) to establish a rough idea of the situation and 2) to dtermine the approximate amount of time available for analysis and attitude maneuvers before the first midcourse correction.

At the same time tracking data is first acquired, telemetry from the attitude sensors can also be expected. The relative speed with which the orbit and attitude can be determined may be more important than assumed here but let us suppose that a rough estimate of the burnout attitude can be obtained from the direction of velocity vector at TLI or from the nominal value of that direction. In any case, it is time for MAESTRO to determine the time and magnitude of the required 1st midcourse correction.

The midcourse sweep mode of the MAESTRO can be run in about 30 seconds (360/75) per guidance law with 10 trial firings ranging from 2 to 20 hours past liftoff. After the initial rough determination of the state, the major resources of the computing system should be turned over to the MAESTRO while three or four guidance laws and an approximate approach analysis are run. The time required will be about five minutes and the computer should then be instantly returned to the Orbit and Attitude Determination Programs (ODP and ADP) for intensive tracking and the refinement of the estimated state.

The early stages of control, then, can be summarized as follows:

GMT	
12:00	Lift off-start of final testing operations
12:15	Launch phase completed
12:30	Acquisition by Tracking System
	Initiation of Orbit and Attitude Determination Operations
12:45	Preliminary Anchor Vector Ready
	Possible Rough Attitude Data

	Preliminary Midcourse Corrections and Approach Analysis
12:50	Initiation of Intensive Orbit and Attitude Determination operations
	Probable Acquisition by 2nd Tracking Station
	Evaluation of Midcourse Sweep Results

Assume, now, that the energy of the translunar orbit is considerably in error and that the midcourse sweep results indicate that the 1st midcourse correction should be performed as soon as possible. The attitude maneuver sequence should be initiated immediately so as to permit the early correction. Suppose that the decision to begin the maneuver is taken in the 10 minutes between 12:50 and 13:00. The remainder of the control sequence might be as follows:

13:00	Accurate Attitude Available
	At least two stations tracking spacecraft
	Decision to initiate attitude maneuver
13:05	Commands to Spacecraft Attitude Control System
	ODP has computer for refined orbit determination
13:15	Refined orbit available
	Attitude maneuver in progress
	Computer to MAESTRO for detailed midcourse analysis
13:20	Attitude maneuver in final stages
	Detailed midcourse analysis complete
	(Desired Attitude Known)
	Final trim pulse of ACS
	Computer to ODP and ADP for verification

The haste with which the above operations have been performed correctly indicate that the hypothetical situation is critical and that further delay will probably result in an unsuccessful mission. At this point, then, a critical decision is required of the mission and flight directors. If the ODP and ADP have relatively good estimates of the state, it may be wise to dispense with any refinements in the control process and to perform the first midcourse maneuver.

The decision-making process would be a trying one in which the risks of making a hasty decision would have to be carefully weighed against the probability of having insufficient fuel to complete the mission.

The consideration of such a rapid 1st maneuver control sequence assumes that very unlikely launch vehicle dispersions have occurred but it seems important to determine the worst possible situation that could still be turned into a successful mission by emergency use of the midcourse correction system. Further, there may be good reasons, of which this writer is unaware, why the initial control sequence outlined above simply cannot be executed in the imaginary time scale of the outline. The outline, then, should be considered as a suggestion that the earliest time at which an emergency 1st midcourse maneuver can be initiated is approximately 90 minutes after liftoff. The schedule above is, in any case, a goal to aim for in establishing the response time of the system. In most cases, the much more conservative outline of the design study final report should be followed.

We come now, to the consideration of the maneuvers to be carried out after the spacecraft has been placed in lunar orbit by the solid retro-rocket. A very important difference in the situation will now be realized; the operations will no longer be time-critical. In the event of a large retro-rocket errors or other complications, the mission may be fuel-critical but we can expect to have plenty of time for analysis and should not unduly rush the trim operations. Indeed, it will be desirable to track the spacecraft for some time after lunar orbit insertion in order to study the effects of the lunar gravity on the orbit evolution and, thereby, to verify the adequacy of the existing models of the lunar potential.

Consider then, as we always should, what might happen in the real-time control center after the news is received that the spacecraft has been successfully placed in lunar orbit. The optimal orbit insertion attitude (from dynamic considerations) will probably not be compatible with the desired cruise-mode

spin-axis orientation and it will probably be necessary to reorient to an attitude that is commensurate with the power and communication requirements of the spacecraft. Of course, the lunar orbit should be checked for short-term stability before a reorientation is performed. This check will guard against an early impact or wild gyrations of the orbit in case of very large deviations from the nominal retro performance. The check, however, should be an integral part of the lunar orbit insertion verification procedure and is not considered as part of the time-uncritical trim maneuvers.

The post-insertion operations, then, should begin with an orbit verification procedure and the operations should approximately follow the outline below.

I. Lunar Orbit Verification Procedure (Time Critical)

   a. Post Injection Orbit Determination.

   b. Post Injection Attitude Determination.

   c. Verification of Short-Term (several weeks) Orbit Stability

      1. Stable Orbit - Go to II
      2. Unstable Orbit - Commence Emergency Trim Maneuvers.

II. Attitude Reorientation Decision (Time Uncritical)

   a. Existing Attitude Suitable for Cruise Mode - Go to III.

   b. Existing Attitude Unsuitable for Cruise Mode - Reorient to Desired Cruise Mode Attitude.

III. Verification of Lunar Gravity Models

   a. Intensive Long-Term Tracking.

b. Existing Gravity Models Adequate for Long-Term Orbit Prediction - Go to IV.

c. Existing Models Inadequate - Perform Lunar Gravity Model Determination (separate program - not in Mission Control program)

IV. Trim Maneuver Policy Decision

a. Number of Maneuvers Required
(Minimum Fuel vs. Risk of Multiple Maneuvers)

b. Effects of Shadowing and Occultation on Trim Policy.

V. Statistical Analysis

a. Probability of Mission Success vs. Trim Motor Ignition Time and Attitude.

b. Definitive Orbit Evolution Prediction.

VI. First Trim Maneuver

a. Reorient Spacecraft for Trim Motor Ignition.

b. Commence Trim Motor Ignition Sequence.

c. Monitor Telemetry During Trim Maneuver.

VII. Post-Trim Evaluation

a. Intensive Calculations.

b. Orbit Evolution Calculations.

c. Mission Requirements Satisfied?

No - Go to IV and repeat.

Yes - Turn over spacecraft to boom - deployment experts.

Flight dynamics control completed.

5.2 CONTINGENCY ANALYSIS

It should be noted at the beginning of this section that the items of discussion are necessarily of a pessimistic nature and that there will probably be a tendency for the people involved to rebel against the consideration of the many possible ways in which the mission might fail of partially fail. No one wants the mission to fail and the discussion of the possibilities may set loose psychological factors that will be detrimental to the objective consideration of the action to be taken in such situations.

For example, if we consider the possibility that the computer logic in the mission control program will fail in some unforseen situation, the planners and programmers may have a tendency to discount the probability of occurrence of such difficulties. If we discuss the possibilities of the failure or partial failure of the spacecraft hardware, the designers of the spacecraft system may feel slighted and unwilling to consider some failure modes as viable possibilities. It seems important to attempt to dispel such inclinations at the outset so that effective contingency measures may be preplanned in a way that will not be clouded by the egocentric factors that affect us all. Let it, therefore, be clearly understood that the following suggestions of possible failure are made with purely constructive intent.

The major areas of possible failures can be classified as follows:

I Hardware Malfunctions

II Computer Software Errors

III Human Errors

Although the Hardware and Computer Software categories might, in a broad sense, be considered human errors, the third category now refers to those

errors in judgement or communication during the in-flight operations that could, in post-flight analysis, be considered causes of an unsuccessful mission.

I Hardware Malfunctions

This category is the most extensive because its possibilities affect the entire in-flight operation to a marked degree. The malfunction of any piece of hardware opens up many possibilities for computer software inadequacies and human error, where-as in-flight failures in categories II and III do not affect the operation of the spacecraft.

The possible hardware malfunctions are numerous and are further classified as follows:

A. Spacecraft Hardware Malfunctions
   1. Launch Vehicle (large Errors)
   2. Midcourse Correction and Lunar Orbit Trim System
   3. Attitude Determination and Control System
   4. Lunar Orbit Injection Retro Rocket
   5. Spacecraft Power and Communication Systems

B. Computer Hardware Malfunctions
   1. Input/Output Hardware Failure
   2. Partial Memory Failure
   3. Mainframe down temporarily
   4. Power Failure

C. Tracking System Malfunctions
   1. Communication link failure
   2. Station malfunctions
   3. Data Processing Equipment failure.

D. Uplink Command Hardware Malfunctions

II Computer Software Errors

A. Orbit Determination Software

1. Preprocessing Software Failure
2. Diffential Correction Program Failure
3. Data Transmission or Storage Errors.

B. Attitude Determination Software

1. Preprocessing Software Failure
2. Attitude Calculation Errors
3. Underestimate of Required Attitude Control Fuel
4. Data Transmission or Storage Errors

C. Mission Control Program Software

1. Midcourse Guidance Calculation Errors
2. Required Attitude Calculation Errors
3. Retro Rocket Ignition Time Calculation Errors
4. Incorrect Evaluation of Required Trim Fuel
5. Data Transmission or Storage Errors

III Human Errors

A. Errors in Planning

1. Errors in assignment of priorities during the flight
2. Errors in scheduling work

B. Errors in Communication

1. Incorrect or Poor Descriptions of Situation
2. Unclear Definition of Work Assignments
3. Unclear Presentation of Results
4. Poor Definition of Objectives and Priorities

C. Errors in Judgement

1. Incorrect Evaluation of the Situation
2. Faulty Evaluation of Probability of Success

The outline above is a compilation of the areas in which malfunctions and errors might occur that would be either totally or partially disastrous. There may be other important possibilities that have not been considered. In the discussion that follows, three of what are thought the most likely failure situations are considered.

Three important failure modes that could cause the mission to be unsuccessful are:

a. Midcourse and Trim Propulsion System Failure

b. Attitude Control System Failure

c. Retro Rocket Failure

These three most drastic possible malfunctions are considered below in order to suggest what might be salvaged in the event of such failure.

a. Midcourse and Trim Propulsion System Failure

The malfunction or failure of the midcourse system at any time prior to lunar orbit insertion would turn the mission control problem into an AIMP-E type decision-making process. The attitude and ignition time for the retro-rocket would then constitute the only control parameters available for use.

The current capabilities of the MAESTRO are adequate to provide sufficient information for the mission director to determine the "best" attitude and retro ignition time from the standpoint of the mission requirements. The approach analysis and retro attitude optimization are integral parts of the current system and could be used in the deterministic or Monte Carlo modes of the program to aid the mission director in making the probably unsatisfactory "best" decision in case of midcourse and trim system failure.

b. Attitude Control System Failure

This possible problem has been considered and steps have been taken to permit inflight evaluation of such a contingency. The solution, in the case

of ACS failure, would be to determine the ignition times and durations of the many midcourse corrections that would be required to salvage the mission.

There seems to be no reason why, with the large propulsive capability of the spacecraft, a satisfactory lunar orbit could not be achieved in many cases. Of course, the results would depend upon when the ACS failed (that is, upon the actual value of the fixed attitude) but it seems obvious that many possible situations could be handled in a satisfactory way be multiple midcourse corrections and trim maneuvers. The capability to analyze such situations has been incorporated into MAESTRO in the form of a fixed attitude guidance law.

c. Retro Rocket Failure

This possibility is probably the most catestrophic of all because of the large energy change supplied by the (single) firing of the solid rocket.

It is this writer's understanding that some of the experiments on-board the RAE-B spacecraft would not be seriously impaired if the orbit were highly elliptic with respect to the Earth. These experiments might be saved or helped by the use of the midcourse correction system after the retro rocket failure to prevent a very close approach to or impact on the Earth.

When the flight plan called for a leading approach to the Moon, it was conceivable that the midcourse and trim propulsion system could be used, after jettison of the faulty retro rocket, to adjust the highly elliptic Earth orbit so that a substantial lifetime could be achieved. Since the revision of the flight plan to yield a trailing approach, it has been found that the nominal trailing swingby precludes the possibility of using the midcourse motor to establish a stable Earth orbit. The energy gained during the close trailing approach is so great that the spacecraft will escape the Earth-Moon system unless the retro-rocket is fired and the midcourse propulsion system cannot provide

enough impulse to reestablish an elliptic orbit about the Earth.

The failure of the retro-rocket, then, should be considered catastrophic for the mission if the lunar approach is near nominal. If, however, there is some early indication that the retro-rocket might not fire, it may be wise to change the aiming point so as to lower the energy gained during the flyby so that the spacecraft will not escape the Earth-Moon system. Studies are underway to evaluate the cost and the Earth orbit options available in case of this not very likely situation.

5.3 SYSTEM TESTING

MAESTRO was tested in December, 1971 during two three-hour sessions on the GSFC 360/75 computer. The program was operated under control of the Graphic Terminal System via the 2250 graphic display console. The various options of the program were tested for a simulated in-flight situation. Unfortunately, due to scheduling problems and computer hardware failures, it was not possible to exercise the program interface with the Orbit Determination Program but some tests were made in which the ODP and MAESTRO were in core at the same time. It was found that either of these highly compute bound programs can cause the other to run considerably slower than it would otherwise. If the 360/75 is to be the primary computer for the launch, it will be necessary to arrange a rigid schedule for assignment of priority to the two programs. In the event of a large translunar injection error it may be necessary to run the two programs on separate computers in order to insure that the first midcourse calculations can be performed in time to make the actual maneuver.

The internal operation of MAESTRO during this simulation was quite satisfactory although several minor problems were discovered and corrected. Had the spacecraft actually been in flight, it would have been possible to execute the first midcourse in a way which, although not optimal, would have resulted in a successful mission. Assuming that the first midcourse was executed correctly, it would have been possible to determine the retro firing time and

attitude which would result in a successful lunar orbit.

The long-delayed first full-participation simulation was held on Wednesday, June 14 and the results were very encouraging. With a few noticeable exceptions, the simulated decision-making process went very smoothly and provided a valuable first step in the consolidation of the three major components of the system. It was obvious that everyone had done considerable homework in preparation for the exercise and that most of the problems were do to interactive aspects of operation father than to lack of preparation. The remainder of this section will be concentrated on the problems so as to focus attention upon them and prevent their future occurrence.

The major operational difficulties can be classified in three areas;

1. System Problems (GTS)
2. Communication Problems
3. Programming Problems

The following is an abbreviated record of the simulation in chronological order:

June 14, 1972

21.00 GMT	360/75 available for use
21.11	Graphic Terminal System (GTS) up
	Two Problems 1. Wrong version of GTS 2. Attitude Determination Program (ADP) not ready for loading
21.24	Attempted reloading of GTS and programs
	Unsuccessful - JCL error
21.37	All programs ready for operation
21.41	Tracking data (simulated) coming in - GPUT processing data
21.43	Orbit Determination Program (ODP) processing data
21.48	Two iterations of differential correction (DC) process complete in ODP
	ADP processing (simulated) data using nominal orbit data
21.55	Flight Director (FD) waived 4th iteration of DC. ODP out, MAESTRO(M) in core.

22.02	Attitude available to within about 3 degrees assuming nominal orbit.
	ADP was not aware that M required attitude information at this time.
22.04	M starting midcourse guidance calculations with anchor vector (AV) from 3rd iteration of DC.
22.08	Fixed Time of Arrival (FTA) Guidance sweep completed
	Problems: 1. Midcourse guidance calculations taking 4 times longer than expected. 2. Rewind error in M - corrected through input array.
22.12	M out - ODP in core GPUT processing second pass of simulated data.
22.19	Problems: 1. ADP unable to read AV from ODP 2. ADP previously unaware that 1st AV was available
	AV entered into ADP by hand.
22.20	ADP running with 1st AV
22.25	Attitude available to about 1^{o}
22.26	ODP beginning to process second pass of simulated data
22.42	First iteration of 2nd pass data finished on DC
22.43	Second AV to M - ODP out of core.
	Start midcourse sweep with 4 guidance laws.
22.46	ADP unaware of new AV
22.57	Midcourse sweeps with 4 guidance laws completed on M.
	Problem: Slow calculations confirmed. Midcourse sweeps required 12 minutes - earlier tests with same software showed 4 minute running time.
22.58	New AV to ADP
23.05	M still in core - Beginning Midcourse Verification at 10 hours with FTA guidance law.
23.10	Midcourse verification still running - should have finished in a few seconds.
23.11	Midcourse run with numerical integration submitted.

23.12	ODP operators confirm very slow running time problem ratio 4 or 5 to 1.
23.21	Midcourse verification run lost. Very large I/O time for run in accounting information.
23.27	Desired attitude to ADP for Attitude Control System (ACS) command sequence calculations.
23.30	M out, ODP in core for simulation of lunar orbit tracking.
23.32	Bad start of ODP - incorrect input caused termination.
23.33	ODP operational again.
23.41	ADP finished with first try at generation of ACS command sequence.
	Problem: Command sequence incorrect. Timing for command sequence approximately correct.
23.47	Two passes of lunar orbit data to ODP - starting DC.
24.04	Starting 7th iteration on DC for lunar orbit - results fair-trying one more iteration.
24.10	Simulation halted.

The outline above shows the general flow of the simulation and the problems that were encountered. Of the most importance are the timing of the separate operations and the interaction (or lack of it) of the major components of the computing system.

After this successful June simulation, testing efforts were devoted mainly to preparation for the IMP-H launch operations in September 1972. These tests were conducted with a modified version of the MAESTRO program and , while the attitude and orbit determination programs were different from the ones that will be used for RAE-B, the required operations were very similar to those for the lunar orbit mission. The use of MAESTRO for IMP-H was, by far, the best kind of testing we could have wished. The differences, both psychological and operational, between a simulation and an actual launch are so great that the experience gained during the IMP-H launch was worth several RAE-B simulations in spite of the differences in the flight profiles.

Since the September launch of IMP-H, there have been several attempts to conduct a realistic RAE-B simulation but these have included little more complexity than the testing of the interfaces between the various computing systems. Very recently, some more thorough simulations have been held but the author was not involved and cannot report on the effectiveness of the tests. A significant feature of the most recent tests is that simulated data can now be generated during the simulation and this capability adds a great deal of flexibility to the operational tests.

A schedule has been established in which simulations are to be held every other week from now until the launch. Every effort should be made to make these simulations as realistic as possible and a standardized schedule of operations should be established as nearly as is possible with the changing computer hardware and software.

There is an important aspect of the entire MAESTRO design and development work that has received no overt recognition but has contributed to the effectiveness of the preparation for the launch. This aspect is the freedom to criticize the launch support operations as the shortcomings become noticeable. It is not usually acceptable for a contractor to criticize the Government but, throughout the MAESTRO development, there have been several points which have been the subject of controversy and for which our opinions have been freely voiced with the most constructive intent. This freedom to discuss what is wrong has been very helpful in allowing us to come to grips with many problems and has increased the usefulness and launch readiness of the MAESTRO program.

Internal checks are constantly being conducted with MAESTRO. This is accomplished by comparing the results of the various program modes against each other and against independent programs. The use of the GSFC 360/91 computer for program development has greatly assisted in the testing of MAESTRO. Goddard personnel are now able to use new program capabilities as soon as they are available or, sometimes, while still in the development stage. The error detection abilities of Goddard's personnel are uncanny. Their help in this area and their general advice is greatly appreciated.

SECTION 6

CONCLUSIONS

A description of the MAESTRO program has been presented. The capabilities and various operational modes have been described in a general way and the reader has been referred to the programmer's and user's manuals for more details. It has been emphasized that the program's flexibility is one of its principal assets and that the all-FORTRAN block-style development is largely responsible for the internal flexibility and ease of modification.

The major operational modes are:

1. Trajectory Propagation
   Method and Integrator Optional
2. Midcourse Guidance or Kick-Motor Firing Analysis
   Includes Statistics of Propagated Errors
3. Lunar or Planetary Orbit Insertion Analysis
4. Orbit Trim Analysis
   One, Two, or Three Impulse Transfer
5. Midcourse and Orbit Trim Verification Analyses
   Simulations of Actual Firings
6. Orbit Evolution Analysis
   Uses numerical averaging or methods of (1) above
7. Monte Carlo Analysis
   Uses any of above in realistic mission sequence

In addition to these capabilities, a modified version of the program has been developed that has the capability to perform parameter estimation analysis to recover the gravitational harmonic coefficients for the central planets' field as well as parameters that describe solar radiation pressure effects. This

parameter estimation version of the program features a numerical integration of the linear variational equations for the method 7 elements or an integration of the averaged linear variational equations analogous to the method 8 numerical averaging. The parameter estimation version is described in Reference (5) which supplements this report.

It has been pointed out that MAESTRO was designed to be a multi-purpose mission analysis tool as well as an in-flight mission control program. The program is capable of use for design of Earth, Moon or planetary orbit or flyby missions and is capable of supporting the mission control operations for such missions. The logic for display of mission-peculiar information is isolated from the program options and it is a relatively simple matter to modify the output for any specific spaceflight mission. It is recommended that care be taken to preserve this isolation and flexibility if the program is modified for use on other missions.

Some care has been taken to make the program as machine independent as was commensurate with the required interface logic for direct communication with the attitude and orbit determination programs. It is suggested that any future modifications be included so as to maintain this flexibility. It is hoped that the MAESTRO program and the techniques described in this report will be useful in the future exploration of space.

APPENDIX A

INTEGRATION OF MODIFIED ELEMENTS

The terms to be integrated are,

1. semilatus rectum, p
2. e sin ω
3. e cos ω
4. ω+ f
5. inclination, i
6. longitude of the ascending node, Ω

where e is the eccentricity

ω is the argument of perigee

f is the true anomaly.

The derivatives of the above quantities are numerically integrated to obtain the instantaneous orbital elements. The derivatives of these quantities are derived in many texts and reports and only the results are presented. The derivatives of the elements are

$$\dot{p} = \left(2\, r \sqrt{\frac{p}{\mu}}\right) S$$

$$(e \sin\omega)^{\cdot} = \sqrt{\frac{p}{\mu}} \left\{ -\cos(\omega+f)\, R + \left[\left(1-\frac{r}{p}\right) \sin(\omega+f) + \frac{r}{p}\, e \sin\omega\right] S \right.$$
$$\left. - e\cos\omega\, \frac{r}{p} \sin(\omega+f) \cot i\, W \right\}$$

$$(e\cos\omega)^{\cdot} = \sqrt{\frac{p}{\mu}} \left\{ \sin(\omega+f)\, R + \left[\left(1+\frac{r}{p}\right) \cos(\omega+f) + \frac{r}{p}\, e\cos\omega\right] S \right.$$
$$\left. + \frac{r}{p}\, e \sin\omega \sin(\omega+f) \cot i\, W \right\}$$

$$(\dot{\omega+f}) = \sqrt{p\mu}\, /r^2 - \left(r\sqrt{\frac{1}{\mu p}} \sin(\omega+f) \cot i\right) W$$

$$\dot{i} = r\cos(\omega+f)\, W \,/\sqrt{p\mu}$$

$$\dot{\Omega} = r \sin(\omega+f)\, W \,/\, (\sin i \sqrt{p\mu})$$

where μ is the gravitational potential

r is the radius

R, S, W are the components of the inertial perturbing acceleration resolved along the radial, circumferential, and orbit normal directions.

Appendix B

Retro Motor Optimization Procedure

The optimization procedure is due to B.A. Glassman et al. (Reference 4) and we are indebted to V.C. Zvonkovich of McDonnell Douglas Astronautics Company for valuable hints on the implementation of the technique.

The procedure finds values of a given set of independent parameters so as to maximize (or minimize) a payoff function while at the same time constrains a set of dependent variables. This procedure is based on first-order perturbation theory and relies on partial derivatives of the independent parameters with respect to the payoff function and the dependent parameters. The partial derivatives are determined by numerical techniques. The payoff function is minimized by treating it as a constrained dependent variable. The constraint value is systimatically reduced until convergence can no longer be obtained. A derivation of the technique follows:

Let the independent variable be x and the dependent variables be y_i, then the error, e_i, and the change in the independent variable can be obtained from

$$e_i = y_i - \bar{y}_i \tag{1}$$

$$x^{r+1} - x^r = \Delta x = -J^T e \tag{2}$$

where the bar denotes the desired values

r is the iteration number and

$$[J] = \frac{\partial y_i}{\partial x_j} \qquad \begin{matrix} i = 1, \text{ m dependent variables} \\ j = 1, \text{ n independent variables} \end{matrix}$$

If n is greater than m, an infinite number of x's satisfy eq. (2). An additional criterion is imposed on the problem such that the vector, x, is chosen which minimizes the step size defined by

$$ds = \sum_{i=1}^{n} \left(\frac{\Delta x_i}{x_i} \right)^2 \tag{3}$$

In matrix form eq. (3) becomes

$$ds = (\Delta x)^T \; D_\alpha^{-1} \; \Delta x \tag{4}$$

where D_α is a diagonal matrix with x_i^2 along the diagonal.

To find the particular solution which minimizes equation (4), first form the augmented function

$$\psi = (\Delta x)^T \; D_\alpha^{-1} \; \Delta x + [\, e^T + (\Delta x)^T J^T] \lambda \tag{5}$$

where the elements of λ are Lagrange multipliers. The term in the square brackets is the transpose of equation (2). Next equate to zero the partial derivatives of ψ with respect to each Δx_i. Repeating the differentiation for all Δx_i and equating all derivatives equal to zero results in

$$2 \; D_\alpha^{-1} \; \Delta x + J^t \lambda = 0 \tag{6}$$

Solving equation (6) for Δx yields

$$\Delta x = -\frac{1}{2} \; D_\alpha J^T \; \lambda \tag{7}$$

Differentiating equation (6) again for Δx_i produces

$$\frac{\partial^2 \psi}{\partial (\Delta x)^2} = 2 D_\alpha^{-1} \tag{8}$$

Since D_α^{-1} is positive definite, the Δx_i obtained by equation (7) is a minimum value for ψ.

Substituting equation (7) in equation (2) and solving for λ yields

$$\lambda = 2 (J D_\alpha J^T) e \tag{9}$$

By substituting equation (9) into equation (7), the final expression for Δx is obtained:

$$\Delta x = -D_\alpha J^T (J D_\alpha J^T)^{-1} e \tag{10}$$

Successive iterations using equation (2) and equation (10) are performed until the constraints are satisfied to within an input tolerance. The payoff function is then inspected and incremented.

For the particular application of calculating the retro attitude, the independent parameters are the right ascension, θ, and declination, δ, of retro firing attitude.

Then:

$$D_\alpha = \begin{bmatrix} \theta^2 & 0 \\ 0 & \delta^2 \end{bmatrix}$$

$$J = \begin{bmatrix} \frac{\partial V_T}{\partial \theta} & , & \frac{\partial V_T}{\partial \delta} \end{bmatrix}$$

where V_T is the trim velocity (payoff function) Equation (10) becomes:

$$\begin{bmatrix} \Delta\theta \\ \Delta\delta \end{bmatrix} = \begin{bmatrix} \theta^2 \frac{\partial V_T}{\partial \theta} \\ \delta^2 \frac{\partial V_T}{\partial \delta} \end{bmatrix} \frac{\Delta V_T}{\theta^2 \left(\frac{\partial V_T}{\partial \theta}\right)^2 + \delta^2 \left(\frac{\partial V_T}{\partial \delta}\right)^2} \tag{11}$$

Where ΔV_T is the error in the payoff function.

The following strategy is used to minimize the payoff function.

1. The initial payoff function is calculated and incremented by an input amount (-.01 for RAE-B)
2. The partial derivatives are determined numerically and the equations (11) used to determine the increment in right ascension and declination.
3. The value of the payoff function is determined at the new attitude.
4. The gain in the payoff function is decreased if the payoff function is increasing or cannot converge to the desired value. The gain is increased if convergence is achieved.
5. Iterations are continued until the gain in the payoff function is within some input stopping criterion.

Figure 3.24 presents an example of a practical situation. This figure shows contours of constant trim fuel required to achieve the desired orbit. The approach trajectory shown is a realistic one in that it resulted from a 1 meter per second execution error in the first midcourse maneuver. The elements of the lunar approach hyperbola are as follows:

$a = -7880.09$ km

$e = 1.392407$

$\omega = 139.715$

$i = 120.335$

$\Omega = -74.131$

} Relative to true lunar equator and prime meridian of date

Time of closest approach June 15, 1973 $5^h\ 15^m$ GMT. The path of the steepest decent procedure is shown on the figure. The initial attitude used was the velocity vector at closest approach. After five iterations, the solution converged to the minimum value of trim fuel.

Appendix C

Targeting Procedure for Inclination and Closest Approach

The impact parameters, B·T and B·R, are components of the vector distance from a central body to the point of closest approach of a hyperbolic asymptote for a hyperbolic trajectory relative to that body. They are of value as targeting parameters for lunar and interplanetary missions. The more direct objectives of inclination and radius of closest approach may be used in defining desired values of B·T and B·R if the hyperbolic excess velocity vector is also specified.

The coordinate reference for the impact parameters is 1) the direction of the incoming asymptote or hyperbolic excess velocity vector, S, of the hyperbola, 2) the outgoing node of the hyperbola, T, on the equator of the target body and 3) the orbit normal, R. The T-vector is defined by

$$T = K \times S \qquad \text{(normalized to unity)} \qquad (1)$$

where K is the polar vector at the planet. R is then defined by

$$R = S \times T. \qquad \text{(normalized to unity)} \qquad (2)$$

The hyperbolic excess velocity vector, S, is computed from the state vector at arrival. Then T and R are computed as indicated in equations (1) and (2). The desired inclination would be achieved (for constant S) by rotating R and T about S until the dot product of R with K is equal to the cosine of the desired inclination. The sketch shows the S, T, R and K vectors prior to this rotation.

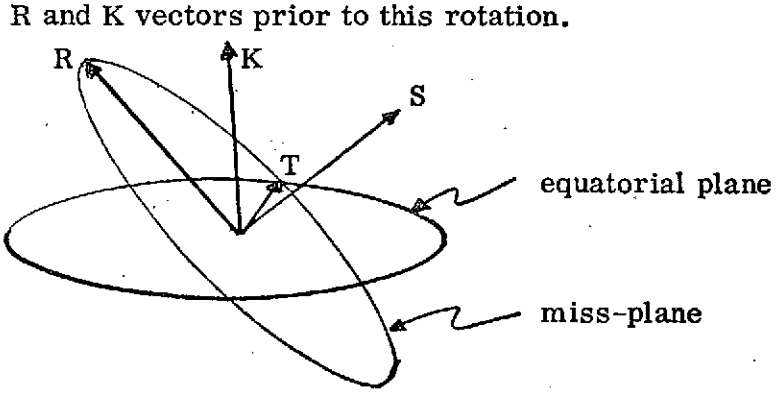

Sketch: Impact Plane and Miss Vector Geometry

Denoting the rotated R-vector by R_r, we may write equation (3).

$$R_r = R \cos\theta + T \sin\theta \tag{3}$$

The desired condition is

$$K \cdot R_r = \cos i_d \tag{4}$$

where i_d is the desired inclination. If the declination of S relative to the equatorial plane is less than the desired orbital inclination, the combination of equations (3) and (4) will provide two solutions for θ. A choice between these solutions may be made based on the sign of i_d. This choice affects the node of the resulting orbit. The desired B-vector will have no component along R_r but will lie entirely along the $-T_r$ direction, where

$$T_r = T \cos\theta - R \sin\theta \tag{5}$$

and θ is the chosen solution of equations (3) and (4). The desired B-vector components are thus given by equations (6) and (7).

$$(B \cdot T)_d = -b \cos\theta \tag{6}$$

$$(B \cdot R)_d = b \sin\theta \tag{7}$$

where b is the magnitude of B. This magnitude is derived from the desired distance of closest approach, r_p, as follows. The hyperbolic excess speed is defined by equation (8).

$$s = \sqrt{S \cdot S} \tag{8}$$

The velocity at closest approach is provided by equation (9)

$$v_p = \sqrt{s^2 + 2\frac{\mu}{r_p}} \tag{9}$$

Equation (10) defines the half-angle of the desired hyperbola

$$\alpha = \tan^{-1} \left(\frac{s\, r_p\, v_p}{\mu} \right) \tag{10}$$

Finally, b is defined by equation (11)

$$b = \left(\frac{\mu}{s^2} + r_p \right) \sin \alpha \tag{11}$$

When b from equation (11) is used in equations (6) and (7) along with the solution θ from equations (3) and (4), impact parameters have been defined from desired inclination and closest approach under the assumption of invariant S. In practice, S varies somewhat during an iteration, but the described impact parameter definition results in convergence to the desired inclination and closest approach regardless of the size of initial errors.

Appendix D

Variable Target Inclination Procedure

This appendix describes the method for computing desired miss vector components, $B \cdot T$ and $B \cdot R$, for an out-of-plane over-burn. The out-of-plane maneuver is assumed to be executed impulsively at periapsis of the approach hyperbola. Sketch B-1 shows the approach hyperbola, the incoming asymptote, S, the miss vector, B, and the periapsis velocity, V_p,

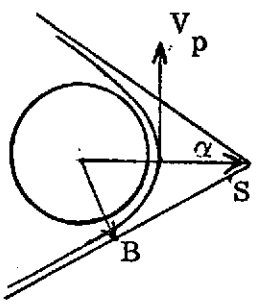

Sketch B-1: Approach Hyperbola

In the sketch, α is the half-angle of the hyperbola. The direction of V_p may be written as equation (1).

$$\hat{V}_p = -\hat{B} \cos \alpha + \hat{S} \sin \alpha \tag{1}$$

The $\hat{}$ symbol indicates "normalized to unity." Both S and α may be computed from the hyperbolic state vector as may also be $\hat{T}$ and $\hat{R}$, the reference miss vector directions. The miss vector B, may be written in terms of $\hat{T}$ and $\hat{R}$.

$$B = (B \cdot T)\, \hat{T} + (B \cdot R)\, \hat{R} \tag{2}$$

The direction of B may be written in terms of a rotation, θ, about S measured from the negative $\hat{T}$ direction toward $\hat{R}$.

$$\hat{B} = -\cos \theta\, \hat{T} + \sin \theta\, \hat{R} \tag{3}$$

The normal to this approach orbit, $\hat{H}$, is given by equation (4).

$$\hat{H} = \hat{B} \times \hat{S} = \cos \theta\, \hat{R} + \sin \theta\, \hat{T} \tag{4}$$

If the over-burn situation exists, the retro velocity is fired out-of-plane at an angle A from V_p such that the resulting velocity is circular. This situation is shown in Sketch B-2.

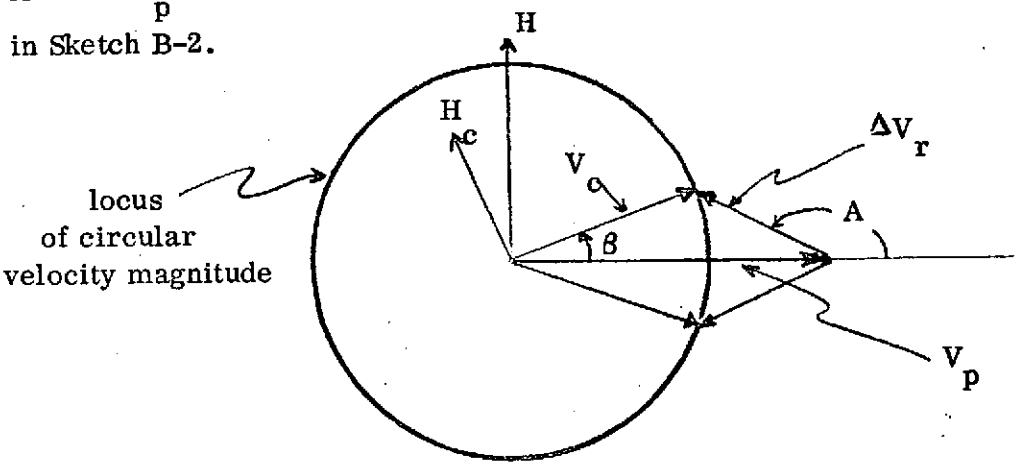

Sketch B-2: Over-burn as Seen from Periapsis

The angle at which to apply ΔV_r is computed from equations (5) and (6).

$$\cos A = (v_c^2 - \Delta v_r^2 - v_p^2) / v_p / \Delta v_r / 2 \tag{5}$$

$$\sin A = \pm \sqrt{1 - \cos^2 A} \tag{6}$$

The azimuth change, β, is then computed from

$$\cos \beta = (v_p + \Delta v_r \cos A) / v_c \tag{7}$$

and

$$\sin \beta = \Delta v_r \sin A / v_c \, . \tag{8}$$

The circular orbit's resultant normal, $\hat{H}_c$, is then written as

$$\hat{H}_c = \hat{H} \cos \beta \pm \hat{V}_p \sin \beta \tag{9}$$

or

$$\hat{H}_c = \cos \theta (\hat{R} \cos \beta \pm \hat{T} \cos \alpha \sin \beta) + \sin \theta (\hat{T} \cos \beta \mp \hat{R} \cos \alpha \sin \beta) \pm \hat{S} \sin \alpha \sin \beta \, . \tag{10}$$

The condition that the circular orbit should have the desired inclination, i_d, is

$$\hat{H}_c \cdot \hat{K} = \cos i_d \tag{11}$$

where $\hat{K}$ is the polar vector.

The algorithm which has been implemented is to call subroutine ORIENT with

$$\hat{H}_c(\theta = 0) = \hat{R} \cos \beta \pm (\hat{T} \cos \alpha - \hat{S} \sin \alpha) \sin \beta \tag{12}$$

to be rotated about $\hat{S}$ until equation (11) is satisfied. ORIENT returns two θ-solutions which, from equations (2) and (3), specify the desired miss vector components.

$$\begin{aligned} (B \cdot T)_d &= - b \cos \theta \\ (B \cdot R)_d &= b \sin \theta \end{aligned} \tag{13}$$

Appendix E

Variable Approach Guidance Procedure

This appendix describes the method for computing "desired" miss-vector components, B·T and B·R, for an in-plane overburn to circularize with retro alone at r_d. The method involves only computation of the magnitude of B, since the direction is governed by the desired inclination as described in Appendix A. The magnitude of B can be defined as a function of the radius of closest approach, r_p.

$$b = (r_p + \mu/C_3) \sin\left(\tan^{-1} \frac{v_{he} r_p \sqrt{C_3 + 2\mu/r_p}}{\mu}\right) \qquad (1)$$

In equation (1), C_3 is energy, v_{he} is hyperbolic excess speed and μ is the target's gravitational constant. The arctangent in (1) is the half-angle between asymptotes of the hyperbola.

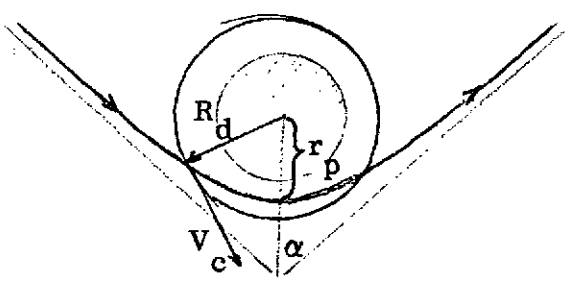

Figure C.1: Variable Approach Guidance Geometry

In attempting to solve for r_p (and also in writing the expression for b), we assume that the energy, C_3, will not change much between trials. Under this valid assumption, the "desired" b will serve to pull radius of closest approach in to its desired value. The retro velocity magnitude changes very little with changes in closest approach distance and is also assumed to be constant in the following derivation of r_p. Let the radius vector to the point on the hyperbola where $r = r_d$ be denoted by R_d and its normalized vector by $\hat{R}$. This point could occur either before or after periapsis. Let $\hat{T}$ denote a normalized vector lying in the orbital plane normal to R_d in the general direction of motion. These vectors $\hat{R}$ and $\hat{T}$, are not to be confused with the miss-plane vectors of the same name.

The velocity vector at R_d can be written

$$V = v_r \hat{R} + v_t \hat{T} \tag{2}$$

where v_r and v_t are radial and tangential components of velocity at r_d. The desired post-retro velocity is the circular velocity at r_d.

$$V_c = v_c \hat{T} \tag{3}$$

The required velocity impulse from the retro maneuver is ΔV.

$$\Delta V = V_c - V = (v_c - v_t) \hat{T} - v_r \hat{R} \tag{4}$$

The problem can be reduced to scalar form by squaring ΔV.

$$\Delta V \cdot \Delta V = \delta v^2 = v_r^2 + (v_c - v_t)^2 = v^2 - 2 v_c v_t + v_c^2 \tag{5}$$

If we assume that δv is the actual velocity impulse expected from the retro burn, we can solve (5) for r_p.

$$v^2 = C_3 + \frac{2\mu}{r_d} \tag{6}$$

$$v_t = \frac{r_p}{r_d} \sqrt{C_3 + \frac{2\mu}{r_p}} \tag{7}$$

$$v_c = \sqrt{\frac{\mu}{r_d}} \tag{8}$$

$$\delta v^2 = C_3 + \frac{3\mu}{r_d} - 2 \sqrt{\frac{\mu}{r_d}} \frac{r_p}{r_d} \sqrt{C_3 + \frac{2\mu}{r_p}} \tag{9}$$

$$C_3 r_p^2 + 2\mu r_p - \left\{ \frac{1}{2\sqrt{\mu r_d}} \left[\delta v^2 - C_3 - \frac{3\mu}{r_d} \right] \right\}^2 = 0 \tag{10}$$

Equation (10) is quadratic in r_p. Denoting the curly-bracketed term by β, we can write the solution as (11).

$$r_p = \left[\sqrt{\mu^2 + C_3 \beta^2} - \mu \right] / C_3 \tag{11}$$

The sign ambiguity in the quadratic solution was eliminated by the fact that r_p cannot be negative. This value of r_p is used in equation (1) to compute b. When the miss-vector errors are nulled by targeting, the radius of closest approach is r_p as computed in equation (11). If, as well, the retro impulse is applied at R_d as in equation (4), the post-retro orbit will be circular at radius r_d.

Appendix F

Attitude Errors on a Minimum Fuel Midcourse Correction

Introduction

It has been observed that for a particular minimum fuel midcourse correction, right ascension and declination errors map into the same straight line when resultant radius of closest approach is plotted against resultant inclination. This result will be shown to be characteristic of minimum fuel corrections.

Attitude Errors

Small attitude errors cause midcourse velocity variations (vectors) which lie approximately in the plane normal to the nominal midcourse velocity vector. Denoting the targeted midcourse correction velocity impulse by ΔV and a polar (or other non-colinear) unit vector by $\hat{K}$, we can describe the general velocity deviation vector, $\delta\Delta V$, which is normal to ΔV.

$$\delta\Delta V = \alpha \hat{K} \times \Delta V + \beta \hat{\Delta V} \times (\hat{K} \times \Delta V) \tag{1}$$

In equation (1), α and β are scalar coefficients of the "east" vector, $\hat{K} \times \Delta V$, and the "north" vector, $\hat{\Delta V} \times (\hat{K} \times \Delta V)$. These coefficients are functions of the attitude errors and $|\hat{K} \times \Delta V|$ in our case.

Mapping

Small midcourse velocity variations map linearly into variations in end conditions. It is this fact that allows targeting of the maneuver in the first place. Suppose that we denote the radius of closest approach (or B·T) by ψ_1 and inclination (or B·R) by ψ_2. Let us also denote their sensitivities to ΔV by

$$A = (\partial\psi_1 / \partial \Delta V)^T \tag{2}$$

$$B = (\partial\psi_2 / \partial \Delta V)^T \tag{3}$$

In equations (2) and (3), A and B are assumed to be column vectors. Midcourse velocity deviations are mapped into end condition variations by equation (4).

$$\delta \Psi = \begin{bmatrix} A^T \\ B^T \end{bmatrix} \quad \delta \Delta V \tag{4}$$

We now perform some vector algebra, the reason for which will soon be apparent.

$$\begin{aligned} \delta\psi_1 &= A^T \delta\Delta V \\ &= \alpha A^T (\hat{K} \times \Delta V) + \beta A^T \hat{\Delta V} \times (\hat{K} \times \Delta V) \\ &= -\alpha \hat{K}^T A \times \Delta V + \beta (A \times \Delta V)^T (\hat{K} \times \hat{\Delta V}) \\ &(-\alpha \hat{K} + \beta \hat{K} \times \hat{\Delta V})^T A \times \Delta V \equiv D^T A \times \Delta V \end{aligned} \tag{5}$$

Similarly $\delta\psi_2 = D^T B \times \Delta V$ (6)

Minimum Fuel Guidance

In what has been done so far, the minimum-fuel aspect has no bearing. It soon will. The MFG velocity correction impulse is computed from

$$\Delta V = -(\nabla\Psi)^{-1} \Delta^{\Psi} \tag{7}$$

where $\Delta\Psi$ is the original constraint error vector and where $(\nabla\Psi)^{-1}$ is the pseudo-inverse of $\nabla\Psi$.

$$\nabla\Psi = \begin{bmatrix} A^T \\ B^T \end{bmatrix} \tag{8}$$

The pseudo-inverse is obtained here by adjoining a third row, C^T, to $\nabla\Psi$. C is selected to be the normalized cross-product of A and B.

$$C = \frac{\hat{A \times B}}{} = (A \times B) / |A \times B| \tag{9}$$

The inverse of the augmented gradient is then (by Cramer's Rule)

$$(\nabla\Psi)^{-1} = \begin{bmatrix} \frac{B \times C}{|A \times B|} & \frac{C \times A}{|A \times B|} & C \end{bmatrix} \tag{10}$$

from whence $\Delta V = - \left[\frac{B \times C}{|A \times B|} \quad \frac{C \times A}{|A \times B|} \right] \Delta\Psi$. (11)

We are interested now in the terms $A \times \Delta V$ and $B \times \Delta V$ from equations (5) and (6). Since $A^T C = B^T C = 0$, we have

$$A \times \Delta V = - \left[\frac{-C (A^T B)}{|A \times B|} \quad \frac{C (A^T A)}{|A \times B|} \right] \Delta\Psi = k_1 C \tag{12}$$

and $$B \times \Delta V = - \left[\frac{-C (B^T B)}{|A \times B|} \quad \frac{C (A^T B)}{|A \times B|} \right] \Delta\Psi = k_2 C \tag{13}$$

We note (perhaps with some surprise) that both $A \times \Delta V$ and $B \times \Delta V$ are proportional to C. If we denote the bracketed vector from (5) and (6) by D as shown there, we may re-write those two equations as (14) and (15).

$$\delta\psi_1 = k_1 D^T C \tag{14}$$

$$\delta\psi_2 = k_2 D^T C \tag{15}$$

The relationship we originally intended to prove is (16).

$$\delta\psi_1 = \frac{k_1}{k_2} \delta\psi_2 \tag{16}$$

The attitude variation is represented by the parameters, α and β, of equation (1). These parameters then appear only in D, which cancels out in forming the quotient of the two end condition variations.

Geometrical Interpretation

It may be observed from equation (11) that the minimum fuel ΔV lies in the plane formed by the constraint sensitivity vectors, A and B.

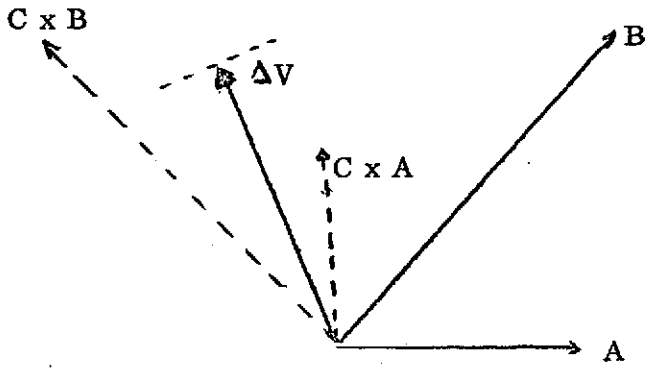

Figure A.1. Sensitivity vectors in the miss-plane

As may be seen from the figure, C x A and C x B lie in the plane of A and B, since C is out of the plane. ΔV is a linear combination of C x A and C x B and therefore lies in the A, B plane. A plane normal to ΔV is also seen to be normal to the A, B plane. Variation vectors in the plane normal to ΔV (epitomized by attitude errors) may be projected along A or B. These projections represent the constraint errors as formulated in equation (4). The projection of the variation vector along A or B is identical to the projection obtained by first projecting the variation vector into the A, B plane and then along A or B as seen in (17), because $A^T C = 0$.

$$A^T (I - CC^T)\, \delta \Delta V = A^T \delta \Delta V \tag{17}$$

The locus of points in the A, B plane corresponding to small attitude variations in ΔV is therefore a straight line along the intersection of the A, B plane and the plane normal to ΔV.

REFERENCES

1. Final Report for Radio Astronomy Explorer-B In-Flight Mission Control System Design Study, Contract No. NAS 5-11796, AMA Report No. 71-23, April 1971.

2. User's Guide to the Mission Analysis Evaluation and Space Trajectory Operations Program (MAESTRO), AMA Report No. 73-9, 1973.

3. Mary Payne, Two Impulse Trajectory Optimization for the RAE-B Orbit Trim Problem, AMA Report No. 72-73, May 1972.

4. F. T. Sun, Analytic Solution for Optimal Two-Impulse 180^{o} Transfer between Noncoplanar Orbits and the Optimal Orientation of the Transfer Plane, AIAA Journal, Vol. 7, No. 10, October 1969.

5. C. Uphoff, Numerical Averaging in Orbit Prediction, AIAA Paper No. 72-934, presented at AIAA/AAS Astrodynamics Conference, Palo Alto, Calif., September 1972.

6. Programmer's Manual for the Mission Analysis Evaluation and Space Trajectory Operations Program (MAESTRO), AMA Report No. 73-10, March 1973.

7. Parameter Estimation Supplement, to be published.